7-12-2017

Cell Dynamics in Three-dimensional (3D) Culture Environments

Rong Fan
rxf4967@rit.edu

R·I·T

Cell Dynamics in Three-dimensional (3D) Culture Environments

by

Rong Fan

A dissertation submitted in partial fulfillment of the requirements
for the degree of Doctorate of Philosophy in Microsystems Engineering

Microsystems Engineering Program
Kate Gleason College of Engineering

Rochester Institute of Technology
Rochester, New York
July 12nd, 2017

Cell Dynamics in Three-dimensional (3D) Culture Environments

By

Rong Fan

Committee Approval:

We, the undersigned committee members, certify that we have advised and/or supervised the candidate on the work described in this dissertation. We further certify that we have reviewed the dissertation manuscript and approve it in partial fulfillment of the requirements of the degree of Doctor of Philosophy in Microsystems Engineering.

_____

Dr. Jiandi Wan Date
Assistant Professor, Microsystems Engineering (Advisor)

_____

Dr. Denis Cormier Date
Earl W. Brinkman Professor, Industrial and Systems Engineering

_____

Dr. Thomas Gaborski Date
Associate Professor, Biomedical Engineering

_____

Dr. Satish G. Kandlikar Date
James E. Gleason Professor, Mechanical Engineering

Certified by:

_____

Dr. Bruce W. Smith Date
Director, Microsystems Engineering Program

ABSTRACT

Kate Gleason College of Engineering
Rochester Institute of Technology

Degree: Doctor of Philosophy **Program**: Microsystems Engineering

Author Name: Rong Fan **Advisor Name: Jiandi Wan**

Dissertation Title: Cell Dynamics in Three-dimensional (3D) Culture Environments

A three-dimensional (3D) cell culture system provides an effective platform to study cell dynamics in *in vivo*-mimicking conditions and thus plays an important role in understanding cell biology, organ function, and disease model. This dissertation investigates cell dynamics in a variety of 3D environments including solid and liquid matrix. We study cell dynamics in 3D hydrogel microparticles and show that cells exhibit significant differences with that from 2D monolayer culture, including cell cycle, survival, morphology and the sensitivity to inflammation. We further develop a 3D printed cell-laden hybrid hydrogel construct to investigate colon cancer cell dynamics in physiologically relevant bowel environment. Such system enables *in vivo*-mimicking cell environment and offers an effective platform to uncover inflammation mechanisms in bowel area. Long-term cell culture in 3D solid matrix, however, is challenged by nutrient delivering problems. We thus engineer a novel leaf-inspired artificial microvascular network to support the long-term cell growth. Apart from the 3D solid environment, we also investigate cell dynamics cultured in 3D fluidic environment and study the regulatory roles of shear stress in circulating cancer cells. Cancer cells are circulated in suspension for mimicking cancer metastasis through blood stream and a previously unrecognized role

of circulatory shear stress in regulating cancer cell dynamics is revealed. The research presented in this dissertation introduces a comprehensive study of cell dynamics in 3D environments and paves a new avenue to establish physiologically relevant model systems for tissue engineering and artificial functional organs.

Acknowledgment

This dissertation was completed with the help of many people and now it is my pleasure to thank all of them for their love, encouragement, support and blessings.

First of all, I would like to express my sincerest gratitude to my advisor, Dr. Jiandi Wan, for providing me the opportunity to work with him, for his valuable guidance on both my academic life and personal development, for his generous support on my career development. His pioneering vision and passions for research always motivate me to grow and become a better man. I believe without his persistent mentoring, this dissertation would not have been accomplished.

I would like to express my deepest appreciation to Dr. Satish Kandlikar, Dr. Thomas Gaborski and Dr. Denis Cormier for being my dissertation committee, guiding me during my Ph. D program, willing to share their precious suggestions and their valuable critiques on my research.

I also would like to thank Dr. Bruce Smith, Dr. Steven Day, Dr. Andrew Herbert and Ms. Lisa Zimmerman for the guidance during my Ph. D program and the help and suggestions for exploring career.

I would like to thank the professor Hela Sweet, Dr. Richard Hailstone, Dr. Patricia Taboada-Serrano, Professor Surendra Gupta and Ms. Dan Xue for providing technical help during my Ph. D research. I also appreciate the technical support from our collaborator at University of Illinois at Chicago and University of Rochester.

I would like to give my gratitude to my lab members, Ms. Sitong Zhou, Mr. Tianyi Lu, Mr. Xinye Chen, Mr. Xi Li, Mr. David Custer, Ms. Kubra Navqi, Ms. Caroline Kruse, Mr. Travis Emery, Ms. Marine Piou, Mr. Hing Jii Mea, Ms. Christine Zhou, Mr. Eyup Cinar and Mr. Scott Christensen, for their always understanding, help and support.

Special thanks should be given to my friends at RIT, Professor Carlos Barrios, Professor Carlos Diaz-Acosta, Professor Ivan Puchades, Ms. Michelle Horan, Mr. Yihang Sun, Ms. Yu Jin, Mr. Wentian Chen, Mr. Fan Wang, Mr. Runchen Zhao, Mr. Xiang Li, Mr. Zhenlin Xu, Mr. Shusil Dangi, Mr. Prashanth Ganesh, Ms. Kailun Jiang, Mr. Yuan Gao and Mr. Jing Ouyang, for their endless and selfless support at all the time. I would also like to thank my team members in MIC soccer teams during RIT intramural games for bring me together to enjoy the passions for competing the championship and the wonderful life time at RIT.

Finally, I would like to express my appreciation to my dearest family, Ms. Huilin Rong, Mr. Qiusheng Fan, Mr. Yong Huang, Ms. Jingyan Sun, Mr. Qingzhou Fan, Mr. Chuncheng Fan, Mr. Fei Fan, Ms. Haikui Wang, and Ms. Yaolin Rong, for their selfless love to me, trust me and always being on my side.

Table of Contents

Abstract ..... **iii**

Acknowledgment ..... **v**

Table of Contents ..... **vi**

Table of Figures ..... **xi**

Table of Tables ..... **xx**

List of Acronyms ..... **xxi**

Chapter 1. Introduction **1**

1.1 Cell dynamics 2

1.2 2D Cell culture 4

1.3 3D Cell culture 7

1.4 Current status of 3D cell culture 10

1.4.1 Materials for 3D cell culture 11

1.4.2 Techniques for 3D cell culture 14

1.5 Application of 3D cell culture 22

1.5.1 Construction for tissue model system 23

1.5.2 Construction for drug testing 24

1.5.3 Construction for artificial organ 25

1.6 Current challenges in 3D cell culture 28

1.6.1 Construction of physiologically relevant scaffolds 29

1.6.2 Construction of vascular networks 30

1.6.3 Realization of *in vivo*-like cellular communication 33

1.7 Research motivation 34

1.8 Dissertation overview 35

Chapter 2. Evaporation-based Microfluidic Production of Oil-free Cell-Containing Hydrogel Particles 38

2.1 Introduction 39

2.2 Motivation 40

2.3 Objective 40

2.4 Design and fabrication 41

2.4.1 Cell culture and maintenance 41

2.4.2 Device manufacture 42

2.4.3 Microfluidic generation of cell-laden microparticles 43

2.4.4 Manipulation and measurement of cell-laden microparticles 44

2.4.5 Statistical analysis 45

2.5 Results and discussion 45

2.5.1 Generation of cell-laden hydrogel microparticles 45

2.5.2 Oil removal and measurement 46

2.5.3 Measurement of cell growth in microparticles 49

2.5.4 Cell dynamics to TNF-α stimulation 52

2.6 Conclusion for Chapter 2 54

Chapter 3. Cell Dynamics in 3D Bio-printing Cell-laden Matrigel/Agarose Construct 56

3.1 Introduction 57
3.2 Motivation 58
3.3 Objective 60
3.4 Design and fabrication 61
3.4.1 Cell culture and maintenance 61
3.4.2 Hydrogel preparation 61
3.4.3 Rheological measurement 62
3.4.4 3D bio-printing 62
3.4.5 Determination of cell growth and cell viability 63
3.4.6 Salmonella bacteria preparation 64
3.4.7 Bacterial treatment for cell-laden tube 64
3.4.8 Evaluation of bacterial adhesion 65
3.4.9 Statistical analysis 65
3.5 Results and discussion 65
3.5.1 3D printing agarose structures 65
3.5.2 3D printing cell-laden agarose structures 67
3.5.3 3D printing Matrigel/agarose hybrid hydrogel 69
3.5.4 3D printing cell-laden Matrigel/agarose hybrid hydrogel structures 71
3.5.5 3D printing Matrigel/agarose hybrid hydrogel at constant temperature 73
3.5.6 Compensation between mechanical and biological property of hybrid hydrogel 76
3.5.7 HCT116 and Salmonella interaction in cell-laden agarose tube 80
3.5.8 Salmonella treatment of cell-laden hybrid hydrogel tube 86
3.6 Conclusion for Chapter 3 88

Chapter 4. Leaf-inspired Artificial Microvascular Networks (LIAMN) for Three-dimensional Cell Culture.....90

4.1 Introduction.....91

4.2 Motivation.....92

4.3 Objective.....93

4.4 Design and fabrication.....94

4.4.1 Cell culture and maintenance.....94

4.4.2 PDMS-based leaf-mimicking microfluidic device.....95

4.4.3 Agarose-based leaf-mimicking microfluidic device.....95

4.4.4 Agarose-based leaf-inspired microfluidic device.....97

4.4.5 Statistical analysis.....98

4.5 Results and discussion.....99

4.5.1 Hydraulic measurement of leaf-mimicking microfluidic device.....99

4.5.2 Agarose-based leaf-mimicking microfluidic device for 3D cell culture.....101

4.5.3 Theories for developing leaf-inspired artificial microvascular networks.....102

4.5.4 Short-term culture of cells in leaf-inspired microfluidic device.....107

4.5.5 Long-term culture of cells in leaf-inspired microfluidic device.....108

4.6 Conclusion for Chapter 4.....109

Chapter 5. Circulatory Shear Flow Regulates the Viability and Proliferation of Circulating Colon Cancer Cells.....111

5.1 Introduction.....112

5.2 Motivation.....113

5.3 Objective.....114

5.4 Design and fabrication....114
5.4.1 Cell culture and maintenance....114
5.4.2 Microfluidic fabrication and circulation of HCT116 colon cancer cells....115
5.4.3 Determination of cell viability and growth after circulation....118
5.4.4 Quantitative real-time PCR....118
5.4.5 Statistical analysis....119
5.5 Results and discussion....119
5.5.1 Cell viability in response to shear stimulation....119
5.5.2 Cell proliferation in response to shear stimulation....121
5.5.3 Expression of critical genes related to β-catenin signaling in response to shear stimulation....123
5.5.4 Correlation between cellular behavior and gene expression....125
5.6 Conclusion for Chapter 5....129
Chapter 6. Conclusion and Future Opportunities....130
6.1 Research Summary....131
6.2 Key contributions....133
6.3 Future opportunities....136
6.3.1 3D Bioprinting ICSs for the development of a functional colon....136
6.3.2 Microfluidically 3D printing construct composed of cell-laden microparticles....138
Chapter 7. References....140
Chapter 8. Publications....160

Table of Figures

Figure 1 Diagram of cell cycle showing different phases of cell dynamics [4]..... 3

Figure 2 Physical, biochemical and physicochemical factors are presented within *in vivo* cell microenvironment [19]..... 6

Figure 3 Schematics shows the difference of cells growing in 2D and 3D environment [35]..... 8

Figure 4 Confocal imaging of cell morphology change in different scaffold materials. Cells are stained by Live/Dead fluorescent assays. Cells display (A) spherical morphology in alginate and (B) spindle-like morphology in gelatin after 7 days culture [66]..... 13

Figure 5 Schematics of 384 hanging drop technique for Murine embryonic stem cell (ES-D3) spheroid culture [27]..... 15

Figure 6 Schematics of bulk hydrogel technique. (A) Concepts of 3D cell culture in bulk hydrogel environment. (B) Fluorescent image of cells cultured in 3D bulk hydrogel scaffold (scale bar: 100 μm, inset: 10 μm) [83]..... 17

Figure 7 Microfluidic technique for 3D cell culture in microparticles. (A) Schematics of microfluidic encapsulation of cells in microparticles (Scale bar: 100 μm) [92]. (B) Fluorescent image of viable fibroblast encapsulated in PEG microgel particles [93]..... 18

Figure 8 Endothelial cells growing in microfluidic channel. Cells are stained with actin-green and nuclei-blue fluorescent dye. (A) Endothelial cells are cultured in microchannel. Scale bar: 50 μm. (B) The change of endothelial cell morphology when subject to static and shear condition respectively scale bar: 50 μm [100]..... 19

Figure 9 Concepts of using microfluidic device for 3D cell culture, metabolite analysis and cytotoxicity assay. (A) The integrated microfluidic device enables co-culturing for drug detoxification. (B) Controlled encapsulation of HLMs inside hydrogel microstructures. (C) Fluorescence image of HLMs entrapped inside PEG hydrogel microstructures. The edge of the microstructure was labeled with dash lines [103]..... 20

Figure 10 Concepts of 3D printing techniques to construct scaffold for 3D cell culture. (A) Schematic of 3D printing process [112]. (B) Schematic illustrations, optical images, and fluorescent images of the vascular networks printed in hydrogel construct [110]. (C) Fluorescent images of the engineered vascular networks lined with TFP HUVECs (red) and GFP Human neonatal dermal fibroblast (HNDF)-laden GelMA ink (green) [110]. (D) 3D printed bone structures [113]. 22

Figure 11 Human mesenchymal stem cell (MSC) spheroid culture in gelatin MPs for 7 days in PDMS microwells [124]..... 24

Figure 12 Concepts of integrated organ-on-a-chip technology by applying microfluidic circulatory system in a physiologically relevant manner [30]. 26

Figure 13 Concept of liver-on-a-chip. (A) Illustration of the basic unit of liver tissue, the classic hepatic lobule. (B) The lobule-mimetic-stellate-electrodes array. (C) The configuration and operation principles of DEP-based heterogeneous lobule-mimetic cell patterning [58]..... 27

Figure 14 Construction of vascular structures realized by (A) scaffold-free 3D bio-printing [102], (B) microfluidics-based bio-printing [100] and (C) direct writing (scale bar: 10 mm) [164]..... 32

Figure 15 Microfluidic encapsulation of HCT116 colon cancer cells in hydrogel particles. (a) Experimental image of a flow-focusing microfluidic device used to encapsulate cells in hydrogel particles (scale bar = 100 μm). (b) Image of hydrogel particles with encapsulated cells. Arrows indicate the encapsulated cells in particles (scale bar = 50 μm). Inset: Size distribution of particles. 46

Figure 16 Schematics of the rapid oil removal process and cell culture in hydrogel particles. 47

Figure 17 Effect of oil on particle aggregation and cell viability. (a) Evaporation-induced change of weight percentage ($W/W_0 \times 100$ %) of the mixture solution of droplets and oil. Inset: Image of aggregated hydrogel particles after the removal of PFP (scale bar = 50 μm). (b) Evaporation-induced change of weight percentage with time when particles are collected in the DMEM cell culture medium. Inset: Image of a centrifuge tube containing layers of culture medium, particles, and PFP (scale bar = 5 mm). 47

F**igure 18** Evaporation-induced change of weight percentage of the mixture solution of droplets and HFE 7500 oil. 48

Figure 19 Conventional method for removing oil phase from the culture environment. (A) Image of a layer of hydrogel particles floating on top of the HFE 7500 oil phase after centrifuge (scale bar = 5 mm). (B) Image of a layer of aggregated matrigel particles sticking to a filter paper after filtration (Scale bar = 50 μm)..... 49

Figure 20 Percentage of living cells in hydrogel particles ($N/N_0 \times 100$ %) at different culture time (t)..... 50

Figure 21 Proliferation of human HCT116 colon cancer cells in hydrogel particles. (a) Time-series image of the growth of a single cell in a hydrogel particle (scale bar = 10 μm).

(b) Percentage of living cells at different time when cells are cultured in petri dish and hydrogel particles. (c) The net growth rate (n_n - n_0)/n_0 × 100 %) of cells encapsulated in hydrogel particles. 52

Figure 22 Effect of TNF-α on the viability of human HCT116 cells cultured in hydrogel particles and petri dish. The change of percentage of living cells, (N/N_0 × 100 %), with time at different concentrations of TNF-α when cells are cultured in hydrogel particles (a) and petri dish (b). 54

Figure 23 Experimental setup of 3D printed agarose constructs. (A) Schematic of the 3D printing setup. (B) 3D printed agarose tubes with different diameters (from left to right: *d* = 12, 17, and 25 mm) (scale bar = 10 mm). (C) 3D printed agarose constructs with a star, triangle, or square shape (scale bar = 8 mm). 66

Figure 24 3D printed tubular structure with a height of 8 cm using 2 wt% agarose. 67

Figure 25 Image of the 3D printed cell-laden agarose tube. (A) Side view and top view microscopic images of the 3D printed cell-laden agarose tube. (B) Confocal imaging of cell distribution at the top, middle and bottom part of the tube. 68

Figure 26 Cell growth in 3D printed agarose tubes. Cells are stained with Live/Dead assays and imaged by confocal microscopy at (A) 0 day, (B) 1 day, (C) 3 days and (D) 7 days. 68

Figure 27 Characterization of Matrigel/agarose hybrid hydrogel. Dependence of the (A) storage modulus (G') and (B) loss modulus (G") of hybrid hydrogel on time at different compositions of Matrigel and agarose. 70

Figure 28 Images of tube printed using hybrid hydrogel composed of (A) 15%, (B) 30%, (C) 50% Matrigel and 2 wt% agarose (scale bar: 5 mm). 71

Figure 29 Percentage of cells that exhibit spreading morphology after 3 days of culturing in 3D printed tubular structures composed of 2 wt% agarose and 15, 30, or 50% (v/v) Matrigel. 72

Figure 30 An image of a 3D printed tubular structure using 50% (v/v) Matrigel and 3 wt% agarose. The tube has a diameter of 17 mm and a wall thickness of 2 mm (scale bar: 5 mm). 72

Figure 31 Cell growth in 3D printed Matrigel/agarose tubes composed of 3wt% agarose and 50% (v/v) Matrigel. (A) Percentage of cells that exhibit spreading morphology for 11 days culturing. Inset: A fluorescent confocal image of spreading cells and clusters formed in the printed tube. Cells are stained with actin-green and Nuc-blue (scale bar = 50 μm). (B) Cell viability over 11 days culturing. 74

Figure 32 3D printing Matrigel/agarose hybrid hydrogel at constant temperature (37^{o}C). (A) An image of the experimental setup in which a syringe heater was wrapped around the printing syringe to maintain the temperature at 37^{o}C during printing. (B) An image of 3D printed tubular structure composed of 3wt% agarose with 50% (v/v) Matrigel (scale bar: 5 mm). (C) Microscopic images of the 3D printed hybrid hydrogel tube cut at the top, middle, and bottom sections (scale bar: 100 μm). (D) Percentage of cells that exhibit spreading morphology for 11 days culturing. (E) Cell viability over 11 days culturing..... 75

Figure 33 Fluorescent images of cells stained with Live/Dead assays in the hybrid hydrogel tubes after culturing for (A) 0 day, (B) 1 day, (C) 2 days and (D) 7 days. Inset: images of a single cell spreading with the culture time and forming into cell clusters in the hybrid hydrogel tubes. 76

Figure 34 COMSOL simulation result shows the diffusion model in thick hydrogel construct. 80

Figure 35 Schematics of experimental process, including 3D printing cell-laden tube, pre-culture tube, Salmonella infection and post-culture for sample collection. 82

Figure 36 Fluorescent images of Salmonella bacterial adhesion at the lumen of agarose tube when HCT116 colorectal cancer cells were encapsulated. While dot line indicates the wall of tube lumen. 84

Figure 37 Fluorescent images of Salmonella bacterial adhesion at the lumen of agarose tube when there were no HCT116 colorectal cancer cells seeded. The while dot line indicates the wall of tube lumen. 84

Figure 38 Bacterial adhesion changes with flow condition and pre-culture time when cells were seeded and not seeded in the agarose tube respectively. Agarose tubes were pre-cultured for (A) 24 h, (B) 48 h and (C) 1 week before infection. 85

Figure 39 Fluorescent images of Salmonella bacterial adhesion at the lumen of hybrid hydrogel tube when there were (A) no cell seeding and (B) with cell seeding respectively. The while dot line indicates the wall of tube lumen. 86

Figure 40 Bacterial adhesion changes with flow condition when cells were seeded and not seeded in the hybrid hydrogel tube respectively. Hybrid hydrogel tubes were pre-cultured for 1 week before infection. 87

Figure 41 Schematics of the fabrication of leaf-mimicking and leaf-inspired microfluidic devices for 3D cell culture. Fabrication process of (A) leaf-mimicking microfluidic device and (B) multilayer leaf-inspired microfluidic device. 94

Figure 42 Analysis of the hydraulic transport efficiency of leaf-mimicking PDMS microfluidic devices. (A) Image of a typical leaf-mimicking PDMS microfluidic device. Scale bar: 2 cm. (B) Schematics of positions of inlets and outlets in the leaf-mimicking PDMS microfluidic devices 96

Figure 43 Analysis of hydraulic transport in leaf-mimicking microfluidic device. (A) Effect of position of outlets on the input pressure. (B) Dependence of fluid coverage on the position of outlets in leaf-mimicking PDMS microfluidic devices. 100

Figure 44 HCT116 colon cancer cells in agarose-based leaf-mimicking microfluidic devices. (A) Image of cultured HCT116 cells in the network area of the leaf-mimicking agarose microfluidic devices. Scale bar: 100 μm. (B) Viability of HCT116 cells cultured near the main vein, the 1st order branch, and the network area. 102

Figure 45 Leaf-inspired microfluidics for 3D cell culture. (A) Schematic of the design of leaf-inspired microfluidics. Unit: mm. (B) Assembly of a three-layer agarose microfluidic device. Scale bar: 2 mm. (C) Image of the cross-sectional view of the assembled three-layer agarose microfluidic device. Scale bar: 200 μm. (D) Image of a three-layer PDMS microfluidic device when fluorescein solution is flowing through the device. Scale bar: 3 mm. 105

Figure 46 COMSOL simulation of fluid velocity through the LIAMN structures. 106

Figure 47 COMSOL simulation of the diffusion model in the thick vascularized hydrogel construct that realized by LIAMN. 107

Figure 48 Cell growth in a short-term manner in leaf-inspired microfluidic device. (A) 3D construction of confocal images of HCT116 cells in the three-layer agarose microfluidic

device. Cells are stained by nucleus-blue fluorescent dye. Scale bar: 200 μm. (B) Viability of HCT 116 cells cultured in the three-layer agarose matrix. 108

Figure 49 Growth of HCT116 cells in the developed three-layer leaf-inspired agarose matrix. 3D construction of confocal images of HCT116 cells stained with cell Live/Dead assay at day 1 (A), 3 (B), and 9 (C) of culture. Scale bar: 200 μm. Inset: Merged bright-field and fluorescent images of cells at the single cell level. Scale bar: 5 μm. (D) Merged bright-field and fluorescent image of cell spheroids stained with actin-green and nucleus-blue fluorescent dye. Scale bar: 100 μm. Inset: Fluorescent image of a single spheroid. Scale bar: 10 μm. 109

Figure 50 Circulation of cells in microfluidic platform. (A) Schematic of the microfluidic facility for cell circulation. (B) A typical microscopic image of cells flowing through the constriction in the microfluidic device. (C) Schematic illustration of the elongation of circulating cancer cells when passing through the constriction due to increased shear stress. 116

Figure 51 Effect of shear on the viability of circulating HCT116 cells. (A) Percentage of living cells in various shear conditions in the microfluidic circulatory system. Fluorescent images of cells stained with Live/Dead assay after circulation at flow rate of 1.0 rpm for (B) 2 min and (C) 20 h, respectively. Scale bar: 50 μm. 121

Figure 52 Effect of shear on the proliferation of survived HCT116 cells after circulation for (A) different durations and (B) shear conditions. 123

Figure 53 Effect of shear on the mRNA expression level of (A) β-catenin, (B) Bmi1 and c-myc, and (C) GSK-3β and p53 mRNA in HCT116 cells circulated at speeds of 0.1 and 1.0 rpm for 2.5 h and 20 h respectively. 125

Figure 54 Effect of concentration of circulation cells on cell viability and proliferation. (A) Immediate cell viability after cells circulated for 20 h with an initial cell concentration of 0.01, 1, or 100 M cells/ml. The circulation speeds were 0.1 and 1.0 revolution per minute (rpm). (B) and (C) are proliferation of cells survived from 20 h circulation at 0.1 rpm and 1.0 rpm respectively. 128

Table of Tables

Table 1 Calculated parameters of the leaf-inspired branching system. Note that the distances between the smallest branches (5^{th} order branches) are from 400 to 500 μm. 106

Table 2 Calculation of average wall shear stress in the microfluidic system. Note that τ_c and τ_w are calculated based on the equation $\tau = \frac{\mu Q}{w^2 \times h}$, ,whereas τ_t is calculated based on the equation $\tau = \frac{32\,\mu Q}{\pi d^3}$ 117

Table 3 Primers used in real-time PCR measurement..... 119

List of Acronyms

2D	Two-Dimensional
3D	Three-Dimensional
5-FU	5-Fluorouracil
AP	Acetaminophen
CO_2	Carbon Dioxide
COX-2	Cyclooxygenase-2
CTC	Circulating Tumor Cells
DEP	Dielectrophoretic
DKK1	Dickkopt-1
DMEM	Dulbeccoo's Modified Eagle's Medium
ECM	Extracellular Matrix
EGF	Epidermal Growth Factor
FBS	Fetal Bovine Serum
G'	Storage modulus
G''	Loss modulus
GSK-3β	Glycogen Synthase Kinase 3 beta
hESCs	Human Embryonic Stem Cells

hiPSCs	Human Induced Pluripotent Stem Cells
HLMs	Human Liver Microsomes
HSCs	Hepatic Stellate Cells
Huh-7	Human Hepatocytes-derived Cell
HUVECs	Human Umbilical Vein Endothelial Cells
IL-6	Interleukin-6
ISC	Intestinal Stem Cell
LIAMN	Leaf-inspired Artificial Microvascular Networks
MAPK	Mitogen-activated Protein Kinase
MMP	Matrix Metalloproteinases
MSC	Mesenchymal Stem Cell
NO	Nitric Oxide
PAECs	Porcine Aortic Endothelial Cells
PBS	Phosphate Buffered Saline
PCR	Polymerase Chain Reaction
PDMS	Poly(dimenthyl Siloxane)
PEG	Poly(Ethylene Glycol)
PET	Polyethylene (Terephtahalate)

PFP	Perfluoro Pentane
ROS	Reactive Oxygen Species
RPM	Ramp per Minute
SEM	Scanning Electron Microscopy
TNF-α	Tumor Necrosis Factor-alpha
TPZ	Tirapazamine
UGT	Uridine 5'-diphosphate-glucuronosyltransferase
μ	Viscosity

Chapter 1. Introduction

Cell dynamics is critical to understand body condition, organ mechanism and disease models, and serves as fundamental knowledge and principle for the development of tissue engineering, biomedical engineering, drug discovery and life science. Therefore, construction of effective systems that enable growing and manipulating cells for investigating cell dynamics becomes increasingly attractive to people in recent decades. In this chapter, cell dynamics is firstly introduced revealing the knowledge of cell growth and metabolism. Methods of two-dimensional (2D) and three-dimensional (3D) cell culture for understanding cell dynamics are then demonstrated and compared. Moreover, the state-of-the-art of 3D cell culture is reviewed that introduces the development of the materials and techniques in the recent decades. In addition, based on literature, the current application of 3D cell culture and potential future development are discussed in this chapter, followed by the review of the current challenges in this field. To this end, the motivations behind this research are first presented.

1.1 Cell dynamics

Cell dynamics is significantly attractive to people in the field of biomedical engineering, tissue engineering, clinical study, because it serves as cornerstone for understanding cell biology and the mechanism of living organisms on earth, and paves avenue for developing life science and technology including the construction of artificial transplantable organ and drug discovery [1-3]. In particular, cell dynamics refers to the change of cell functions and structures at both behavioral and molecular level, because as known by all, the metabolism and structure of cells are not static, instead, they are subjected to sustained change responding to the intracellular demand and the variation of local biological environment, and therefore the organelles, specialized domains, molecule inside the cells become significant dynamic [2].

One of the typical examples of cell dynamics is cell division, which is an important criteria to evaluate the vitality of an organism. If a tissue or an organ is vigorous, rapid cell growth is needed to maintain the proper renewal and growth [4-6]. For each cell division, cells will go through a series of events inside the cell body leading to the division and duplication of their DNA, resulted in two daughter cells, so called a cell cycle [7]. As shown in Figure 1, several phases are happened during each cell cycle, including G_0 phase (resting phase between two cell cycles), G_1 phase (also called growth phase, where biosynthetic activities of cells are motivated at a high rate that causes the growth in size, the increase of proteins supply and number of organelles, such as mitochondria, ribosomes), S phase (DNA replication), G_2 phase (protein synthesis and cell growth becomes rapid for preparing cell mitosis) and M phase (mitosis). The cell cycle keeps repeating that lets the cells grow in numbers, which is a dynamics process at all time before cell death.

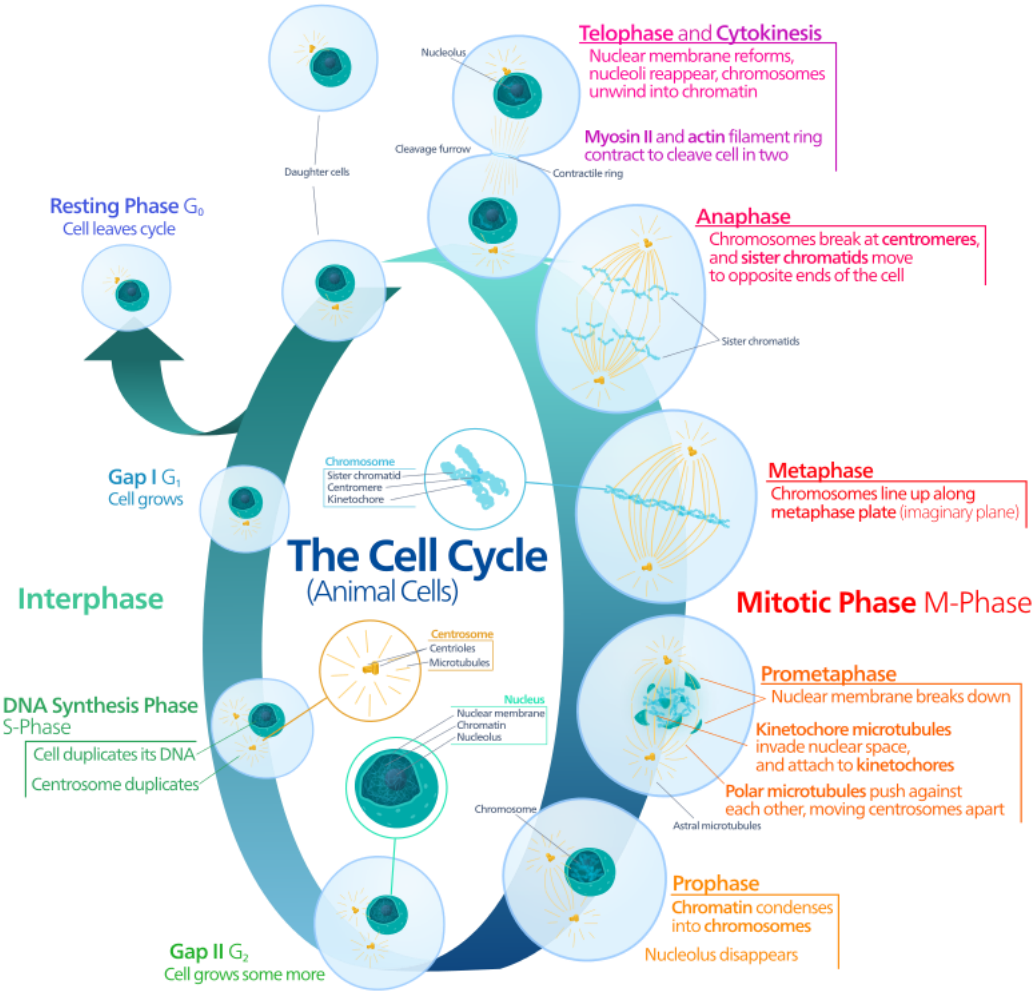

Figure 1 Diagram of cell cycle showing different phases of cell dynamics [4].

On the other hand, signals induced by extracellular matrix (ECM), surrounding cells, hormones, growth factors, and mechanical stimuli are sensed by cells and then trigger rapid response in cell membrane dynamics and behaviors, cell shape, cytoskeletal organization, and gene expressions [8, 9]. Cell migration, for example, responses to external cues that initiate the metabolism including dynamic reorganization of the actin, microtubule and intermediate filament cytoskeletons, coordination with membrane trafficking situation, which involves the transportation of receptors, secretory and

endocytic cargo to appropriate location that is necessary for cell function [8, 10]. As a result, new membrane can be delivered to the leading edge and internalize adhesive receptors from the cell near. It should be noted that each cell serves as a basic unit for the tissue, whereas several tissues form the organ structure and realize the organ function. Therefore, studying cell dynamics is essential for understanding the cellular function and dysfunction at various biological system that enables people understanding the mechanism of organism and body system.

1.2 2D Cell culture

In order to investigate the cell dynamics, construction of artificial system that enables culturing cells out of natural environment, treating cells with stimuli and testing cell metabolism becomes a necessary task to accomplish. The development of cell culture technique provides a powerful platform for understanding biological mechanism of organism, studying cancer and disease model, researching drugs and methods for curing patients, and opening new avenues to explore other aspects of life science and technology [11-15]. In particular, cell culture is a technique that extracting living cells from animal or plant tissues through surgical method and subsequently grow them in well-controlled condition, which is usually outside of their natural environment but artificial engineered [15]. The cell culture condition can vary with cell types, including the supplement of essential nutrients, such as carbohydrates, amino acid, vitamins, and minerals, growth factors, hormones, gasses (CO_2 and O_2) and physio-chemical environment that containing pH, osmotic pressure and temperature [15, 16]. It has been well-known that most cells

require an artificial substrate that can provide a surface for adherence, whereas others can grow in culture medium at the status of suspension.

When cells, especially mammalian cells, grow on the surface at adherent status, where cells are spreading to form focal adhesions and a mono-layer culture could be achieved by culturing, it is called 2D cell culture. Apart from bringing researcher a platform for studying cell dynamics, it has other obvious advantages including simple operation, easy-controlled microenvironment, cell observation, measurement and manipulation. For example, cells in culture medium suspension could be simply seeded into petri dish and cells will grow into mono-layer to confluence through incubation at proper condition (temperature, O_2, CO_2 and nutrient). Moreover, manipulation of cells, such as drug treatment, bacterial infection and growth factor stimulation could be achieved by simple addition. Due to the mono-layer of cell growth on 2D surface, it is optimal to observe the cell behavior and response through placing the petri dish on microscope and extract samples from petri dish via pipette.

In the recent decades, however, cell culture on 2D flat surface has been demonstrated to miss key metabolic activities of found *in vivo* and leads to biased data acquired from animal experiments because it is unable to mimic and satisfy neither the structural requirements nor the biological demands in complex physiological condition (Figure 2) [12, 17]. In particular, first of all, cells growing in 2D environment only contact with each other on edge and most part of cell body are in contact with plastic substrate, whereas cells at *in vivo* situation are surrounded by 3D matrix, in which a strong interaction between cell and matrix can be triggered that plays critical roles in regulation of cell behaviors and signaling transduction at molecular level (Figure 3). On the other hand,

instead of forming mono-layer structure, 3D physiological environment allows cells forming into clusters that called spheroid, in which cells attach tightly with each other that realizes cellular communication. Moreover, cells growing in 2D environment can reach to nutrients without limitation from the surrounding medium and cellular wastes could be released to the medium directly, which are different from physiological condition where both nutrients and wastes should be delivered through diffusion and a possible limitation is presented. Additionally, 2D environment is hard to realize areas of hypoxia, varying cell proliferation zone (quiescent and replicating), heterogeneous cell populations, gradient effect, and differential nutrient and metabolic waste transport [14]. Therefore, all of the issues described above render the conventional 2D culture system lack of biological relevance to *in vivo* situation and fail to serve as a reliable platform to disease study and drug testing [14, 18].

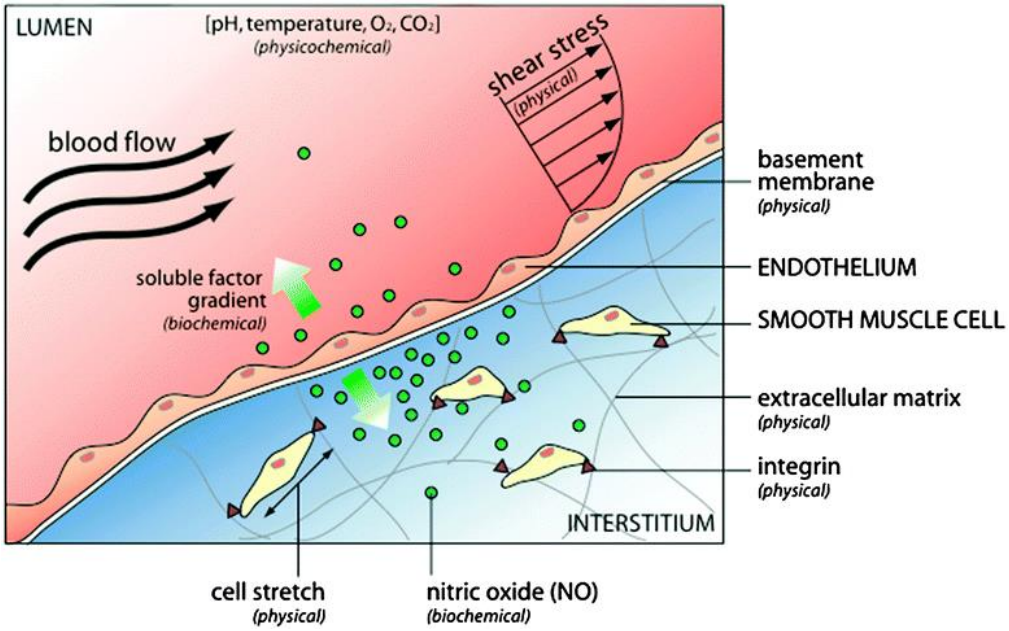

Figure 2 Physical, biochemical and physicochemical factors are presented within *in vivo* cell microenvironment [19].

1.3 3D Cell culture

In recent decades, due to the realization of the limitations of 2D culture system, 3D construction of biological matrix possessing the structural and functional features of *in vivo* tissues is of great interest and importance in tissue engineering and biomedical engineering [20-22]. In particular, building 3D biological matrix that is physiologically relevant significantly contributes to the study of cell dynamics and providing reliable results of cell metabolism, which are advantageous for various applications such as investigation of tumor model [23, 24], drug delivering [25, 26], testing and screening [27, 28], and development of transplantable organ constructs [29, 30].

3D culture system is desirable for studying cell biology, because 3D environment allows cells growing and interacting with surrounding matrix at all three dimensions, and therefore providing more contact space for cell adhesion and stimulation input (Figure 3). This is critical for achieving *in vivo*-like cellular function, for example, cell contraction, integrin ligation and signaling transduction at molecular level [31, 32]. In such system, cells would grow into 3D spheroid structure or 3D colonies, which are believed to enable closely resembling *in vivo* tissue in terms of cellular communication and the development of extracellular matrices. As a result, cell behaviors are different from those in 2D culture environment. For example, in order to achieve cell migration and proliferation, cells are required to modify the surrounding matrix through secreting enzymes to create space, which involves the activation of dynamic reorganization of the actin, microtubule and intermediate filament cytoskeletons, coordination with membrane trafficking situation. The produced daughter cells will tightly attach with each other due to the limited space that enhances cell communication and formation of tight junction. Moreover, it has been

revealed that, in contract to monolayer culture, fibroblasts can grow faster in 3D and become asymmetrical that close to the status at *in vivo* [33]. The lifespans of cells growing in 3D environments are also found to be longer than 2D, and 3D spheroids have been reported to be cultured continuously for 302 days with healthy status and non-cancerous growth, suggesting the potential for conducting long-term investigation of cell growth and effects of drugs [34].

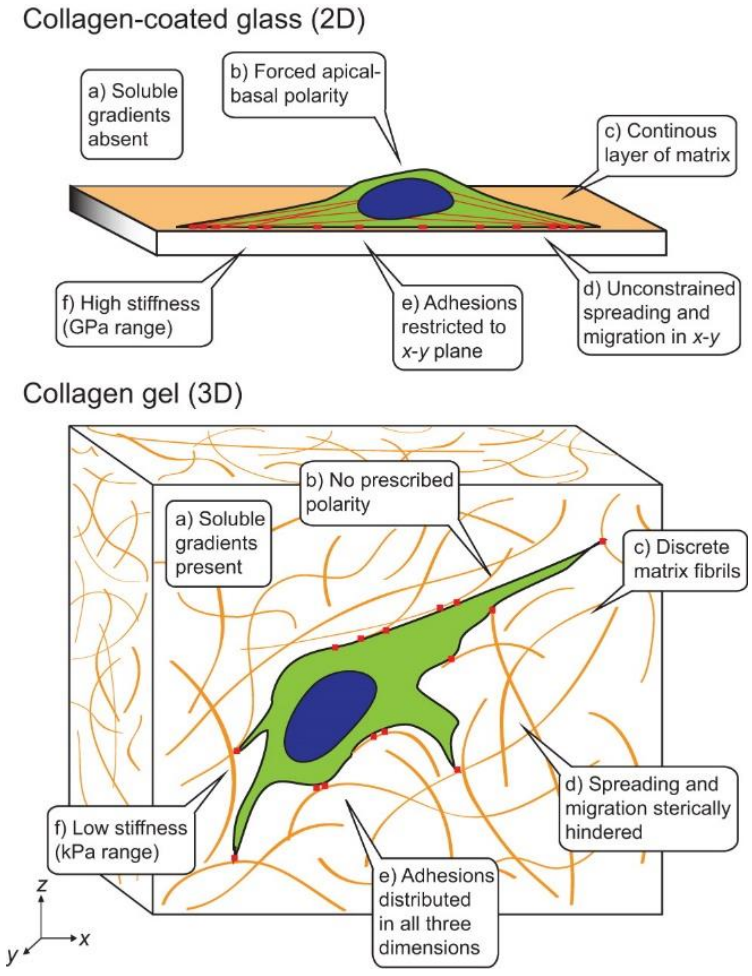

Figure 3 Schematics shows the difference of cells growing in 2D and 3D environment [35].

Not only morphological changes of cells when cultured in 3D environments, signaling transduction and gene expression are also significantly modified by 3D culture systems. For example, when breast carcinoma cells are cultured in 3D environment, the beta 1-integrain antibodies hinders the intracellular signaling transmission from receptors of epidermal growth factor (EGF), and meanwhile, the receptor EGF antibodies are able to inhibit the activity of beta 1-integrain, neither of which are observed when cells are cultured in monolayer [36]. In addition, integrin is known as the media for cells to sense dimensionality and other physical and biochemical properties of ECM, which controls cells to behave in difference according to the environment. During fibroblast cell migration, a non-muscle myosin II-B is required for achieving $\alpha 2\beta 1$ integrin-mediated transport of collagen fibers and subsequent contraction of cells when cultured in 3D collagen environments, but such mechanism is not required for migration on 2D surface [37].

Moreover, in 3D culture system, the delivery of nutrient, oxygen, hormones, effector protein such as growth factor and enzymes, and removal of cellular waste are subjected to complex transport dynamics through diffusion, and hypoxia conditions are usually created at the center of 3D cell spheroids, which is critical for the establishment of tissue scale solute concentration gradient [38, 39]. For example, depending on the action modes of anticancer drugs, various responses are observed when cells are cultured in 2D and 3D environments respectively. The anticancer drug 5-fluorouracil (5-FU) performed higher anti-proliferative effect on monolayer cell culture, whereas tirapazamine (TPZ) becomes more effective in 3D culture due to the effective activation by hypoxia condition. Such results indicate culture environment and cell status, to some extent, will lead to bias results during the testing of drug and other stimulation.

Therefore, it is a necessary task to build up a physiologically relevant system for creating cell and tissue models, not only at the prospective of developing biomaterials that possess similar properties to tissue, but also the exploration of techniques that could be helpful to realize the 3D artificial environments. In this way, the knowledge of cell biology and potential application, especially drug testing and resembling artificial transplantable organs could be conducted with accuracy and efficacy.

1.4 Current status of 3D cell culture

3D culture environments have been applied to culture different types of cells, including carcinoma cells, fibroblast cells, and stem cells, in which obvious cell-type dependent manner is usually observed. Cells have various requirements regarding to the structures, properties and components of the 3D matrix, the addition of nutrients, hormones and growth factors due to the different natural growing environments *in vivo*. Carcinoma cells are growing in similar way that form the spheroid clusters, whereas endothelial and fibroblast cells connect with each other into networks [40, 41]. Stem cells usually have very strict requirements and exhibit different dynamics in response to the variety of environments. For example, intestinal stem cells (ISCs) can only be successfully cultured in protein-rich environments, such as Matrigel. They tend to perform proliferation dynamics when Wnt signaling pathway is dominating but proceed to differentiation function when Notch Signaling pathway is active [42, 43]. Also, special circle or crypt structures are formed when intestinal stem cells are growing in 3D Matrigel matrix that different from others. Therefore, to satisfy the requirements from different types of cells,

it is critical to develop various biomaterials and techniques to create the physiologically relevant 3D matrix.

1.4.1 Materials for 3D cell culture

Materials for constructing 3D culture environment is essential for realizing proper cellular metabolism, because materials are well-known to be able to interact with cells and even regulates the cell behaviors, signaling transduction and gene expression. Hence, in order to create a microenvironment that is more close to physiological condition for 3D cell culture, significant progresses have been achieved in developing biological materials. Traditional materials are solid scaffolds, which are fabricated by a wide range of biocompatible materials including ceramics [44, 45], glass [45, 46], polymer [47, 48] and metal such as titanium [49] and stainless steel [50]. For example, polymers are the most commonly used materials, because the controllability over organic synthetic process enables the tuning of stiffness, elasticity, porosity, and permeability, which benefits the fabricating process of scaffolds with diverse size, structures and properties, as well as facilitates the cellular functions in 3D cell culture applications [51, 52]. Polyethylene (terephtahalate) (PET) has been reported to fabricate a 3D stacked sheets mesh scaffolds that enabled to apply oxygen gradients through layers for studying the mechanism and responses of MDA-MB-231 cells [53]. When cultured porcine aortic endothelial cells (PAEC) on PEG or dextran scaffolds, increased nanoparticles cytotoxicity has been observed in 3D cell culture than 2D [54, 55]. Moreover, ceramics have been mostly applied to the fabrication of replacement parts such as artificial joints, hip or dental parts, in which a high mechanical strength is required [56, 57], but to guarantee the safety of replacement, testing the biocompatibility is necessary. On the other hand, ceramics are usually used as supportive scaffolds for 3D cell culture.

Bone regeneration was reported by seeding bone marrow mesenchymal stem cells and osteoblast cells on ceramic scaffolds [58, 59]. Solid scaffolds have already been applied to wide applications, however, major disadvantages including difficulties in cell imaging and recovering cells from the matrix, and failures to create tissue-like environment for 3D cell culture, limit the further development.

Hydrogel, as the most attractive biomaterial, has been developed significantly and widely applied in recent. The most common type is the polysaccharide-based hydrogel, such as alginate, agarose, and hyaluronic acid. This type of hydrogel usually performs a rapid gelation kinetics that contributes to good mechanical properties, which is advantageous to the construction of scaffolds containing complex design due to the requirements of maintaining the stability of the scaffolds [60, 61]. Vessel-like structures [62], porous constructs [63], and aortic valve conduits [64], for example, have been reported to be fabricated by using polysaccharide-based hydrogel. However, mechanical property is not the only factor critical to the construction of 3D scaffolds for cell culture, the biocompatibility also plays significant roles in managing cell fate [65]. Polysaccharide-based hydrogel is usually criticized for the lack of essential protein components and consequently subjected to the limitations with respect to cellular adhesion and functions that compromise the purpose of mimicking *in vivo* environments [66]. For example, cells growing in agarose were found with spheroid morphology and failed to spread into the spindle-like morphology as observed protein-based hydrogel and *in vivo* situation (Figure 4), which results from the missing of protein component, RGD-containing peptide, and the absence of bioactive cell attachment ligands with the polysaccharide-based hydrogel [66].

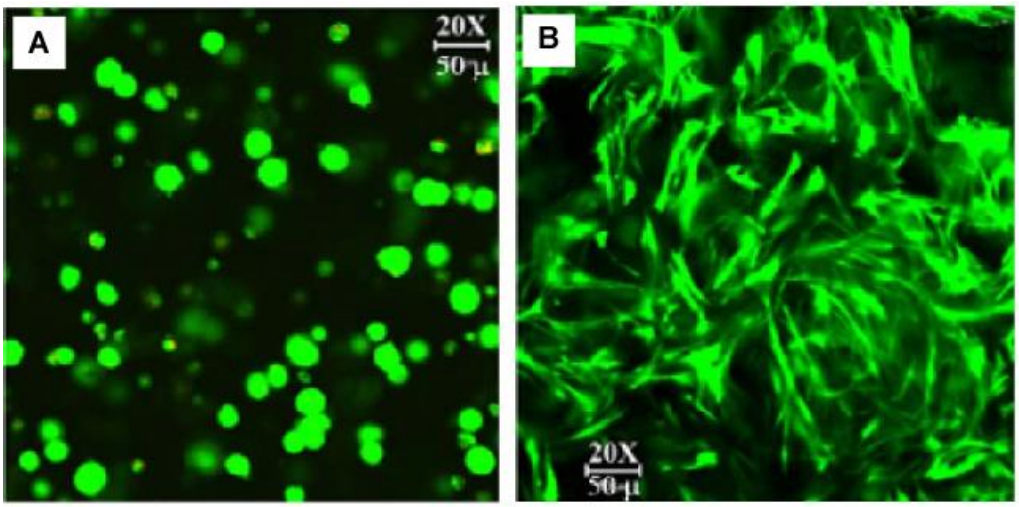

Figure 4 Confocal imaging of cell morphology change in different scaffold materials. Cells are stained by Live/Dead fluorescent assays. Cells display (A) spherical morphology in alginate and (B) spindle-like morphology in gelatin after 7 days culture [66].

Protein-based hydrogel, such as collagen, gelatin and Matrigel, contains a comprehensive recipe of growth factors and peptides, and therefore can facilitate cell growth and adhesion in 3D matrix (Figure 4B) [54, 67]. Recently, collagen has been proved to be beneficial to the 3D cell culture and effective to simulate cellular *in vivo* behaviors. Collagen scaffolds were found to enhance the cell proliferation and significantly increase the expression of pro-angiogenic growth factors and the transcription of matrix metalloproteinases (MMPs) when MCF-7 breast cancer cells were cultured in 3D collagen matrix [68]. Human embryonic stem cells (hESCs) and human induced pluripotent stem cells (hiPSCs) were co-cultured with Swiss 3T3 cells in collagen type I scaffold to mimic the hepatic maturation, and found the gene expression levels of hepatocytes-related markers such as P450 enzymes and conjugating enzymes, and the albumin secretion in hEHs or hiPHs were significantly up-regulated by 3D collagen matrix comparing to 2D culture environment [69]. On the other hand, Matrigel was found to enable a long-term culture for intestinal stem cells [6]. Intestinal crypt and organoid were successfully cultured

and maintained by using 3D Matrigel scaffold [70]. In addition, a hepatocytes-like polarized system was demonstrated by a Matrigel-embedded 3D culture of human hepatocytes-derived cell line (Huh-7 cells), in which a continuous networks of functional proto-bile canaliculi structures was successfully formed [71]. Even though protein-based hydrogel exhibits outstanding performance in improving 3D cell culture, most of them exhibit poor mechanical properties that would cause problems during the construction of complex structures [72].

Synthetic hydrogel such as PEG and PEGDA provides advantages of tailorable physical properties through the controllable synthetic process to suit particular applications [73]. For example, the using of PGM4/PEG-4Mal hydrogel enabled highly cyto-compatible gelation in a spatiotemporally controlled manner, while controlling gel stiffness via appropriate light dose during the fabrication of 3D scaffold for cell culture [54]. A thermo-responsive hyper-branched PEG-based copolymer (PEGMEMA-MEO_2MA-PEGDA) with multiple acrylate functional groups in combination with thiolated HA was synthesized for 3D stem cell culture, which possess desired mechanical properties and gelation kinetics [74]. The synthetic hydrogel enables novel applications through modifying physical properties, but it usually has disadvantages including poor biocompatibility, degradation, toxic degradation products, and loss of mechanical properties [73].

1.4.2 Techniques for 3D cell culture

1.4.2.1 Scaffold-free technique

In addition to the development of biological materials, a variety of techniques has been explored as well aiming to apply a more controllable manipulation over 3D cell culture and

create a more physiologically relevant environment for long term culture. Scaffold-free approach, which does not contain biomaterials and ECM, has been widely applied to 3D cell culture due to its simplicity and homogeneity of the cultured spheroids [75, 76]. Cells growing in the platform can generate and organize their own 3D ECM, and therefore the cell spheroids formed in such platform are believe to closely resemble *in vivo* tissues [75, 76]. Hanging drop plate is a good example of scaffold-free approach [27, 77]. In particular, there is no supportive structure or porosity. The platform containing a hanging drop culture plate, in which the cell suspension could be hung, and a water reservoir around the plate (Figure 5). Because there is no bottom substrate for cell attachment, so cells in suspension would aggregate into spheroid during the culture. The overall size of spheroid could achieve 500-600 μm in diameter, however, a central necrosis may be caused due to the insufficient diffusion of nutrient and oxygen. It has been reported that 384 hanging drop array plate enabled high-throughput capabilities and significant improvements of spheroid culture over existing 3D cell culture method [77]. Well-controlled manipulation, homogeneous size, and uniform structures of monkey kidney fibroblast cell (COS7), murine embryonic stem cell (ES-D3), and human epithelial carcinoma cell spheroids were achieved at high throughput, which provided accurate, controllable, reliable, and efficient method for the 5-fluorouracil (5-FU) and tirapazamine (TPZ) anti-cancer drug testing [27].

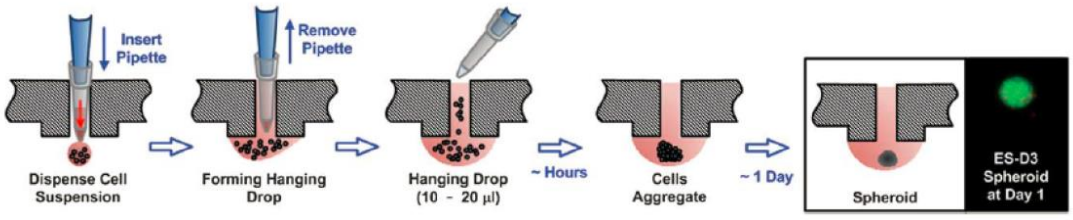

Figure 5 Schematics of 384 hanging drop technique for Murine embryonic stem cell (ES-D3) spheroid culture [27].

1.4.2.2 Bulk hydrogel technique

To well mimic the *in vivo* ECM of the specific tissue being modeled, the materials with different porosities, permeability, and mechanical characteristics are used to construct the 3D scaffold. Hydrogel as the most qualified candidate has been widely applied for 3D cell culture [65, 78], which turns the bulk hydrogel technique into a popular conventional method due to the simple operation and effectiveness for growing cells. Particularly, cells usually are dispersed to the bulk aqueous hydrogel and then gel through manipulation of chemical, thermal, or UV crosslinking mechanism in container, after which cells would be encapsulated into the 3D hydrogel matrix (Figure 6) [79]. It has been proved bulk hydrogel could grow cells into clusters or spheroids and could be maintained for about one week with desired viability [80]. Cells were mostly growing better in protein-based hydrogel, especially Matrigel, in which cells could spread into spindle-like morphology [71], whereas spherical morphology was presented when cultured in polysaccharide-based hydrogel [66, 81]. Moreover, bulk hydrogel technique can be effective to investigate the influence of matrix stiffness due to the simplicity and repeatability [65], and it does not cause any concern with the mechanical properties of protein-based hydrogel because of the simple structure. With respect to the sustained culture, however, bulk hydrogel has challenges with the delivery of nutrient and oxygen. Because the limitation of the diffusion is only 150-200 μm in hydrogel [82], whereas the dimension of scaffold is usually much larger than the threshold, which usually caused the problem of sustained cell culture and resulted in cell necrosis and death at early stage. In addition, bulk hydrogel system has problem with representing physiological factors, such as cell patterning, zonation and structure design.

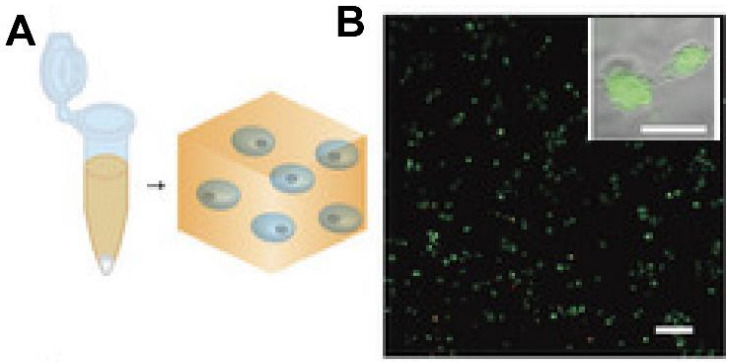

Figure 6 Schematics of bulk hydrogel technique. (A) Concepts of 3D cell culture in bulk hydrogel environment. (B) Fluorescent image of cells cultured in 3D bulk hydrogel scaffold (scale bar: 100 μm, inset: 10 μm) [83].

1.4.2.3 Microfluidic technique

Recent advances in microfluidics have yielded unprecedented control over the construction of physiologically relevant environments, and have significantly improved the controllability, feasibility and sustainability of 3D cell culture [84-86]. First of all, microfluidics enables cell encapsulation into micrometer diameter hydrogel particles which provides a well-controlled, physically isolated microenvironment for studying cellular mechanism in 3D matrix (Figure 7A) [25, 87]. By simple manipulation over the double-phases fluids, cells can be encapsulated into uniform size of drops at ultra-high throughput [88], which serves as thousands of homogeneous micro-bioreactors (Figure 7B). The encapsulation efficiency can be obtained over 98.5% [88]. Moreover, it is also possible to control the number of cells being encapsulated into each drop [89]. Method of encapsulating exact one cell per droplet was reported with the efficiency over 96%, which will be helpful to study single cell response to the 3D hydrogel matrix. Encapsulation of multi-cells or even multi-type of cells into each droplets were developed that is advantageous to investigate the intercellular communication and influence on each other [90]. In addition, microparticles can be produced into different morphology through using

microfluidics coupled with stop-flow lithography techniques [91]. Cells were successfully encapsulated and cultured in hydrogel particles with different morphologies, such as rectangular and triangle, and hence provide a useful approach to study the effect of geometrical factors of hydrogel matrix on cell homeostasis as well as mimic the *in vivo* geometry.

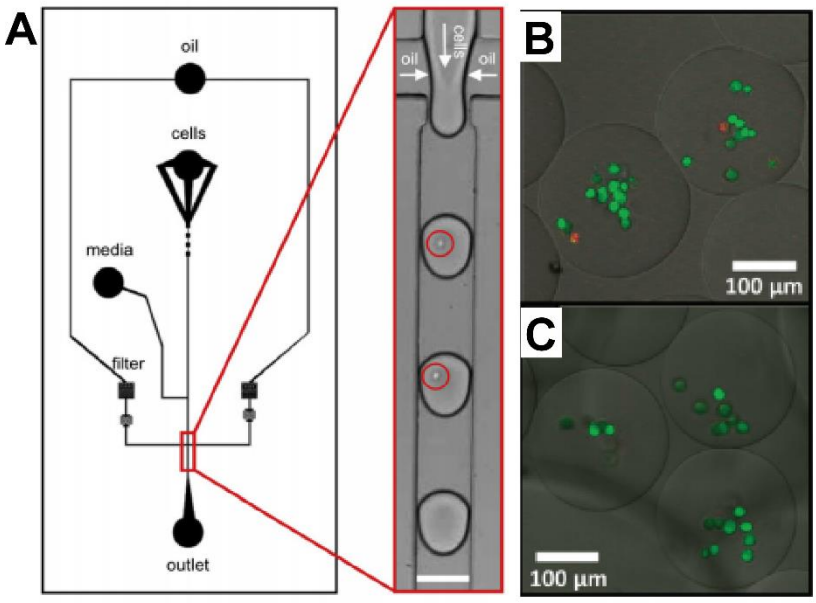

Figure 7 Microfluidic technique for 3D cell culture in microparticles. (A) Schematics of microfluidic encapsulation of cells in microparticles (Scale bar: 100 µm) [92]. (B) Fluorescent image of viable fibroblast encapsulated in PEG microgel particles [93].

Secondly, microfluidics possesses the significant advantage of manipulating fluids, which can be used to construct nutrient delivering systems that favors sustained cell culture, as well as investigate the effect of extra stimulation, such as concentration gradient [94-96] and shear stress [97, 98] that mimics the physiological factors (Figure 8). For example, microwell has been fabricated in microchannel that could trap the cells flowing in suspension [99]. Culture medium flowing through the microchannel could supply nutrient

to the cells growing in the microwell that supports the cell growth and development of clusters and spheroids. Uniform COS-7, HepG2 and

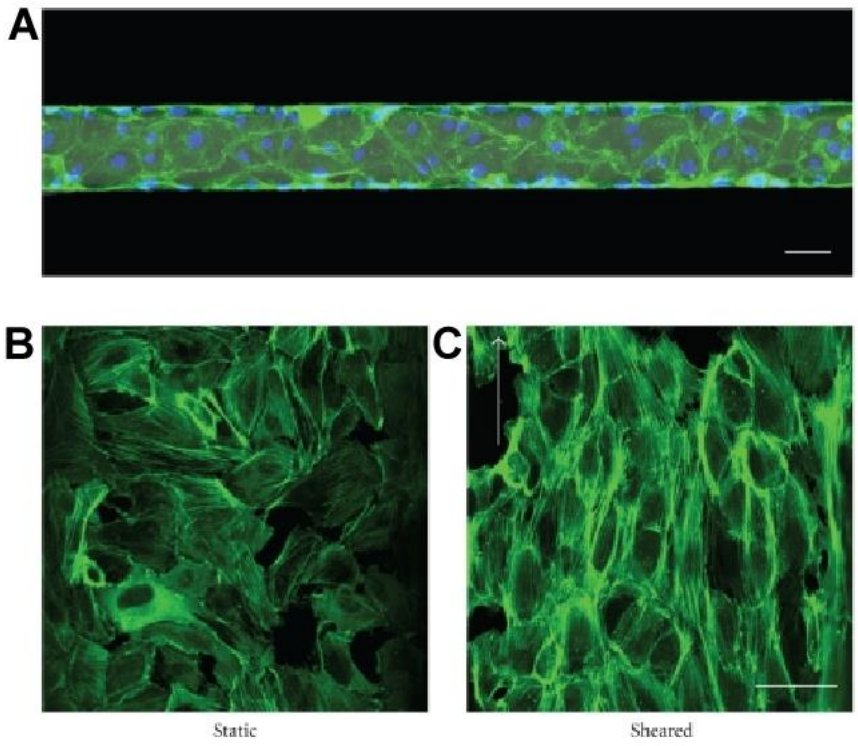

Figure 8 Endothelial cells growing in microfluidic channel. Cells are stained with actin-green and nuclei-blue fluorescent dye. (A) Endothelial cells are cultured in microchannel. Scale bar: 50 μm. (B) The change of endothelial cell morphology when subject to static and shear condition respectively scale bar: 50 μm [100].

MCF-7 cell spheroid were obtained from 3D cell culture and achieved average diameters of 80, 200, and 150 μm [84, 101] respectively after 3 days. HT-29 cells grew into spheroid and kept high viability for 12 days [95], indicating the perfusion of culture medium through microchannel is favorable to achieve sustained 3D cell culture that not only can supply fresh nutrients but also remove the cellular waste from the culture environment. On the other hand, cells could be cultured in gradient environments by using microfluidics, in which cells in hydrogel were cultured in central microchannel, whereas drug solution at

different concentration are introduced from adjacent side channel [102]. HepG2 spheroids, for example, were cultured in gradient concentration of rifampicin for 48 and 96 hours for testing the toxicity of rifampicin to cells [94]. HT-29 spheroids were cultured for 12 days and test the toxicity of 5-fluorouracil under gradient concentration range of 0.125-1 mM [94]. Clear dose-dependent manner was observed for the drug testing studies in microfluidic platform, which indicates the microfluidics can be effective techniques for both of the sustained 3D cell culture and the application of extra stimulation. Such system could also be developed to realize cellular communication by simply connecting different microfluidic scaffolds through tubing, in which cellular metabolites will be transported via the flow and start to communicate and influence the cell metabolism at downstream. This is significant useful for building the liver-on-chip models, which involves the interaction and cooperation between multi types of cells to achieve the function of drug detoxification (Figure 9).

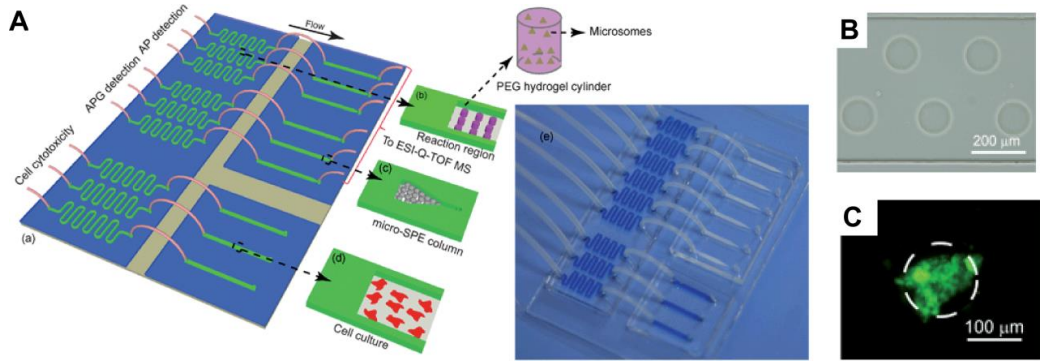

Figure 9 Concepts of using microfluidic device for 3D cell culture, metabolite analysis and cytotoxicity assay. (A) The integrated microfluidic device enables co-culturing for drug detoxification. (B) Controlled encapsulation of HLMs inside hydrogel microstructures. (C) Fluorescence image of HLMs entrapped inside PEG hydrogel microstructures. The edge of the microstructure was labeled with dash lines [103].

1.4.2.4 3D bio-printing technique

3D bio-printing, as an outstanding alternatives, has rapidly evolved as a “bottom-up” approach to fabricate complex biological constructs for 3D cell and tissue culture. It is able to apply additional factors, such as materials, cell types, growth and differentiation factors and print the 3D construct with extraordinary spatial control at high resolution through a layer-by-layer process (Figure 10A) [104]. Functional skin and cartilage, for example, have been fabricated using inkjet printing techniques where controlled deposition of cell-containing aqueous droplets on a substrate is used[105, 106]. Laser-assisted printing, a nozzle-free technique that deposits droplets using focused laser pulses, enables high resolution printing (30-100 μm) of cell-containing constructs. This technique has been used to fabricate cellularized skin constructs [107]. Microextrusion, on the other hand, extrudes continuous viscous bio-ink (up to 6×10^7 mPa/s) on substrates with a wide range of spatial resolutions (5 μm to millimeters) and hence can fabricate tissue structures with complex geometries such as aortic valves [64], branched vascular systems [108] and tumor models [109].

Additionally, many vascular system has been demonstrated by using 3D bioprinting techniques. A rapid prototyping bioprinting method for scaffold-free small diameter vascular reconstruction, for example, has been demonstrated for the fabrication of single- and double-layered small diameter vascular tube (OD ranging from 0.9 to 2.5 mm) [108]. Vascularized cell-laden tissue constructs have also been fabricated by 3D printing a fugitive ink (Pluronic F127) in cell-containing gelatin methacrylate hydrogel (Figure 10B) [110]. Furthermore, 3D printed filament networks of carbohydrate glass [55] and agarose template fibers [111] have been used as cyto-compatible sacrificial templates to generate

vascular network in engineered tissue, where improved mass transport, cellular viability and differentiation within the cell-laden tissue constructs have been observed (Figure 10C). Therefore, 3D printing techniques are believed to be able to open new exciting opportunities to generate more physiologically relevant constructs, and may also achieve next milestone towards the construction of artificial organs such as bone (Figure 10D).

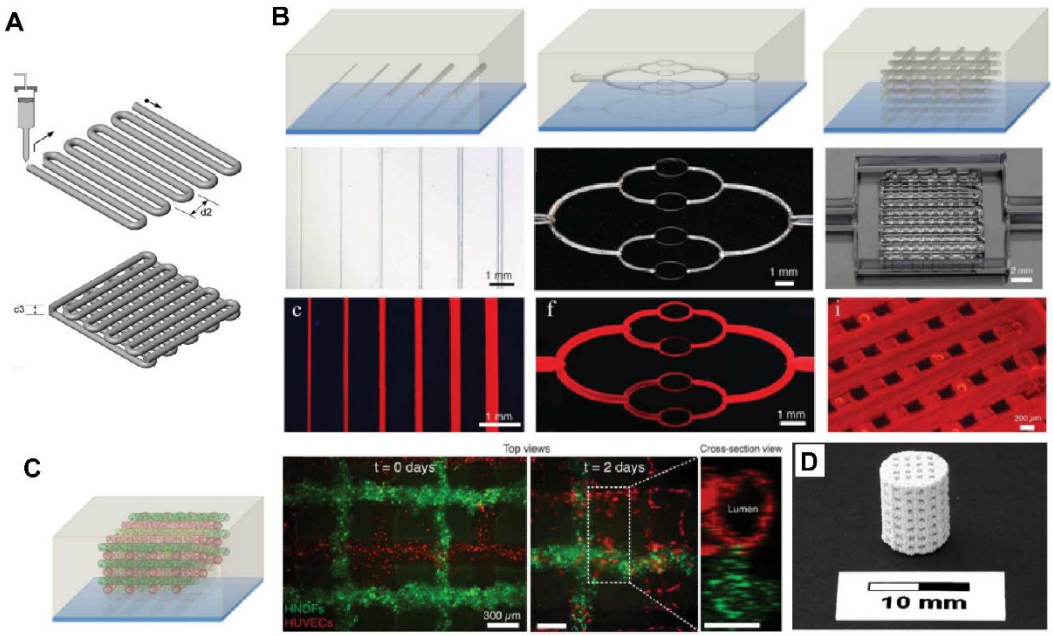

Figure 10 Concepts of 3D printing techniques to construct scaffold for 3D cell culture. (A) Schematic of 3D printing process [112]. (B) Schematic illustrations, optical images, and fluorescent images of the vascular networks printed in hydrogel construct [110]. (C) Fluorescent images of the engineered vascular networks lined with TFP HUVECs (red) and GFP Human neonatal dermal fibroblast (HNDF)-laden GelMA ink (green) [110]. (D) 3D printed bone structures [113].

1.5 Application of 3D cell culture

3D cell culture attracts increasing attention because it can realize cell dynamics and tissue organization that is impossible to achieve in conventional 2D system. 3D culture technique not only contributes to the understanding of fundamental knowledge of cell biology, but

also creates effective platforms for accomplishing wide range of applications in the field of biomedical engineering, tissue engineering and drug discovery.

1.5.1 Construction for tissue model system

Tissue model system, for example, is a 3D biological structure formed by single cells in physiological environment that can represent basic biological functions. Such model can be potential to be constructed through 3D cell culture technique. To be specifically, it has been found that 3D hydrogel matrix supports cells to grow into clusters and then develop into spheroid, which is self-assembled spherical clusters of cell colonies [23, 114]. 3D spheroids can closely resemble *in vivo* tissue that effectively realize cellular communication and the development of extracellular matrix. It enables the improvement of models for cell migration, differentiation, survival and growth, as well as providing accurate depiction of cell polarization [23, 114]. With inherent metabolic, such as oxygen, carbon dioxide, nutrients, and waste, and proliferative gradients, spheroids are becoming excellent model systems to mimic solid tissues, vascular tumors, embryoid bodies, and contribute to the applications in tumor therapy and stem cell research (Figure 11) [23, 114].

For instance, previous studies have developed approaches to grow cell spheroid with defined structure and size at a large production by 3D culturing different types of cells, such as embryonic stem cells [115], carcinoma cells [95, 116], and fibroblast cells [117]. Cell spheroid composed of multi-type of cells has been accomplished by co-culturing, such as HepG2 and fibroblasts [94, 117], MDA-MB-23 breast cancer cells and NIH/3T3 fibroblasts [118]. Manipulation over spheroid development are reported either by using 3D matrix with defined geometry [119, 120] or taking advantages of microfluidics [96, 121, 122]. By using the current techniques, spheroid cultures can be prolonged from 5 to 45

days with cell viability over 90% [84, 123]. It should be noted that it is not necessary to grow the spheroid with extremely long duration, but reaching critical size (e.g., 500 μm) that could represents the features of tissue will be desirable for biological testing. However, relative long term culture of cells is the pre-requisite for growing the size of spheroid and realizing the cell dynamics, therefore, approaches to extend the culture duration with high cell viability become popular for the investigation on tissue function, formation and tumor growth.

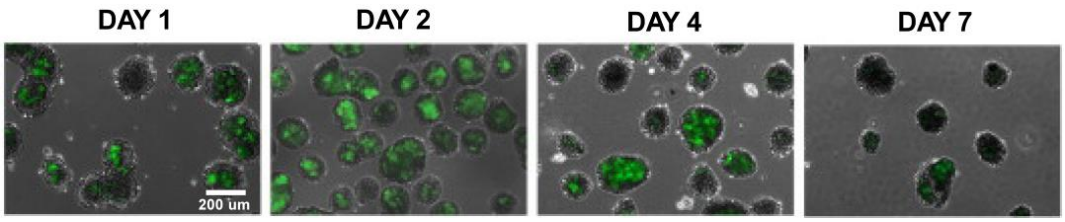

Figure 11 Human mesenchymal stem cell (MSC) spheroid culture in gelatin MPs for 7 days in PDMS microwells [124].

1.5.2 Construction for drug testing

3D cell culture can be particular attractive to drug testing and screening. Investigation of cell-drug interactions is crucial for validating and screening potential drug candidates, which pose significant challenges to develop efficient, robust, and high-throughput instrumentations for pharmacological applications [125, 126]. Current therapeutic strategies mostly rely on *in vivo* animal test which has been drawing serious concerns with biological relevance to human and ethical reasons [122, 123]. Therefore, 3D cell culture based assays can be developed as *in vitro* models to fill the gap between molecular level drug discovery and animal test, in which the drug-induced impact on cell proliferation, apoptosis and migration can be readily studied simultaneously while achieving higher throughput [17, 28, 127].

Cellular behaviors and responses to extracellular stimulation in 3D culture environment are reported to be different from 2D traditional method, and 3D matrix is more effective to realize cellular function due to the similarity to *in vivo* situation, such as cell spreading, migration, and differentiation [65, 114, 128], so the 3D cell culture platform is believed to provide a more accurate results and convenient method. Previous studies have developed several systems to investigate the drug testing, screening and delivery. HT-29 colon carcinoma cell cultured in 3D matrix, for example, has been used to test the anti-cancer drugs, 5-Fluorouracil (5-FU), and found spheroid was more resistant to drug than regular 3D cell culture, and higher dose of drug induced stronger resistance [95]. A549 lung adenocarcinoma cell spheroid was treated by twelve drugs to investigate the inhibition of signal transduction regarding to epithelial-mesenchymal transition (EMT), which is a critical process of switching carcinoma to metastatic tumors [129].

1.5.3 Construction for artificial organ

In addition, 3D cell culture is the fundamental technique but a critical step towards the future development of organ-on-chip and even the construction of transplantable artificial organs [30]. Because cell culture in 3D scaffolds resemble and simulate various functions of real tissue, and it would be possible to grow artificial functional organs *in vitro* if physiological requirements can be satisfied, such as vascular transportation, cell-cell interaction, and structural guidance [30, 130]. Organ-on-chip or even human-on-chip has become increasing popular because it could be the milestones of achieving artificial organ and provide not only the biological relevance but also the requisite high-throughput applications (Figure 12) [30, 130].

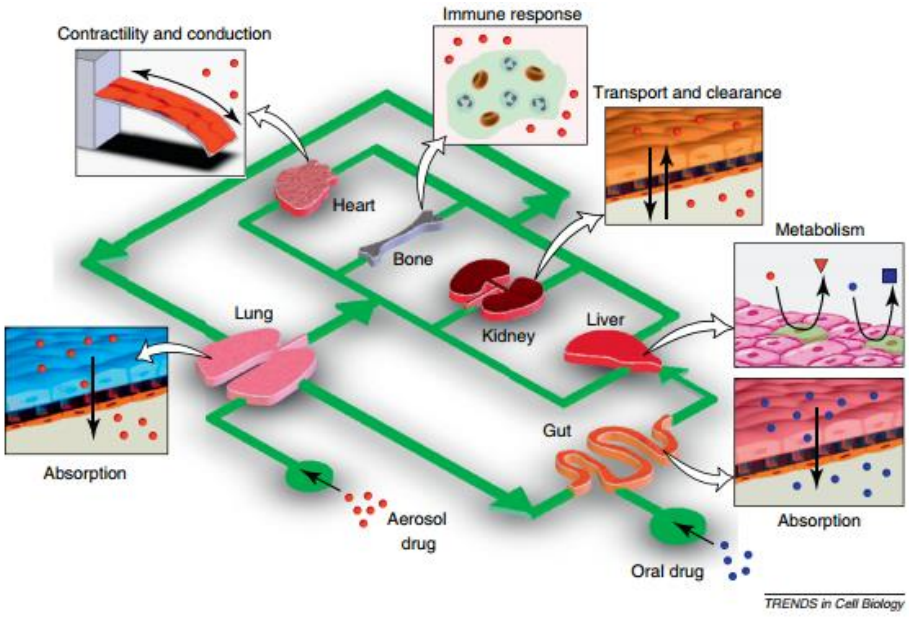

Figure 12 Concepts of integrated organ-on-a-chip technology by applying microfluidic circulatory system in a physiologically relevant manner [30].

Liver-on-chip, for example, possesses 3D features and achieves co-culturing of multiple types of cells such as Kupffer cells and stellate cells that ensures proper functionality [131]. In order to simulate human liver, liver-on-chip should also enable a gradient zone of oxygen and the unique morphology of liver lobules [132], which performs a cylindrical shape and composes of a hypatocytes core in the middle with cord-like shape, non-parenchymal cells at surrounding, and a tiny network of capillaries (Figure 13A) [132-134]. Previous studies demonstrated the experimental approach for arrangement of cells in order to construct the unique morphology of liver. Dielectrophoretic (DEP) force was used to direct cell movement in desired directions by applying electric field for cell patterning [135, 136]. To be specifically, to arrange the cell pattern, hepatocytes suspension was first flowed into microchannel with collagen treatment that enhanced cell adhesion, and pushed by positive DEP forces toward the assembly gap in the middle and trapped on the surface to resemble the hepatocytes core in liver lobule (Figure 13B). Endothelial cell suspension

was then flushed into microchannel to surround the hepatocytes by applying the same manipulation. Both the simulation and experimental results showed successful trapping of two types of cells as well as the desired sinusoidal arrangement (Figure 13C). On the other hand, by using similar approach, radial non-parenchymal cells arrangement of human umbilical vein endothelial cells (HUVECs) into sinusoidal morphology on a so-called lobule-mimetic-stellate-electrode array was developed [64].

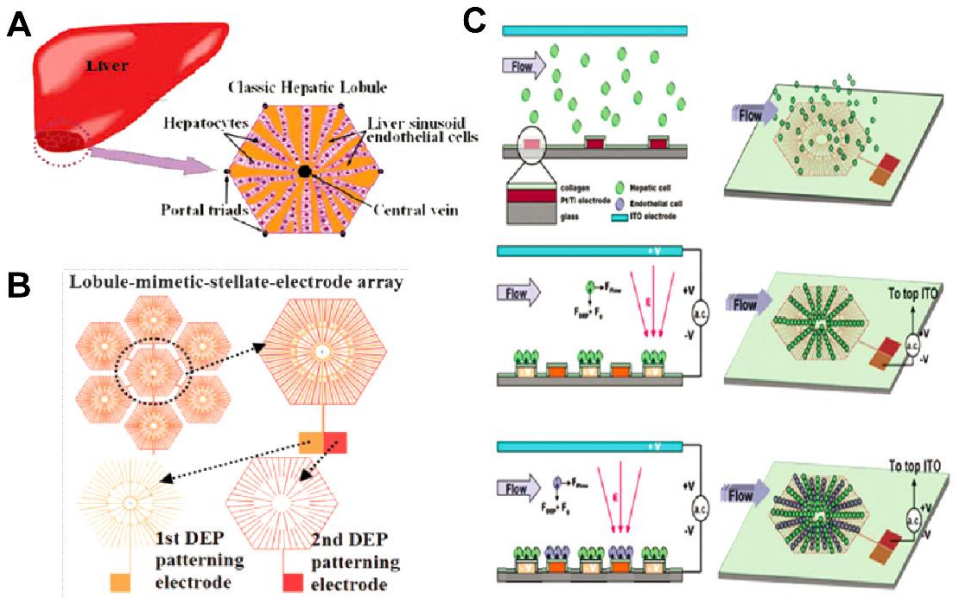

Figure 13 Concept of liver-on-a-chip. (A) Illustration of the basic unit of liver tissue, the classic hepatic lobule. (B) The lobule-mimetic-stellate-electrodes array. (C) The configuration and operation principles of DEP-based heterogeneous lobule-mimetic cell patterning [58].

In addition, co-culturing of hepatocytes spheroids and hepatic stellate cells (HSCs) was achieved in a 3D liver-on-chip device. Because HSCs play crucial roles in producing hepatocytes growth factor [137] and liver regeneration [131, 138], these two types of cells were cultured in two microchamber respectively and connected by microchannel, which facilitated the interaction between cells by releasing and receiving metabolites through continuous flow [131]. Results showed that the co-culture system improved the albumin and urea secretion rates of hepatocytes spheroid after 9 days comparing to mono-cultured

system, indicating the designed liver-on-chip co-culture system is potential to realize the physiological function of livers.

Moreover, liver-on-chip composed of co-culture system has already been applied to test the functionality of drug detoxicity [129]. Human liver microsomes (HLMs) were encapsulated in hydrogel and cultured in upstream microchamber, whereas hepatic HepG2 cells were cultured in downstream chamber [103]. Acetaminophen (AP), the most common cause of liver disease, was used as drug to introduce into co-cultured system, and could be detoxified by Uridine 5'-diphosphate-glucuronosyltransferase (UGT) of HLMs. It was found that the co-cultured system improved the viability of HepG2 cells by more than 20%, due to the detoxifying function of HLMs, providing potential insights to mimic the liver function and knowledge for construction of artificial liver. Furthermore, construction of artificial skin [139], cardiac tissue [140], aortic heart valve [64], and bone [141] has been reported by seeding cells to pre-constructed supportive scaffolds composed of artificial materials such as hydrogel and ceramics.

1.6 Current challenges in 3D cell culture

As discussed in previous section, breakthrough progresses and momentous milestones have been achieved in these years [17, 142], however, several critical issues still remained challenging. For example, most of the 3D matrix constructed could not satisfy the *in vivo* structural or functional requirements, which renders the scaffolds lack of the realization of some critical factors, such as structural guidance of stem cell differentiation, cell-matrix interaction, and promotion of cell spreading and migration [17, 30, 142].

On the other hand, the construction of vascular architectures capable of distributing oxygen and nutrients is critically important for 3D sustained cell culture, tissue engineering, and the culture of functional organ [143, 144]. Building blood vessel-like vascular system in 3D biological matrix for nutrient delivery, however, is difficult. So far, controlled fabrication of complex, hierarchical microvascular networks, such as the degree of branching, capillary density, and connecting microvascular networks with large vascular vessels is still poorly solved.

In addition, other problems like realizing the culture multi-type of cells and cell-cell interactions, guiding stem cell differentiate into multi-type of matured cells, and cell arrangement have not been well-solved yet [14, 30, 78]. Without solving these critical challenges, fully understanding cell dynamics and disease model *in vivo* as well as stepping toward the construction of artificial transplantable organs would be impossible.

1.6.1 Construction of physiologically relevant scaffolds

3D scaffolds that enable mimicking physiological characters are attractive, but difficult to be constructed yet. Encapsulation of cells in hydrogel microparticles, for example, could provide isolated environments for studying the cell growth, differentiation, survival in 3D matrix, and the co-culture of multi-type of cells in the microparticles indeed provides good platforms to investigate cellular influence and communication with each other, which can be used to understand the tumor model [145]. However, due to size limitation and the lack of critical factors, such as nutrient delivery and oxygen gradient, it would be insufficient to grow tumor into physiological size and structures [75, 146].

Spheroid culture in microwell by using microfluidic system, on the other hand, brings new insights for combining 3D cell culture with nutrient perfusion in a smart

manipulation, which is potential to accomplish sustained cell culture and achieve a high throughput analysis with large production of cell spheroid [99]. But cell culture in microwell would be challenged to mimic the physiological 3D environments, especially the construction of tissue structures and arranging multi-type of cells into specific pattern.

3D printing technique combines the applicability of wide range of biological materials with the extraordinary spatial control and high constructing resolution. 3D Printing of bone tissues and liver-inspired detoxification device were reported to mimic the function of bone [141] and live lobule [73, 147] respectively. Several constructs including functional skin [105], cartilage [106], and aortic valves [64] have been achieved to mimic the *in vivo* tissue structures.

These studies indeed provided a prototype for constructing tissue or organ-mimicking structures at a relative large scale, the resolution of unique structures, development of zonation, application of gradient factors, and possible flow effect, however, are still challenged to be realized in the model, which could potentially cause the failure of obtaining functional and structural guidance of cell migration, patterning, and differentiation, as well as the cellular responses to the extracellular stimulations.

1.6.2 Construction of vascular networks

Fabrication of blood vessel-like artificial microvascular networks in 3D physiologically relevant construct, which can ensure the delivery of sufficient nutrients and oxygen to the cells cultured in the 3D matrix that supports a sustained cell culture, is challenging. In particular, effective vascularization in engineered tissues is critical to the development of living organs and remains one of the highest priorities in tissue engineering [143, 148, 149]. Without a vascular network, for example, the maximal thickness of an engineered tissue is

approximately 150-200 μm due to the limited oxygen diffusion [150]. As a result, large 3D engineered tissue constructs quickly develop necrotic regions [151]. Thus, an effective transport system including both large vascular vessels and microvascular networks is required to sustain the biomimetic functions of thick, complex tissue constructs. To date, tissue engineered large and small blood vessels have been demonstrated by using porous scaffolds [152] and cell sheet technology [53]. However, controlled formation of complex, hierarchical microvascular networks, such as the degree of branching, capillary density, and connecting microvascular networks with large vascular vessels is challenging.

Recent advances in micro-fabrication technology have enabled the generation of microvascular networks in tissue constructs. Microfluidic-based systems, for example, have been developed to control the fabrication of vascularized patterns in a variety of bio-substrates where endothelial cells can be seeded and form monolayers [153]. To be specifically, the development of biodegradable microfluidics and 3D vascularized microfluidic scaffolds [154, 155] highlights the potentially implantable 3D microfluidic tissue constructs. 3D bioprinting, on the other hand, is essentially a microfluidic technology and has been emerged rapidly as an effective bottom-up approach to fabricate vascularized 3D tissue constructs (Figure 14A) [156, 157]. A rapid prototyping bioprinting method for scaffold-free small diameter vascular reconstruction has been demonstrated for the fabrication of single- and double-layered small diameter vascular tubes (OD ranging from 0.9 to 2.5 mm) (Figure 14B) [108]. Vascularized cell-laden tissue constructs have also been fabricated by 3D printing a fugitive ink (Pluronic F127) in cell-containing gelatin methacrylate hydrogels [158]. Furthermore, 3D printed filament networks of carbohydrate glass [159] and agarose template fibers [111] have been used as cytocompatible sacrificial

templates to generate vascular networks in engineered tissues. Improved mass transport, cell viability and differentiation within the cell-laden tissue constructs have been observed. Formations of microvascular architectures using methods such as direct writing (Figure 14C) [160] and electrical discharge [161, 162] have also been demonstrated. In addition, studies using micropatterning and microfluidics have been investigated to fabricate vascularized hydrogel for 3D cell culture, such as grid networks and hollow hydrogel fibers [159] [163]. The majority of the studies, however, failed to demonstrate the rationale of the construction of hierarchical networks that enables to mimic the blood vascular system, e.g., how the diameter of the channel and the degree of branching change with hierarchical levels, in order to maintain the maximum flow efficiency in the network. This is particularly of interest when maximum flow efficiency for material delivery at a given input pressure or flow rate is required or becomes a concern. Most importantly, establishments of artificial vascular networks into physiologically relevant 3D construct are still less reported.

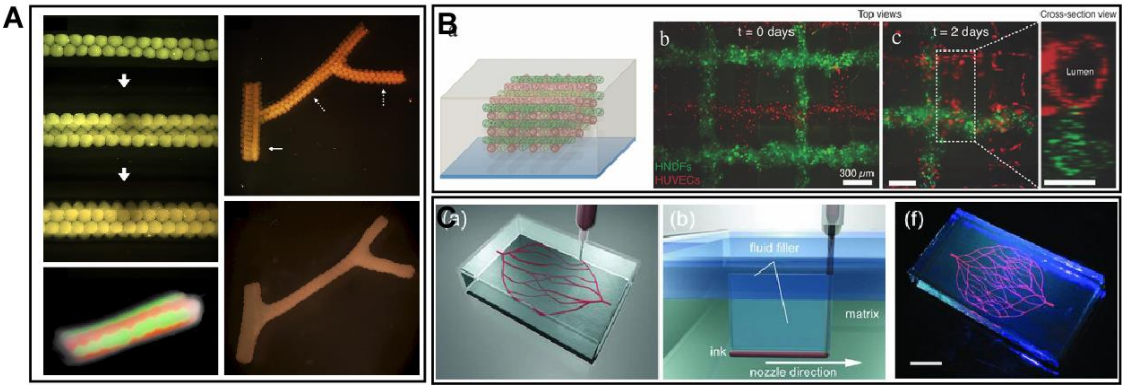

Figure 14 Construction of vascular structures realized by (A) scaffold-free 3D bio-printing [102], (B) microfluidics-based bio-printing [100] and (C) direct writing (scale bar: 10 mm) [164].

1.6.3 Realization of *in vivo*-like cellular communication

Realization of the cellular communication between cell and cell or cell and matrix in an appropriate manner is critical but difficult. It has been well-known cell growth, migration, differentiation, and survival are under the influence of other cells and surrounding environments [165, 166]. To realize specific functions, such as detoxification of hepatic cells and development of crypts, cellular interactions and matrix guidance are required. For example, Hepatic stellate cell (HSC) is a type of non-parenchymal cells presenting about 5-8% of total cells in human liver [167], which plays crucial roles in hepatocytes growth factor [131] and liver regeneration [167], [168]. Co-culture of HSCs and hepatocytes showed that with the support of growth factor secreted from HSCs, viability of hepatocytes increased significantly and surface of spheroid becomes smoother [169]. The arrangement of cells into *in vivo*-like pattern, however, was still not realized, even though cellular communication was achieved. On the other hand, it was reported that only when human liver microsomes (HLMs) were presented in the cultured environment, the detoxifying functions can be realized and protect the HepG2 cells from death, indicating the growth of liver tissues and obtain of tissue function require cellular cooperation and communications [103], but the pattern of lobule that enables function such as zonation and oxygen gradients has not be developed. Therefore, even though several techniques have been proposed to study the cell-cell interaction and communication, desirable methods that can pattern multi-type of cells into complex physiologically relevant structures with high resolution and ensure the proper cellular communication and functions have not been well demonstrated.

1.7 Research motivation

Significant advances have been achieved in 3D cell culture and provides fundamental knowledge of cell mechanism at both cellular behavioral and molecular level that are advantageous for the application of tissue model construction, transplantable organ resembling, and drug discovery. Current 3D culture systems, however, could not fully represent the physiological features at either structural or functional aspects, which could refer to the missing of several critical factors, such as vascular delivering system, gradient effect, and fluidic shear stress, or the failure of providing *in vivo*-like environment by using the constructed 3D system. As a results, the cell dynamics in such 3D culture system cannot perform as it presents in physiological condition, and therefore would not be able to provide a sufficient scaffold for growing artificial transplantable organ, or exhibit reliable results for disease model testing and drug screening.

In this dissertation, several researches are presented aiming to make the contributions toward the development of artificial organ. In particular, the objective of this dissertation is constructing 3D biological *in vitro* toolbox that could mimic the physiological conditions for investigating cell dynamics in 3D environments. Microfluidics and 3D printing techniques are employed to create physiologically relevant systems, in which several various critical biological factors could be addressed, including 3D physical-isolated microenvironment, extracellular matrix, cell-matrix interaction, cell-cell communication, gradient zone, fluid shear stress, vascular structures for nutrient delivery, circulatory microenvironment, colon shape-like tubular structures and Salmonella interactions. In these developed systems, cancer cell dynamics in either solid or liquid 3D environments has been elucidated and different biological features of cells, such as cell

proliferation, cell survival, cell aggregation, formation of spheroid, cell-Salmonella interaction, and gene expression are investigated. Moreover, the mechanism of cell metastasis and cell sensitivity to inflammatory factors have been studied through using the developed 3D system, which provides potential application for therapeutically method of cancer and drug testing.

1.8 Dissertation overview

The dissertation presents the experimental design, theoretical development, manufacture, characterization and implementation of the 3D culture systems that are constructed by either microfluidics or 3D printing techniques for investigating cell dynamics.

Chapter 1 introduces the background of cell culture in 2D conventional method and recent developments of 3D system with the review on the advantages and disadvantages respectively. The State-of-the-art and current challenges remaining in the field of cell biology are presented based on the literature review. Chapter 1 also includes the motivation behind the research and the proposed microfluidic and 3D printing methods for studying cell dynamics in 3D culture environment.

Chapter 2 presents a study about using microfluidic approach to encapsulate HCT116 colon epithelial cells into hydrogel particles that could mimic the physiological environment of tumor model. The advantage of this study could be the realization of producing cell-laden hydrogel microparticles in an oil-free environment through using microfluidics, while maintaining the extraordinary controllability of production rate, microparticle size and numbers of cells encapsulated in microparticles. The model of cell

growth in this physical-isolated microenvironment and cell sensitivities to inflammatory factor (TNF-α) are exhibited with the comparison with 2D monolayer culture, which contributes to the knowledge of cancer cell proliferation and homeostasis.

Chapter 3 demonstrates a study of using 3D printing techniques to construct hydrogel tubular structures to mimic the physiological bowel microenvironment and thus investigate the dynamics of colorectal epithelial cells. In this study, different types of hydrogel are used for building the tubes and the measurement of both the mechanical and the biological properties are describe in details in this chapter. In addition, the proliferation, survival and cellular response to Salmonella interaction of HCT116 cells are analyzed and presented that reveals the cell dynamics in tubular structural oriented and bacterial microenvironment. The developed system addresses several key influencing factors in colon environment that could be potential for creating intestinal tissue model and studying bowel disease.

Chapter 4 describes a study of creating artificial microvascular networks for nutrient and oxygen delivery throughout the 3D hydrogel construct by using leaf skeleton and designed model. This study is aiming to solve the delivering problem in 3D hydrogel culture environment. An artificial model of vascular system construction has been proposed and tested by applying several advanced laws that summarized from lumen and branching system on earth. Efficiency of water transport phenomena and supportive role of vascular structures are examined. Long-term cell growth and formation of spheroid tissue are achieved in such developed 3D vascular system that will be advantageous for using as the platform of drug testing system and provide necessary techniques for constructing artificial organ in future opportunities.

Chapter 5 introduces a study about creating microfluidic circulatory system to mimic the blood circulation for understanding regulatory role of shear stress in colon cancer cells under 3D liquid environment, which is expected to enrich the knowledge of cell dynamics during cancer metastasis *in vivo*. Such system addresses several key factors, such as close-loop circulation, periodic change of shear stress, physiological condition of shear stress, suspension status of cancer cells and peristaltic driving forces of *in vivo* blood circulation. The manufacture of such circulatory system is described in detail and cell dynamics is analyzed in both behavioral (survival and proliferation) and molecular (RNA expression) level. This study reveals previously unrecognized role of circulatory shear stress and contributes significantly to the core knowledge of cancer metastasis.

Chapter 6 addresses a summary of the research along with the potential opportunities to explore in this field following the research present in this dissertation.

Finally Chapter 7 includes all the references cited in this dissertation.

Chapter 2. Evaporation-based Microfluidic Production of Oil-free Cell-Containing Hydrogel Particles

3D hydrogel microparticle can be employed as a good scaffold to investigate the cell dynamics and tumour model, because it provides a physically isolated microenvironment to study cell-cell communication, cell-matrix interaction and cellular response to drugs without being influenced by the surrounding environments. Microfluidics is the most effective method to generate cell-laden microparticles with extraordinary control over the size, shape and number of microparticles and encapsulating efficiency. However, oil phase has to be unavoidably participated into the process to generate the microparticles based on the emulsion science and it becomes extremely hard to remove that may interfere with the cell metabolism. Here, we demonstrate an evaporation-based microfluidic strategy to produce oil-free cell-containing hydrogel particles. Perfluoro-n-pentane, which is used as the continuous oil phase to generate cell-containing hydrogel particles, is removed at an elevated temperature. Hence, human colon cancer cells can be encapsulated and cultured in the hydrogel particles without the oil disturbance, and cell dynamics in 3D solid environment and the mechanism of interaction between cells and 3D matrix can thus be investigated. This study reveals that cell dynamics including cell survival, cycle and sensitivity to inflammation in 3D environment perform significant difference from 2D

monolayer, highlighting the necessary roles of 3D matrix for realizing *in vivo*-like cellular function.

2.1 Introduction

Cells cultured in a 3D hydrogel matrix resemble and simulate various functions of real tissue, and have drawn significant attentions in the fields of tissue engineering [22], stem cell research [20], drug screening [21] and cell-based drug delivery [170]. In particular, because micrometer diameter hydrogel particles provide a well-controlled, physically isolated microenvironment for 3D cell culture [171, 172], numerous methods including extrusion [173], complex coacervation [174], and emulsification [175] have been developed to encapsulate cells in hydrogel particles. The majority of approaches, however, produce hydrogel particles with relatively large sizes (hundreds of micrometer to millimeter in diameter) and a broad size distribution. Most importantly, cell encapsulation efficiency, i.e., the percentage of particles with encapsulated cells, is low and the number of cells per particle is poorly controlled. Recent advances in microfluidics, on the other hand, have yielded unprecedented control over the generation of hierarchical emulsion drops and hydrogel particles [176-178], and thus have significantly improved the efficiency of cell microencapsulation. By adjusting the size of aqueous droplets via microfluidic approaches, for example, cell-containing drops with a narrow size distribution [179] and 98.5 % of cell encapsulation efficiency have been achieved [88]. Furthermore, microchannel with a high aspect-ratio has been developed to control the number of cells in droplets and exact one cell per droplet can be obtained with an encapsulation efficiency of 96.6 % [89]. When hydrogel precursors are included in these cell-containing drops,

hydrogel particles with encapsulated cells can be obtained by polymerizing the hydrogel precursors. Last but not the least, stop-flow lithography, a recently developed microfluidic-based approach for particle synthesis, has been used to encapsulate cells in hydrogel particles with different morphologies, such as rectangular and triangle particles, and thus provides a useful approach to study the effect of geometrical factors of hydrogel matrix on cell homeostasis [91].

2.2 Motivation

Although microfluidic-based approaches are effective in encapsulation of cells in drops and particles, generation of cell-containing aqueous drops and/or particles usually occurs in a continuous oil phase, which unavoidably results in oil contamination of particles and cells. Most importantly, oil contamination is toxic and can inhibit cell growth, accelerate cell death and damage the formation of tissue [180]. Therefore, oil removal is necessary for acquiring accurate knowledge of cell dynamics in 3D culture environment and precise results of drug testing.

2.3 Objective

In this study, we are aiming to create an oil-free environment for investigating cell dynamics in 3D hydrogel microparticles by using microfluidics, in which cell metabolism under 3D solid matrix could be revealed and provide essential knowledge of tumor model. In particular, during the microfluidic production micro-droplets, perfluoro-n-pentane (PFP) is used as the continuous oil phase to generate aqueous cell-containing droplets. Because

PFP has a boiling point of 29 °C, it can be removed effectively by evaporating the oil phase at 37 °C. Meanwhile, hydrogel precursors, which are widely used for cell culture including colon cancer cells [181], are added to the aqueous cell-containing droplets and become gelation at 37 °C. As a result, oil-free hydrogel particles can be generated by simultaneously evaporating the PFP oil phase and solidifying the hydrogel precursor-containing aqueous drops at 37 °C. Cell viability in hydrogel microparticles produced by PFP oil and HFE7500 oil is compared. In addition, the regulatory role of 3D matrix in HCT116 cell cycle and the cell sensitivity to inflammatory stimuli are going to be investigated under the comparison with 2D monolayer culture system. Hence, the knowledge of cell dynamics under the interaction with 3D solid matrix can be acquired and the advantage of 3D culture environment can be validated.

2.4 Design and fabrication

2.4.1 Cell culture and maintenance

HCT116 human colon cancer cells (kindly provided by Jun Sun, Medical Center at University of Rochester) [182] were cultured in DMEM (Life Technologies, CA) containing 10 % (v/v) fetal bovine serum (Life Technologies), 1 % (v/v) penicillin/streptomycin (Life Technologies). The cells were maintained in a T-25 culture flask and incubated in an incubator at 37 °C with 5 % CO_2.

For cell passage, cells growing on the surface of culture flask were rinsed by PBS for three times, followed by trypsizing for 5 min incubation, which cause the detachment of cells from the surface. Fresh DMEM was then added to cease the trypsin stimulation.

Cell suspensions were transferred to centrifuge tube and centrifuged at 1500 rpm for 5 min. Supernatant was then removed and cell pellets were suspended with fresh DMEM culture medium, followed by transferring to T-25 culture flask and incubation at 37 °C with 5 % CO_2.

For preparing the cell samples for experiment, the protocol is same as the operation of cell passage until centrifugation. After the removal of supernatant, cells were dispersed in controlled volume of fresh DMEM medium (depending on experimental requirement), which were then mixed with other reagents.

2.4.2 Device manufacture

Flow-focusing microfluidic devices were fabricated according to the established soft lithography technique in Semiconductor Manufacture Fabrication Laboratory (SMFL) at Rochester Institute of Technology (RIT) [183]. In particular, 3 inches wafers were purchased from UniverstiyWafer and cleaned by using acetone and isopropyl alcohol (IPA). Then photoresist SU-8 (MicroChem) was deposited on the silicon wafer by spin coating following recipe. 2 min soft bake at 95 °C was conducted to remove the parts of the solvents and promote the adhesion between substrate and resist. Lithography mask was then aligned on the silicon wafer with SU-8 coating and exposed to UV light following protocol. After the UV exposure, silicon wafer was post baked at 105 °C for 2 min, in order to remove parts of the solvent and improve the resist sidewall profile by reducing the effect of standing waves. The photoresist coated on the silicon wafer was next developed by using SU-8 developer (MicroChem) and rinsed by acetone. Finally, wafer was baked at 115 °C for 2 min to improve the mechanical robustness of the resist for subsequence process and

measured the dimension of pattern by using profilometer. In this study, the height of the microchannel is 37 μm everywhere. The widths of aqueous inlet channels are 100 μm; the widths of oil and main channels are 150 μm; the width of the orifice is 50 μm.

By using the silicon wafer, which is called master for poly(dimenthylsiloxane) (PDMS) mode, PDMS was prepared through mixing the monomer reagent with the crosslinker, followed by vacuum for 60 min. Then PDMS was poured on the silicon master and incubated at 95 °C for 1 hour, in which crosslinking reaction was triggered and PDMS would form into solid status. PDMS replica was then cut out by using knife and attach on clean glass slide after punching inlet and outlet holes. The final step is heating the resembled device at 85 °C for 1 hours to ensure the proper attachment.

2.4.3 Microfluidic generation of cell-laden microparticles

To generate hydrogel particles with encapsulated HCT116 cells, a HyStem-C Hydrogel Kit (BD Biosciences) was utilized as the hydrogel precursors, which consisted of Glycosil (thiol-modified sodium hyaluronate), Gelin-S (thiol-modified gelatin), Extralink (PEGDA, polyethylene glycol diacrylate), and degassed, deionized water (DI water). The Glycosil and Gelin-S powder were dissolved in 1 mL DI water separately and Extralink powder was dissolved in 0.5 mL DI water. The cell-monomer mixture was prepared by well mixing 150 μL Glycosil and 150 μL Gelin-S in a 1 mL centrifuge tube, followed by adding 150 μL HCT116 cell suspension (1×10^8 cells mL^{-1}). Oil as continuous phase was prepared by adding 2 wt % PEG-157 surfactant, which is synthesized based on the previous report, into perfluoro-n-pentane (Strem Chemicals). 7500 Engineered Fluid (3M™ Novec™) (HFE 7500) was prepared by adding 2 wt % Krytox.

In the experiment, 1 mL monomer solution and 1mL crosslinker solution were loaded into two 1 mL syringes (Med Lab Supply), which were connected to the inlets of the microfluidic device via polyethylene tubing (Scientific Commodities Inc., 0.015" (0.38 mm) I.D. × 0.043" (1.09 mm) O.D.). A syringe pump (KD Scientific) was then used to inject the solution to the microfluidic device. Oil was introduced from the side channel via another syringe pump (New Era) as the continuous phase. The typical flow rates of both aqueous phases and the oil phase varied from 3 to 5 μL min^{-1}, and 30 to 50 μL min^{-1}, respectively, which give a generating efficiency of 500 droplets per second. The generation process of droplets was monitored directly by a high-speed video camera (Phantom, Ametek) mounted on the microscope (AmScope).

2.4.4 Manipulation and measurement of cell-laden microparticles

To evaporate the oil phase, cell encapsulating droplets with excess oil were collected in a 1 mL centrifuge tube and then incubated at 37 °C. The tube was taken out and weighed every 5 min to monitor the weight change.

For cell culture in hydrogel particles, a 35 mm petri dish (In Vitro Scientific) was used to collect hydrogel particles with encapsulated cells, which were then incubated in an incubator. The number of cells in each hydrogel particle throughout the whole petri dish was counted under a Leica microscope (DMI 6000, Leica Microsystems) from day 0 to day 4.

To study the proliferation of single cells in particles, a time-lapse video of cell growth was recorded by using a camera (C10600-10B-H, Hamamatsu) coupled to the Leica microscope. To study the effect of TNF-α (Sigma-Aldrich) on the cell viability, HCT116

cells or encapsulated HCT116 cells were cultured in different concentrations of TNF-α (0.1, 1.0, 10, 50, 100 ng mL^{-1}) at 37 °C in an incubator. TNF-α was diluted in DMEM culture medium containing 10 % FBS and 1 % P-S. Normal culture medium without TNF-α added was used as control.

2.4.5 Statistical analysis

The size of cell-laden droplets was analyzed by using Image J. The viability of cells in microparticles was measured based on microscopic image and time-lapse video, and was then characterized by $N/N_0 \times 100$ %, where N is the number of living cells measured every day by counting, and N_0 is the number of living cells at Day 0. Plots were prepared by using Igor software, whereas figures were drew by Canvas software.

2.5 Results and discussion

2.5.1 Generation of cell-laden hydrogel microparticles

To control the generation of hydrogel particles, we have developed a flow-focusing microfluidic device that has two individual inlets to prevent hydrogel precursors from gelation during the process of sample introduction (Figure 15A). One of the inlets is for hydrogel monomers (Glycosil and Gelin-S) and the other inlet is for the crosslinker (Extralink). The crosslinker solution and hydrogel monomers mixed with a HCT116 cell suspension (1×10^8 cells mL^{-1}) are injected respectively into the two separated inlet channels, flowing through the confluence area and form droplets downstream in a continuous oil phase. Because a droplet with a diameter of 50 μm has a volume of 6.5×10^{-8} mL and a cell suspension with a concentration of 1×10^8 cells mL^{-1} gives a volume of

3×10^{-8} mL per cell, controlled generation of drops with a diameter of 50 μm is expected to encapsulate approximately two cells per droplet. Indeed, when a typical aqueous flow rate of 4 μL min^{-1} (for both aqueous phases) and oil flow rate of 40 μL min^{-1} are used, we are able to generate cell-containing aqueous drops with an average diameter of 50 μm. As shown in Figure 15B inset, the diameters of the majority of particles (> 70 %) fall into the range of 46-54 μm. Only 6 % and 5 % of the particles have the diameters in the range of 30-38 μm and 54-62 μm, respectively. Cells encapsulated in drops are clearly evident in Figure 15B. The percentage of droplets with two cells is 65 % among all the cell-containing drops.

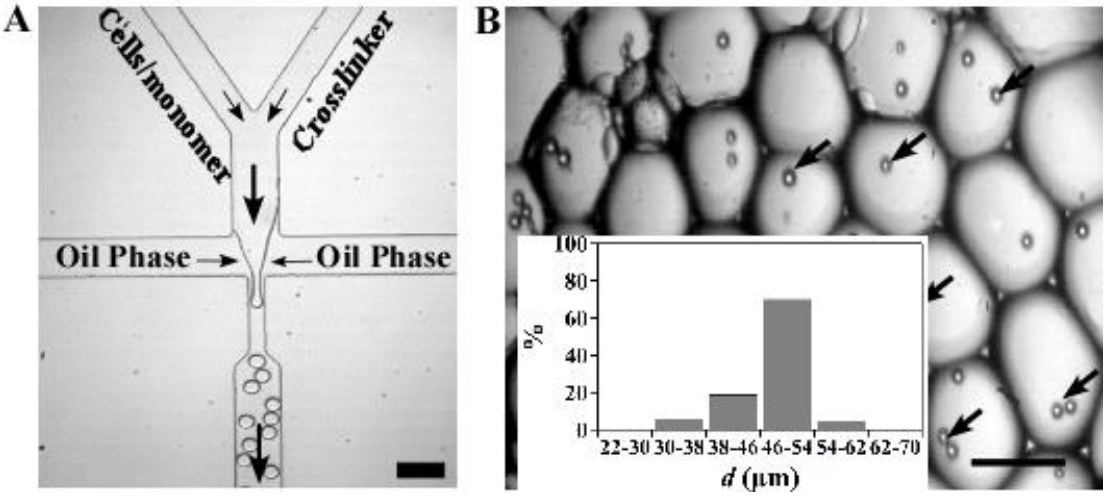

Figure 15 Microfluidic encapsulation of HCT116 colon cancer cells in hydrogel particles. (a) Experimental image of a flow-focusing microfluidic device used to encapsulate cells in hydrogel particles (scale bar = 100 μm). (b) Image of hydrogel particles with encapsulated cells. Arrows indicate the encapsulated cells in particles (scale bar = 50 μm). Inset: Size distribution of particles.

2.5.2 Oil removal and measurement

To remove the PFP oil phase by evaporation, we collect the cell-containing drops in a 1 mL centrifuge tube and incubate the mixture solution at 37 °C. The progress of evaporation is monitored by measuring the weight of the mixture solution at different incubation time

(Figure 16). For comparison, we also generate cell-containing drops in a HFE 7500 oil phase.

The results show that the weight of the PFP mixture stops decreasing after incubating at 37 °C for 35 - 40 min, suggesting that the oil phase is evaporated completely (Figure 17A). In contrast, the removal of the HFE 7500 solution via evaporation is ineffective and the weight of HFE 7500 solution remains almost constant within 40 min.

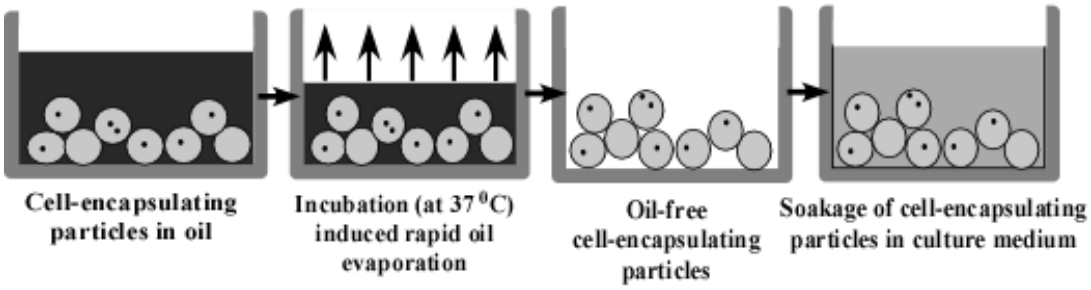

Figure 16 Schematics of the rapid oil removal process and cell culture in hydrogel particles.

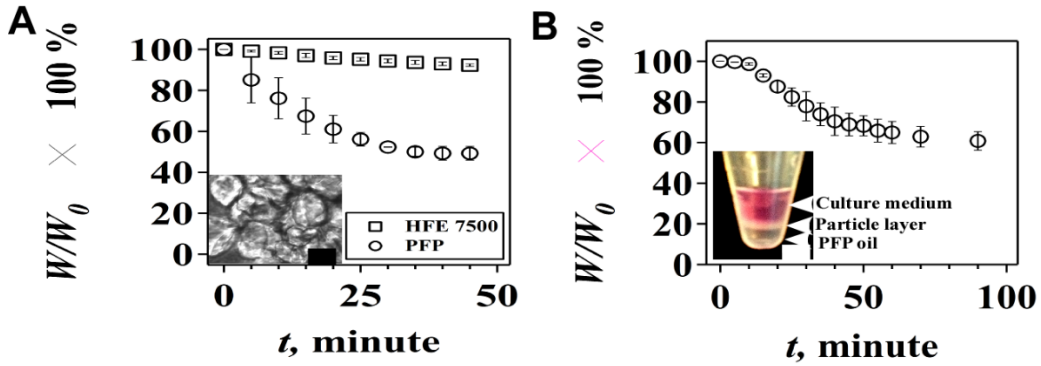

Figure 17 Effect of oil on particle aggregation and cell viability. (a) Evaporation-induced change of weight percentage ($W/W_0 \times 100$ %) of the mixture solution of droplets and oil. Inset: Image of aggregated hydrogel particles after the removal of PFP (scale bar = 50 μm). (b) Evaporation-induced change of weight percentage with time when particles are collected in the DMEM cell culture medium. Inset: Image of a centrifuge tube containing layers of culture medium, particles, and PFP (scale bar = 5 mm).

For a long time incubation, the weight of HFE 7500 solution decreases slowly over 1200 min (Figure 18). Note that separation of the oil phase from particles by using

conventional approaches such as centrifugation and filtration is not effective (Figure 19). Rapid evaporation of PFP, however, results in an aggregation of cell-containing particles (Figure 17A inset). To prevent particles from aggregation, we collect the cell-containing drops in a centrifuge tube that is prefilled with a DMEM culture medium. As shown in Figure 17B inset, PFP from the continuous oil phase remains at the bottom of the centrifuge tube and the cell-containing drops form a layer between the culture medium and PFP. After the mixture is incubated for about 90 min, the weight of the mixture stops decreasing (Figure 17B) and particles are obtained without any aggregation in the DMEM culture medium.

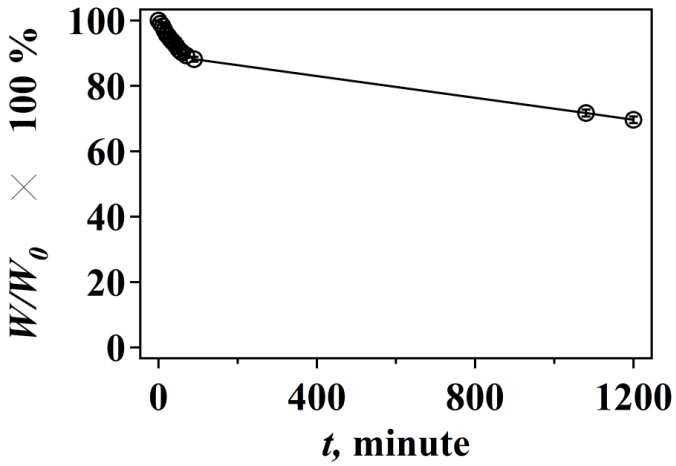

F**igure 18** Evaporation-induced change of weight percentage of the mixture solution of droplets and HFE 7500 oil.

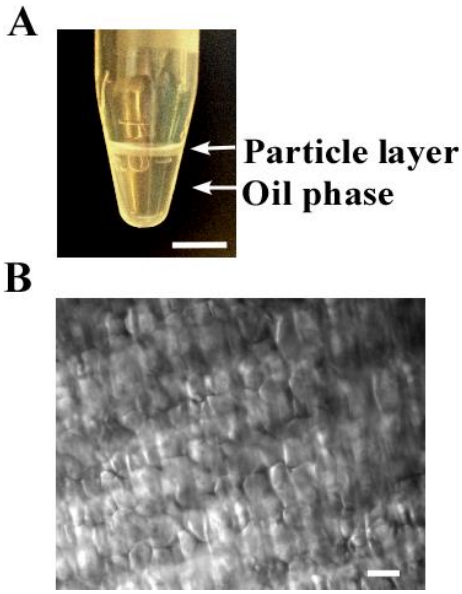

Figure 19 Conventional method for removing oil phase from the culture environment. (A) Image of a layer of hydrogel particles floating on top of the HFE 7500 oil phase after centrifuge (scale bar = 5 mm). (B) Image of a layer of aggregated matrigel particles sticking to a filter paper after filtration (Scale bar = 50 μm).

2.5.3 Measurement of cell growth in microparticles

We then study the cell viability by culturing the cell-containing particles at 37 °C in the DMEM medium where nutrients in the medium are expected to be delivered to cells through diffusion. Our results show that the majority of cells (> 90 %) survive in the first 72 hours, but the percentage of living cells shows a descending trend within the next 144 hours (Figure 20). In contrast, when HFE 7500 is used as the oil phase to generate cell-containing hydrogel particles, the percentage of living cells starts to decrease sharply after 24 hours and drops to 0 % within 120 hours. HFE 7500 has been used extensively as the continuous oil phase in microfluidic-based generation of droplets or micro-particles due to its inertness and ability to provide superior droplet stability [184]. Our results, however, demonstrate a toxic effect of the residue HFE 7500 oil on the growth of encapsulated colon cancer cells.

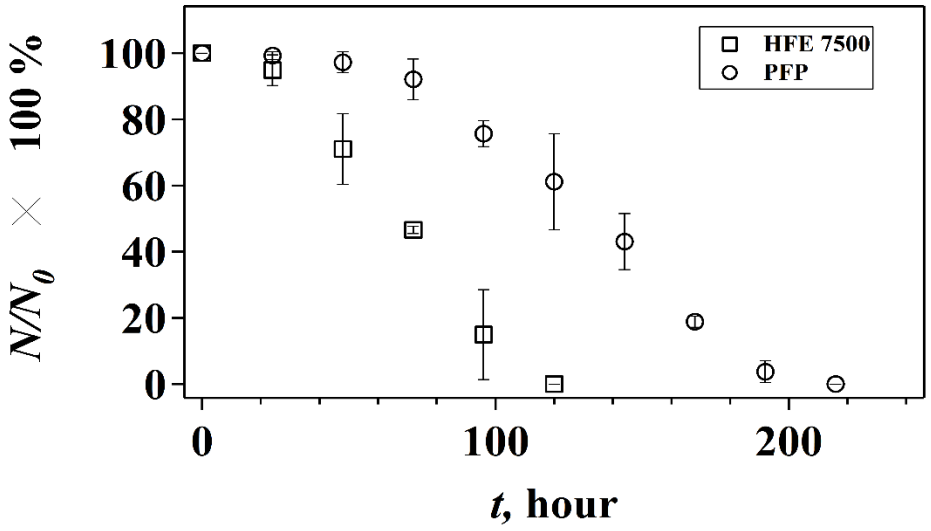

Figure 20 Percentage of living cells in hydrogel particles ($N/N_0 \times 100$ %) at different culture time (t).

We further investigate the cell proliferation dynamics at the single cell level and find that cells encapsulated in hydrogel particles have a prolonged cell cycle and a relatively low proliferation rate. Encapsulated cells spend 3 days to grow before reaching the division stage and the division process normally takes about 2.5 hours, which is much longer than that of cells growing in petri dish. In particular, encapsulated cells always keep a spherical morphology in contrast to the spindle-like shape of cells cultured in petri dish. During cell division in particles, cells elongate firstly, followed by the formation of two daughter cells. Notably, newborn daughter cells always stick tightly to their maternal cells and keep their spherical morphology. Occasionally, remerging of newborn daughter cells with their maternal cells is observed (Figure 21A). As a result, the proliferation rate of encapsulated HCT116 cells is much lower than that of HCT116 cells growing in petri dish (Figure 21B).

In addition, we notice that when encapsulated HCT116 cells are cultured for 4 days, there are more particles containing 3 cells than that with 2 cells (Figure 21C). In particular, when the number of cells at different culture time is evaluated by using $(n_n - n_0)/n_0 \times 100$

%, where n_n is the number of particles containing 2 or 3 cells quantified at day n, (n = 1, 2, 3, and 4) and n_0 is the number of particles containing 2 or 3 cells collected at day 0, the percentage of particles containing 3 cells increases dramatically within 4 days. The observation might result from a declined proliferation rate when more cells are encapsulated in one particle. Assuming cells encapsulated in particles with 3 cells stop growing on day 3, for example, there would be more particles containing 3 cells on day 4 because of the high proliferation rate of cells encapsulated in particles with 1 or 2 cells. Thus, accumulation of particles containing 3 cells is expected when the growth rate of cells in particles with 3 cells is lower than that of particles with 1 or 2 cells. Indeed, because encapsulated cells are required to overcome the effect of physical impediments from the matrix and remodel their extracellular microenvironment to create enough space to migrate and proliferate [185, 186], it is likely that a crowded microenvironment due to increased numbers of cells per particle exerts additional physical confinement that suppresses the proliferation of encapsulated cells.

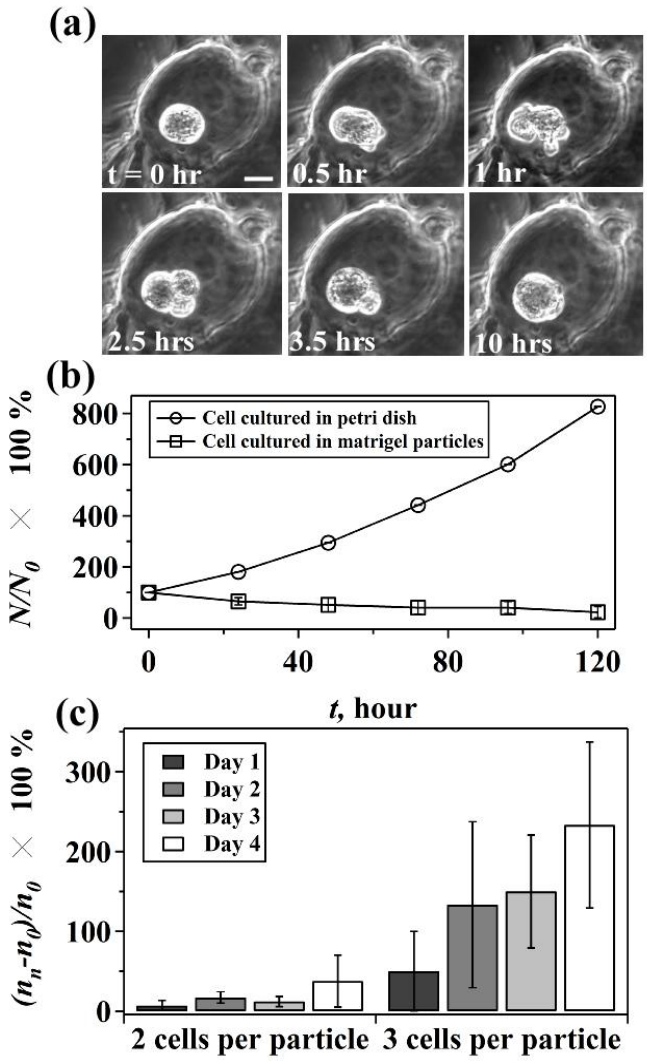

Figure 21 Proliferation of human HCT116 colon cancer cells in hydrogel particles. (a) Time-series image of the growth of a single cell in a hydrogel particle (scale bar = 10 μm). (b) Percentage of living cells at different time when cells are cultured in petri dish and hydrogel particles. (c) The net growth rate $(n_n - n_0)/n_0 \times 100$ %) of cells encapsulated in hydrogel particles.

2.5.4 Cell dynamics to TNF-α stimulation

Last, because chronic inflammation is associated with colon cancer, we further study the dynamic responses of encapsulated colon cancer cells to inflammatory cytokines such as TNF-α [187]. TNF-α is a cytokine involved in systematic inflammation and stimulation of acute phase reaction [188]. It has been demonstrated previously that TNF-α is able to inhibit the growth of HCT116 cells cultured in petri dish and induces programmed cell

death [189]. In our experiment where encapsulated human HCT116 cells are treated with different concentrations of TNF-α, the cell viability decreases with the increase of concentration of TNF-α. High concentrations of TNF-α, e.g., above the pathological concentration of TNF-α in colon (5 ng mL^{-1}) [188], accelerate cell death (Figure 22A), which is similar with the results obtained from cells cultured in petri dish (Figure 22B). Cells cultured in petri dish, however, live longer than cells cultured in particles, and can adapt to a low TNF-α concentration, e.g., 0.1 ng mL^{-1}. Cells cultured in particles undergo apoptosis rapidly between 70 and 140 hours depending on the concentration of TNF-α and do not show the ability to adapt to a low concentration of TNF-α. The observed phenomena may arise from the fact that there is a critical concentration of TNF-α above which cells start to undergo apoptosis [190]. When cells are encapsulated in a 3D hydrogel matrix, e.g., hydrogel particles, however, hydrogel matrix may act as a constrained, stiff network that impairs cell migration and proliferation via regulations of cellular signaling pathways such as integrin ligation, protein kinase activity and activation of Rho family GTPases [191, 192], and thus leads to a descending cell viability. In this case, the additional stimulation by TNF-α may accelerate cell apoptosis by further activating TNF-α–induced cell apoptosis pathways. However, it should be noted that in the first 24 hours cells encapsulated in particles have a higher viability than cells cultured in petri dish do. The reason for this phenomenon remains unclear to us. A possible explanation is the slow diffusion rate of TNF-α in hydrogel particles or a gradient of TNF-α across the particle that may delay the effect of TNF-α on cell viability in the early stage of treatment.

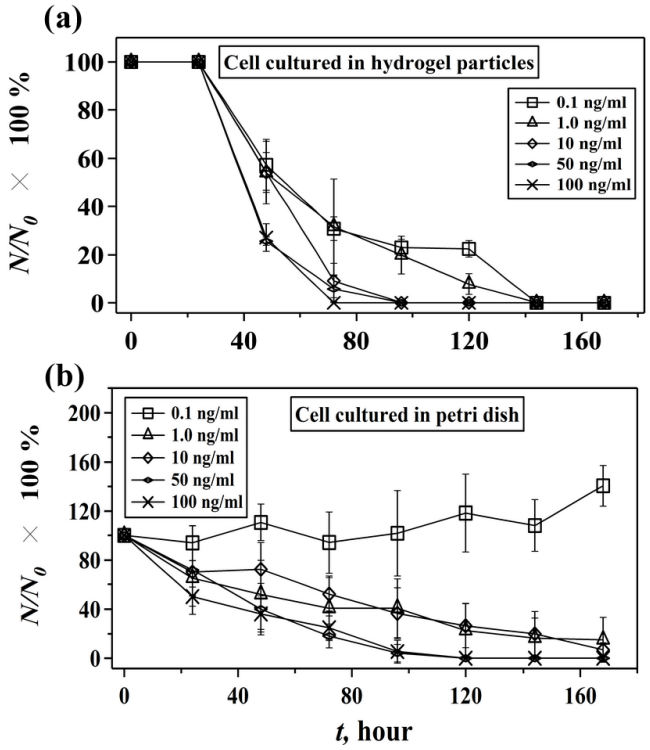

Figure 22 Effect of TNF-α on the viability of human HCT116 cells cultured in hydrogel particles and petri dish. The change of percentage of living cells, ($N/N_0 \times 100$ %), with time at different concentrations of TNF-α when cells are cultured in hydrogel particles (a) and petri dish (b).

2.6 Conclusion for Chapter 2

We have demonstrated a microfluidic approach to generate oil-free, cell-containing hydrogel particles by utilizing PFP as the continuous oil phase. Highly efficient removal of PFP by evaporation contributes to a comparably long time, 216 hours, culture of encapsulated human HCT116 colon cancer cells. Cell cycle is found to become slower than 2D monolayer culture. An apparent cell growth in hydrogel particles is observed at both population and single cell levels. In addition, when cells are treated with an inflammatory cytokine TNF-α, encapsulated cells are more susceptible the TNF-α stimuli than cells cultured in petri dish, highlighting the regulatory role of matrix in cancer cells growth under inflammatory conditions. The present study declares useful understanding of cell dynamics

in 3D solid environment and the necessary role of 3D matrix for achieving *in vivo*-like cell function and accurate results in biological application. On the other hand, the developed strategy provides an effective approach to obtain cell-containing hydrogel particles without oil contamination and may serve as a potentially useful platform for the development of hydrogel particle-based 3D cell culture, tissue engineering, and cell-based drug delivery.

Chapter 3. Cell Dynamics in 3D Bio-printing Cell-laden Matrigel/Agarose Construct

3D printing of biological architectures that mimic the structural and functional features of *in vivo* tissues is of great interest in tissue engineering and the development of transplantable organ constructs. In this study, we are aiming to create a platform that can mimic the physiological bowel environment by 3D printing cell-laden hydrogel tubular structures for investigating colon cancer cell dynamics, which addresses several critical influencing factors including 3D tubular biocompatible environment, bacterial interaction and flow condition. The rheological and biological properties of hydrogel construct is firstly evaluated, and cell growth and morphology are assessed according to various hydrogel condition. The interaction between colon cancer cell and Salmonella bacteria is further studied, which offers valuable knowledge of colon cancer cell dynamics and bowel disease mechanism. Therefore, the developed 3D printed hybrid hydrogel system enables addressing several critical factors *in vivo* and will be effective to mimic the physiological bowel environment for studying intestinal stem cell dynamics and bowel inflammation disease.

3.1 Introduction

3D bio-printing has evolved rapidly as a "bottom-up" layer-by-layer manufacturing technique for the construction of complex biological constructs. Functional skin and cartilage, for example, have been fabricated by applying the inkjet bio-printing technique, in which controlled volumes of cell-containing aqueous droplets can be deposited on substrate via using thermal or acoustic forces to fabricate construct [105, 106, 193], but rapid post solidification of bio-ink is required and resolution may become a concern. Laser-assisted bio-printing, a nozzle-free technique that deposits droplets by applying well-controlled focused laser pulses, enables high resolution printing (30-100 μm) of cell-containing structures and thus has been used to fabricate cellularized skin construct [107]. However, the stability of the printed structures depends on the gelation kinetics due to the use of aqueous drops which resulted in challenge for printing construct with complex geometry. Microextrusion, on the other hand, extruding uninterrupted viscous bio-ink (up to 6×10^7 mPa/s) on substrate with good spatiotemporally controlled deposition while keeping a proper resolution (5 μm to millimeters), is able to fabricate complex tissue structure, such as aortic valves [64], branched vascular system [108], and tumor models [108]. The high pressure applied during the extrusion is concerned to affect cell viability, however, the strong mechanical properties of the viscous bio-ink are desirable for building organ-like complex construct as well as maintaining the printed structures for biomedical applications.

In addition to the development of printing technique, the composition and material properties of bio-ink play essential roles in 3D bioprinting complex structure for cell and tissue culture. For example, polysaccharide-based hydrogel, such as alginate, hyaluronic

acid, and agarose, has rapid gelation kinetics and perform excellent mechanical property after printing, which contributes to the construction of vessel-like structures [62, 194], porous constructs [63, 195] and aortic valve conduits [64] for cell culture. However, due to the lack of essential proteins, polysaccharide-based hydrogel is usually criticized for the failure of supporting cellular function [66]. On the other hand, protein-based hydrogel has been well-known as one of the most biocompatible materials for 3D cell culture, since the containing of necessary growth factors and peptides facilitates the cellular activities and performs desired cell viability [65, 145, 196, 197]. For example, Matrigel composed of collagen IV, entactin, and laminin has been reported for construction of vascular network and culture of colonic crypt, as well as used as additives in 3D printed structures for bone regeneration [65, 145, 196, 197]. Nevertheless, the obtain of the outstanding biocompatible properties sacrifices the mechanical property and resistance to the enzymatic degradation that leads to the difficulties for bioprinting and structural maintenance [72]. Additionally, synthetic hydrogel like polyethylene glycol is developing for printing complex 3D structures, such as vessel-like structures and mechanically heterogeneous aortic valve construct [198, 199]. It has tailorable physical property, but poor biocompatibility and toxic degradation products, and the synthetic process is time consuming [200].

3.2 Motivation

From the technical issue, at current stage of 3D printing biological construct for 3D cell culture, finding proper materials that are not only compatible with biological function and printing process, but also has desired mechanical property to maintain the printed 3D complex structures is still challenging. Apart from the materials, although significant

progresses of constructing 3D structures have been accomplished, most of the system cannot represent the physiological condition for realizing cell dynamics and metabolism, which renders the problem for culturing tissue with proper structures and functions, and testing the drug efficacy.

From the aspect of life science, on the other hand, bowel environment is one of the most complex environment in human body, which involves bowel inflammation disease and cancer metastasis. It has been reported that over 50% patients with colorectal cancers developed cancer metastasis, which leads the colorectal cancer to become the second leading cause of cancer-related death in United States [201]. Hence, construction of a bowel-like physiologically relevant system is necessary for understanding the dynamics of colorectal cancer cells and method for cancer therapy. In addition, self-renewing stem cells in intestinal crypts play a critical role in maintaining the vigorous proliferation of intestinal epithelium [202, 203]. Impaired activity of intestinal stem cells has been linked to colorectal cancer [204, 205]. Therefore, achieving the ability to modulate ISCs in a well-controlled microenvironment is of great interest for both fundamental research of stem cells and clinical applications. Development of *in vitro* culture systems to sustain the growth and differentiation of ISCs, however, is challenging and in part this is because of the loss of 3D architecture of the tissue [206] and preservation of epithelial viability is difficult [207]. Such demands push the development of a 3D architecture that enables supporting ISCs growth and differentiation to understand ISCs dynamics. The successful completion of this research will contribute a missing, fundamental element to our base of knowledge of colorectal cancer and ISCs, without which the long-term culture of ISCs for tissue engineering and ISCs-based therapy can hardly be achieved.

3.3 Objective

The overall goal of this present study is aiming to build up a biological system by applying 3D printing technique that can mimic the physiological bowel environment for studying the dynamics of colon cancer cells and contributing to the knowledge of bowel inflammation disease. In particular, hydrogels are firstly being investigated for not only supporting the cell growth and cell to matrix interactions, but also are 3D printable and stable for maintaining the 3D structures, and hence provides a proof-of-concept for 3D printing intestinal stem cells at the final stage. Colorectal cancer cells are used as model to test the feasibility of 3D printing system and its supportive role for cell dynamics. Several critical factors in physiological bowel environment will be addressed, including 3D tubular biocompatible environment, bacterial interaction and flow condition. Moreover, to improve the biocompatibility of the 3D culture system and prepare for seeding ISCs in future steps, the development of hybrid hydrogel by incorporating Matrigel into agarose will be studied. The hybrid hydrogel is expected to take the advantages of the mechanical stability from agarose and the biological property from Matrigel, which can achieve proper cellular function and structures while maintaining the stable tubular structures. In addition, the interaction between the seeded colorectal cancer cells and Salmonella bacteria, which is a common bacteria found in bowel environment, is going to be evaluated according to various pre-cultures and flow conditions from behavioral and molecular examination. Therefore, such 3D printed biological architectures are expected to mimic the structural and functional features of human bowel environment, which can contribute an effective platform for ISCs differentiation and intestinal tissue growth.

3.4 Design and fabrication

3.4.1 Cell culture and maintenance

Human colonic epithelial HCT116 cells (ATCC) were cultured in a T-25 culture flask supplied with DMEM (Life Technologies) containing 10% (v/v) fetal bovine serum (FBS) (Life Technologies) and 1% (v/v) penicillin/streptomycin (Life Technologies) under 37°C and 5% CO_2. For preparation of the cell suspension, cells were washed by a PBS solution (Life Technologies) and treated by Trypsin (Life Technologies) for 5 minutes to detach them from the culture flask. The cell suspension was then centrifuged and re-dispersed in a fresh DMEM solution without adding FBS (1×10^8/ml) for further experimental use. Since dead cells were not attached on the culture flask and could be washed away by the PBS buffer during the washing step, the viability of cells in the suspension was approximately the same for all experiments.

3.4.2 Hydrogel preparation

Agarose stock solution was prepared by dissolving agarose powder (Sigma) in DI-water at 2 wt% or 3 wt%, and then homogenized and sterilized by boiling. The stock solution was then stored in an incubator at 37°C. Matrigel (50 μg/ml) (Corning) was stored at -18°C and pre-warmed overnight at 4°C before experimental use. To produce a gel mixture for 3D printing, agarose stock solution was first poured into a tube (Cristalgen) that had been pre-warmed at 37°C. Matrigel was then added by continuously mixing with a sterilized spatula, followed by the addition of cell suspension (1×10^8 /ml). The gel mixture was homogenized by continuously stirring, and then transferred to the printing head of the 3D

printer (Seraph Robotics) for printing or to the plate of a rheometer (Discovery Hybrid Rheometer, TA Instrument) for rheological testing.

3.4.3 Rheological measurement

The storage modulus (G') and loss modulus (G") of the hydrogel mixture at each concentration ratio were measured using a Discovery Hybrid Rheometer (TA Instrument) with a 40 mm diameter parallel plate. The measurements were conducted at room temperature and performed using six different angular frequencies from 1 to 10 rad/s. As soon as the Matrigel and agarose were mixed, the G' and G" of samples were measured every 3 minutes for 21 minutes.

3.4.4 3D bio-printing

A dual syringe 3D printer (Seraph Robotics) was used for the 3D bio-printing. The printing process was controlled by Seraph Print (Seraph). The programming code was written to design the shape of the printing structures point by point and imported to the Seraph Print software to be recognized by the printer. The 3D printer was sterilized with 70% ethanol before printing and was placed in a bio-cabinet to avoid contamination. During the printing process, a 0.9 mm diameter dispensing needle was used which produced printed line width on the order of 2 to 2.5 mm. The printing head was moved in *x*- and *y*-directions, and the platform was moved in *z*-direction. A motorized plunger inside the printing syringe continuously pushed the hydrogel out of the syringe. Hydrogel was printed layer-by-layer at a speed of 6 mm/s to build tubular structures in a collecting petri dish (Corning) or on glass slides (VWR) in air. The printed cell-laden tube was then filled with a DMEM culture medium and placed in an incubator at 37°C with a 5% CO_2 atmosphere for culturing. In

order to facilitate microscopic imaging and observation of cell growth, some of the tubular structures were controlled at a height of 5 mm during printing.

All printing experiments without the syringe heater were conducted at room temperature and each printing cycle took approximately 20 minutes. Note that the initial temperature of agarose has to be kept at 37°C. This is due to agarose gelation process at temperature below 37°C, which results in blockage of the printing head. When the temperature is above 37°C, on the other hand, agarose solution has a relatively low viscosity, which compromises the printing resolution and 3D constructs. For 3D printing with temperature control, a syringe heater (New Era) was wrapped around the printing syringe and the temperature was maintained at 37°C during printing.

3.4.5 Determination of cell growth and cell viability

The growth and morphology of HCT116 cells cultured in hydrogel were examined using an inverted fluorescence microscope (Leica Microsystems, DMI 6000). Cell viability was determined using Live/Dead assays (Life Technologies) following the manufacture's protocol. To image cells encapsulated in the printed hydrogel, cells were stained with nucleus-blue (Life Technologies) and/or actin-green (Life Technologies) and imaged using a confocal microscope (Leica, TCS SP5). The percentage of cells that exhibited spreading-out morphologies was calculated by dividing the total number of cells counted each day with the number of spreading cells. Each set of experiments was repeated three times with at least 100 cells being counted for each experiment. Error bars are presented as the standard deviation of the mean.

3.4.6 Salmonella bacteria preparation

Bacteria LB plate was prepared by seeding bacteria on agar plate through streaking. After overnight incubation at 37 °C overnight, a clone from LB plate was picked and dispersed in 7 mL LB broth, followed by shaking at 37 °C for about 5h. Inoculate 100 mL of LB with 0.1 mL of a stationary phase culture followed by overnight incubation at 37 °C without shaking for 18h. The LB broth was then centrifuged at 5000 rpm for 10 min at room temperature, and supernatant was removed for acquiring the bacteria pellets. Finally, bacteria was suspended in HBSS using ratio at 100:3 (LB: HBSS) for treating samples.

3.4.7 Bacterial treatment for cell-laden tube

Cell-laden tubes were cultured for 0 h (control), 24 h, 48 h and 168 h before bacterial infection, which is called pre-culture. Then culture medium were removed and tubes were placed into petri dish horizontally. When treated the tubes at static condition, bacterial suspension was added into the petri dish and emerged the tubes. When treated the tubes at flow conditions, bacterial suspension was loaded into syringe and injected into the lumen of tube through polyethylene tubing with the control of syringe pump. The flow rates were controlled at 63, 126, and 413 μl/min, which produced shear stress at 0.00075, 0.0015, and 0.005 dyne/cm^2 that within the physiological magnitude of bowel environment. The bacterial infection was controlled at 30 min for both static and flow condition, then tubes were rinsed by HBSS for three times, followed by confocal imaging or incubation with DMEM containing gentamicin (100:1) for 30 min (post-culture). Finally, after post-culture, tubes were collected for PCR analysis and medium were collected for cytokine analysis. This part was conducted by our collaborator at University of Illinois at Chicago.

3.4.8 Evaluation of bacterial adhesion

After the infection and rinse by HBSS, cell-laden tubes contained in petri dish were placed on the stage of microscope. Because the Salmonella bacteria was genetically labeled and could be detected by GFP fluorescent mode, the bacterial adhesion at the lumen of the tubes was assessed through microscopic imaging under GFP fluorescence.

3.4.9 Statistical analysis

The viability of cells growing in 3D construct was measured based on using Live/Dead fluorescent assay and microscopic image, and was then characterized by $N/N_0 \times 100$ %, where N is the number of living cells measured every day by counting, and N_0 is the number of living cells. To determine the bacterial adhesion, Matlab program was coded to measure the area of fluorescent and calculated based on a standard image. To determine significant differences of data between experimental parameters, Student's *t*-test was performed where $P<0.05$ was considered significant. Each set of experiment was conducted for more than three times. The data was expressed as mean +/- standard deviation. Plots were prepared by using Igor software, whereas figures were drew by Canvas software.

3.5 Results and discussion

3.5.1 3D printing agarose structures

Agarose has desirable temperature-based gelation features and proper mechanical properties for 3D printing [208, 209]. The printability of agarose was initially examined using a Seraph Robotics 3D printer. A circular pattern was designed by defining the

coordinates of printing pathways in the Seraph Robotics code, which was then imported to the Seraph Print program to control the movement of the printing head. 2 wt% agarose solution heated at 37 ºC and cooled down during the printing process, which improved its elastic properties. Agarose solution was loaded into the print head syringe, and was continuously extruded while printing (Figure 23A). As a result, agarose extruded from the printing head had enough mechanical strength to support the printed structure. By adjusting the tool path and the number of printed layers, tubular structures of agarose with a height of 5 cm, a wall thickness of 2 mm and diameters of 12, 17, or 25 mm were printed (Figure 23B). By changing the design of printing patterns, tubular structures with star, triangle, and square morphology were constructed (Figure 23C). In addition, our study shows that tubular structures with a height of 8 cm can be achieved in air without the need of external structural support (Figure 24). However, it shall be noted that the printing process is accomplished within 20 min, otherwise the gelation of agarose will block the printing head.

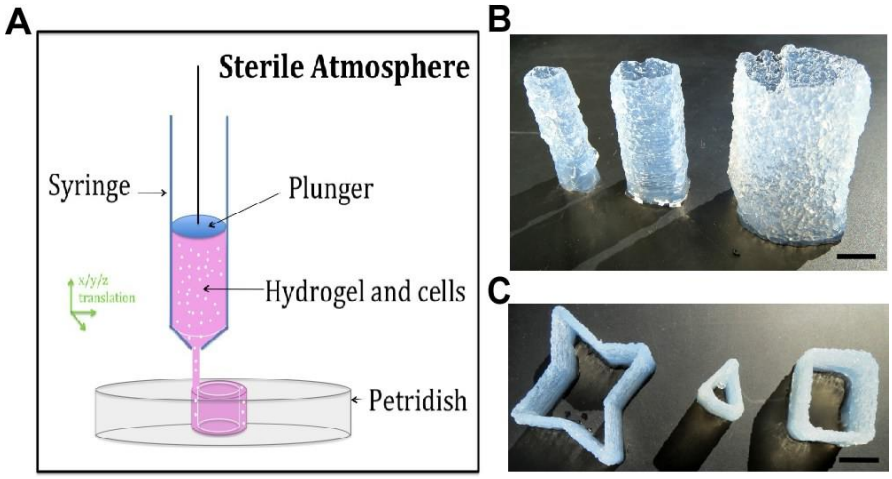

Figure 23 Experimental setup of 3D printed agarose constructs. (A) Schematic of the 3D printing setup. (B) 3D printed agarose tubes with different diameters (from left to right: *d* = 12, 17, and 25 mm) (scale bar = 10 mm). (C) 3D printed agarose constructs with a star, triangle, or square shape (scale bar = 8 mm).

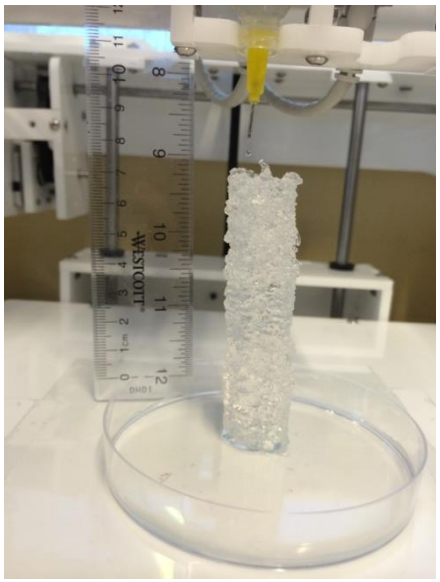

Figure 24 3D printed tubular structure with a height of 8 cm using 2 wt% agarose.

3.5.2 3D printing cell-laden agarose structures

We then printed agarose with encapsulated human HCT116 colonic epithelial cells to study the cell viability in such printed constructs (Figure 25A). As shown in a 3D constructed confocal image of the tube (Figure 25B), cells were dispersed throughout the entire structure of the agarose tube including the inner and outer surfaces. We found that cells were able to stay alive in the agarose tube after printing. However, the cell viability started to drop rapidly after 3 days culture (Figure 26). It was also observed that in contrast to the spindle shaped cells cultured in protein-based hydrogels such as Matrigel [67], cells growing in the agarose tube exhibit spherical morphology (Figure 26), indicating the lack of essential proteins that support cell attachment and spreading in agarose [210].

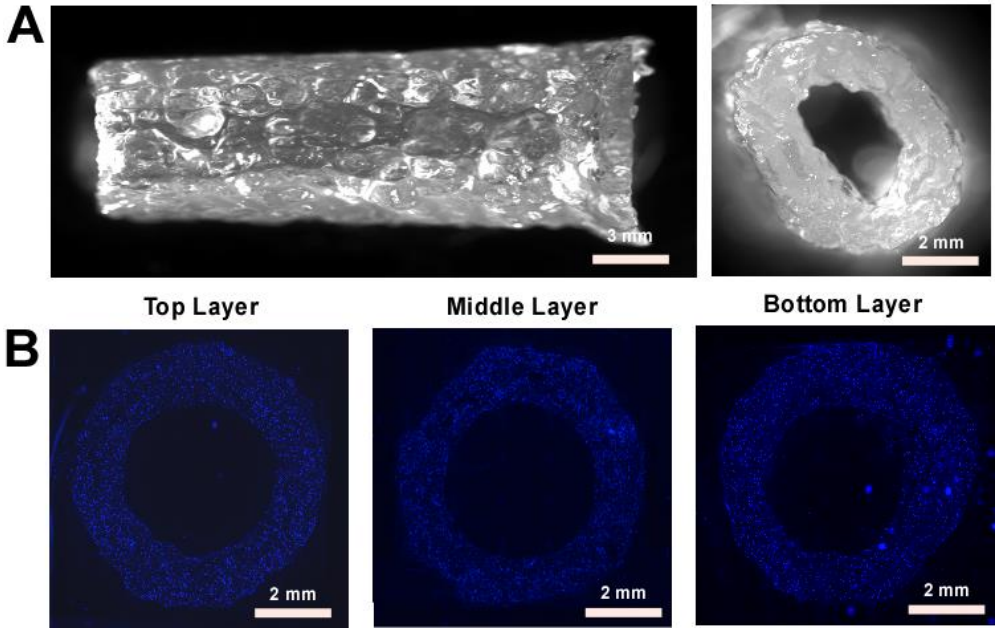

Figure 25 Image of the 3D printed cell-laden agarose tube. (A) Side view and top view microscopic images of the 3D printed cell-laden agarose tube. (B) Confocal imaging of cell distribution at the top, middle and bottom part of the tube.

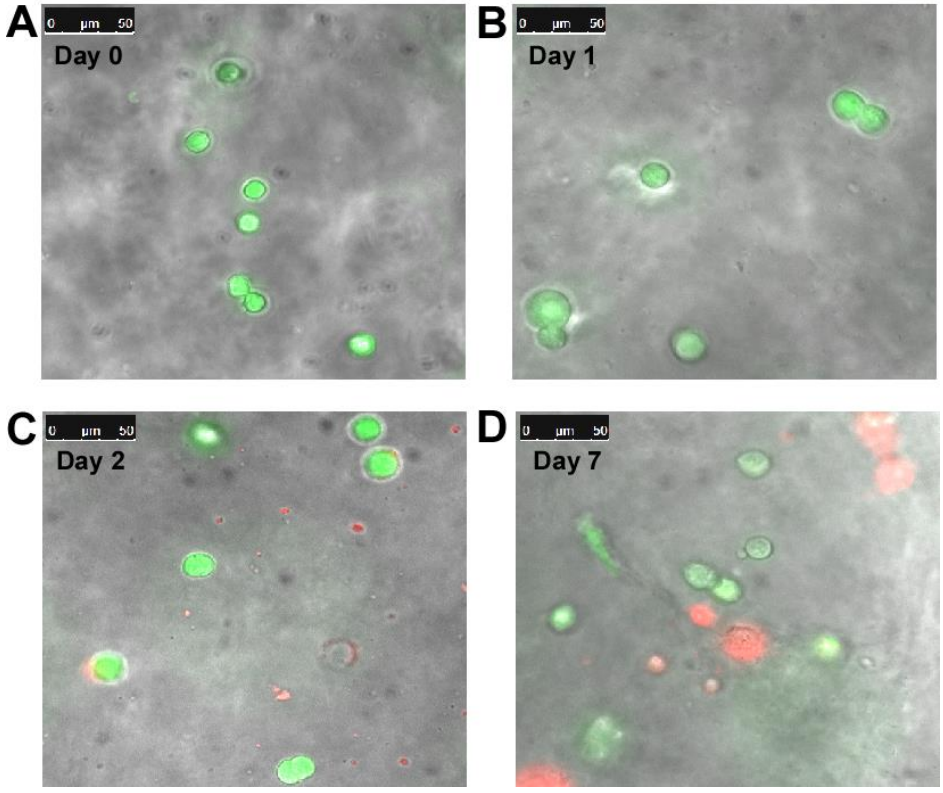

Figure 26 Cell growth in 3D printed agarose tubes. Cells are stained with Live/Dead assays and imaged by confocal microscopy at (A) 0 day, (B) 1 day, (C) 3 days and (D) 7 days.

3.5.3 3D printing Matrigel/agarose hybrid hydrogel

In order to improve cell growth and attachment in printed agarose constructs, we added Matrigel into the agarose matrix to form the Matrigel/agarose hybrid hydrogel. Agarose solidifies at temperatures below 32°C, whereas gelation of Matrigel occurs at temperatures above 4°C. The mixing of cold Matrigel with hot agarose solution therefore causes partial gelation of the hydrogel mixture immediately. We thus investigated the time-dependent change of the storage modulus (G') and loss modulus (G") of the agarose solution mixed with different volumetric fractions of Matrigel. Briefly, Matrigel was added to a 2 wt% agarose solution in volumetric ratios of 15%, 30%, or 50%. G' and G" as a function of time were then measured using a rheometer. As shown in Figures 27A and B, increase of G' and G" with time was observed for all formulations. However, G' was much larger than G" and increased fourfold within 21 min, indicating that the mixed hydrogel became a more elastic-like polymer along gelation. When volumetric fractions of Matrigel increased from 15% to 50%, the value of G' decreased, suggesting that adding Matrigel compromises the elastic property of the hybrid hydrogel.

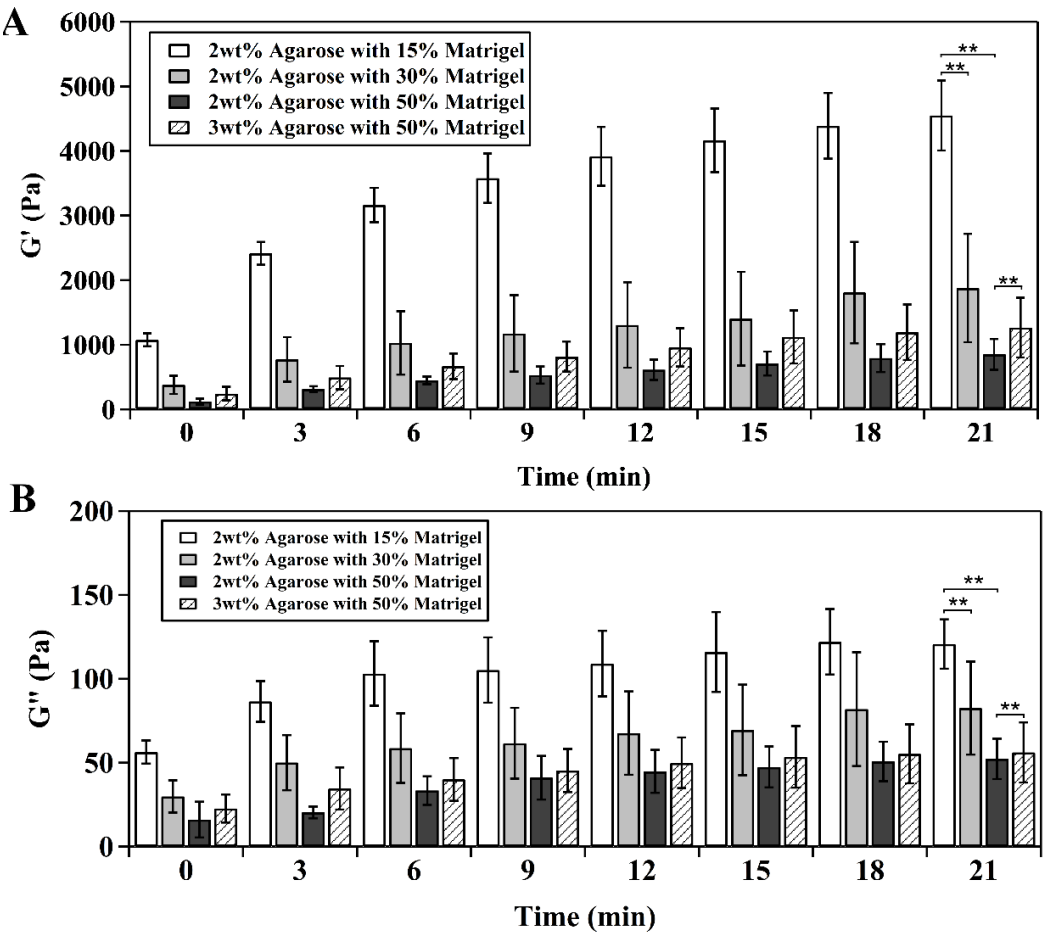

Figure 27 Characterization of Matrigel/agarose hybrid hydrogel. Dependence of the (A) storage modulus (G') and (B) loss modulus (G'') of hybrid hydrogel on time at different compositions of Matrigel and agarose.

We further tested the printability of these hybrid hydrogels and found that 15% and 30% Matrigel possessed the desired mechanical properties (G' > 1800 Pa at 21 minutes) for printing (Figure 28A and B), whereas 50% Matrigel (G' ~ 850 Pa) failed to maintain the printed structure (Figure 28C). Note that since the printing process was usually completed within 20 minutes, the rheological performance and printability of Matrigel/agarose hydrogels were examined within 21 minutes.

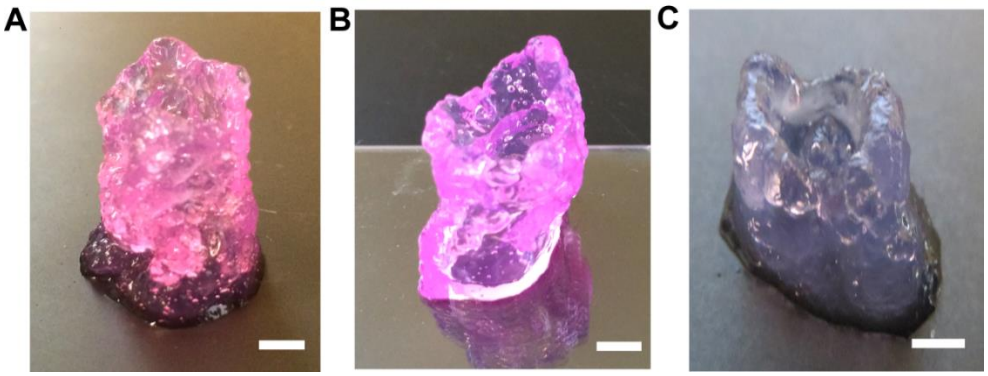

Figure 28 Images of tube printed using hybrid hydrogel composed of (A) 15%, (B) 30%, (C) 50% Matrigel and 2 wt% agarose (scale bar: 5 mm).

3.5.4 3D printing cell-laden Matrigel/agarose hybrid hydrogel structures

We further tested cell viability in the hybrid hydrogel with different volumetric factions of Matrigel. Our results showed that the percentage of spreading cells increased with the increase of volumetric factions of Matrigel (Figure 29). When the volumetric factions were 15% and 30%, there were 9% and 23% of cells that exhibited spindle-like morphology after 3 days culture (Figure 29). Higher percentage of spreading cells (37%) was found when Matrigel fraction was 50%, which was consistent with a previous study of 3D colonoid culture in Matrigel [196]. Although hybrid hydrogel with 50% Matrigel supported more cells to spread and grow, it had poor printability due to the low G' (Figure 27A and 28C). In order to increase G', the concentration of agarose stock solution was increased to 3 wt% while the volumetric faction of Matrigel was kept unchanged as 50%. As a result, a relatively high G' (1250 Pa) of Matrigel/agarose hydrogel system was obtained. The hybrid hydrogel with 3 wt% agarose and 50% (v/v) Matrigel were then printed into a stable tubular structure with a diameter of 17 mm and a wall thickness of 2 mm (Figure 30).

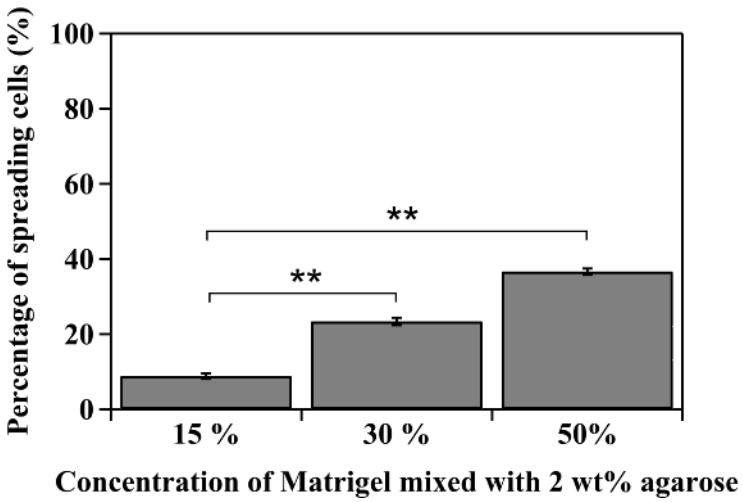

Figure 29 Percentage of cells that exhibit spreading morphology after 3 days of culturing in 3D printed tubular structures composed of 2 wt% agarose and 15, 30, or 50% (v/v) Matrigel.

Figure 30 An image of a 3D printed tubular structure using 50% (v/v) Matrigel and 3 wt% agarose. The tube has a diameter of 17 mm and a wall thickness of 2 mm (scale bar: 5 mm).

Therefore, human HCT116 cells were introduced to the tube composed of 3 wt% agarose and 50 v/v% Matrigel and culture the cells for 11 days. The results showed that, before day 8, the number of cells with spindle-like shape increased and that 72% of cells maintained spreading morphology (Figure 31A). Cells also tended to form clusters and spheroids (Figure 31A, inset) after seeding, consistent with reported 3D cell culture in hydrogel [208, 209]. The percentage of spreading cells, however, decreased from 70% to

47% between day 8 and day 11. Cell viability remained relatively high within the first 6 days (77%) but dropped after 7 days (Figure 31B), which was consistent with the observed decrease of the percentage of spreading cells after day 8 (Figure 31A).

3.5.5 3D printing Matrigel/agarose hybrid hydrogel at constant temperature

Because printing was conducted at room temperature (25^{o}C) whereas the initial temperature of the hybrid hydrogel was 37^{o}C, the change of temperature along printing led to the change of rheological properties of the hybrid hydrogel with time (Figure 27). We therefore tested whether the hybrid hydrogel could be printed at constant temperature (37 ^{o}C). A syringe heater was used to wrap around the printing syringe and maintained the printing temperature at 37 ^{o}C (Figure 32A). By repeating the printing process described above, a tubular structure with the same dimensions as the one printed without temperature control (a diameter of 17 mm and a wall thickness of 2 mm) was printed (Figure 32B). The tube printed at constant temperature was more transparent than that printed without temperature control (Figure 30), probably due to a more homogeneous composition. When the tube was cut at its top, middle and bottom sections and examined under a microscope, no massive hydrogel clusters or granular structures were observed, indicating a relatively homogeneous composition (Figure 32C). Most importantly, when HCT116 cells were introduced to the hybrid hydrogel and printed at constant temperature (37 ^{o}C), percentage of spreading cells increased with culture time and reached 75 % after 11 days culturing (Figures 32D and 33). Cell viability was also improved and maintained over 70 % after 11 days culturing, even though a slight decrease was found at the end of the culture (Figures 32E and 33). Most importantly, formation of cell clusters, or called cell spheroids, was

observed at day 7, indicating this 3D printed architecture is effective for growing tissues and studying cell dynamics.

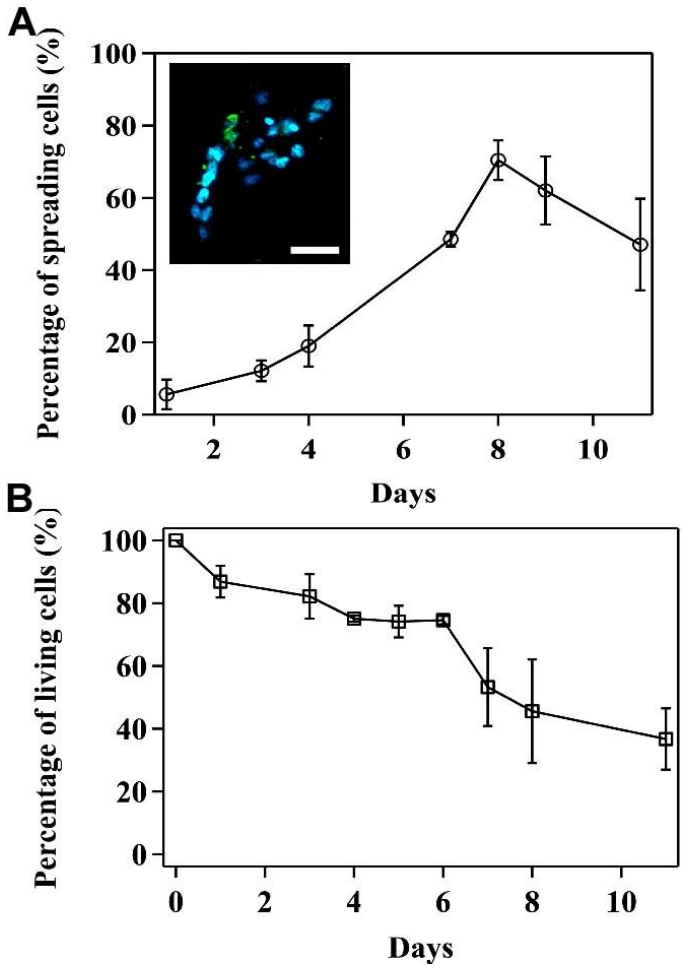

Figure 31 Cell growth in 3D printed Matrigel/agarose tubes composed of 3wt% agarose and 50% (v/v) Matrigel. (A) Percentage of cells that exhibit spreading morphology for 11 days culturing. Inset: A fluorescent confocal image of spreading cells and clusters formed in the printed tube. Cells are stained with actin-green and Nuc-blue (scale bar = 50 μm). (B) Cell viability over 11 days culturing.

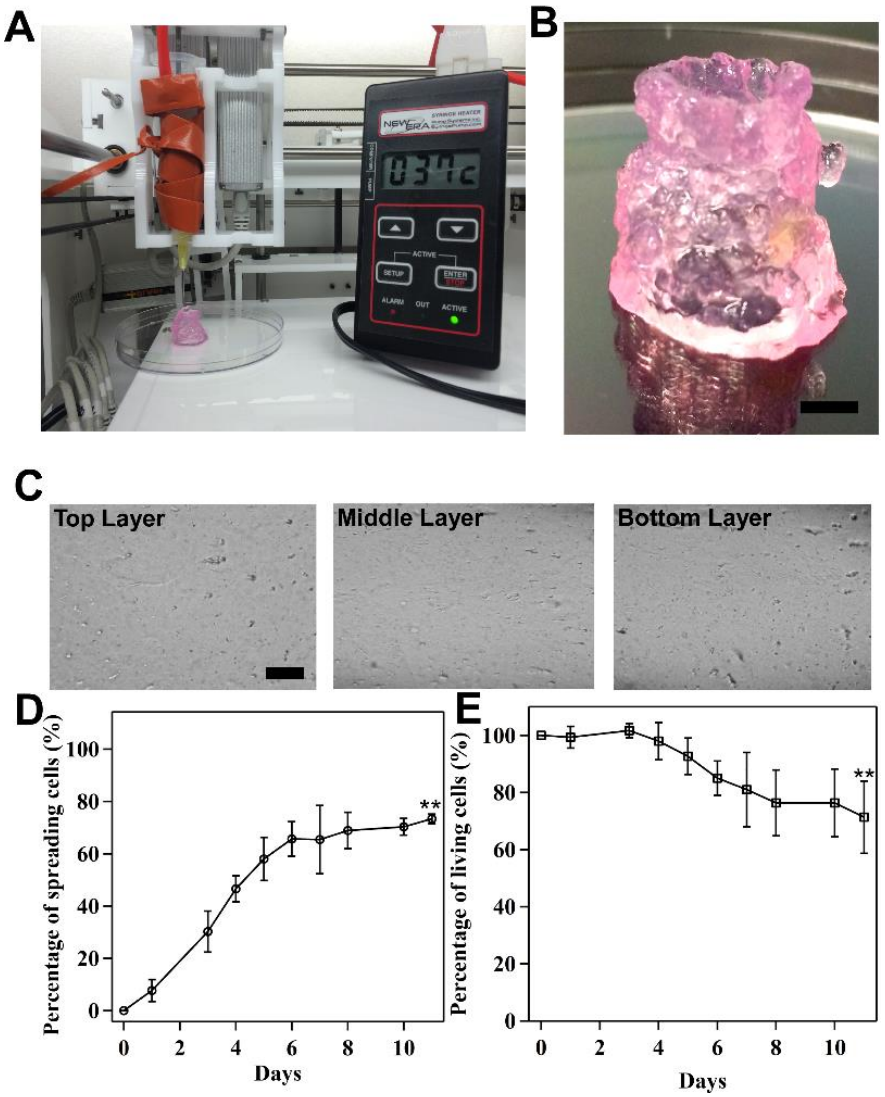

Figure 32 3D printing Matrigel/agarose hybrid hydrogel at constant temperature (37ºC). (A) An image of the experimental setup in which a syringe heater was wrapped around the printing syringe to maintain the temperature at 37ºC during printing. (B) An image of 3D printed tubular structure composed of 3wt% agarose with 50% (v/v) Matrigel (scale bar: 5 mm). (C) Microscopic images of the 3D printed hybrid hydrogel tube cut at the top, middle, and bottom sections (scale bar: 100 μm). (D) Percentage of cells that exhibit spreading morphology for 11 days culturing. (E) Cell viability over 11 days culturing.

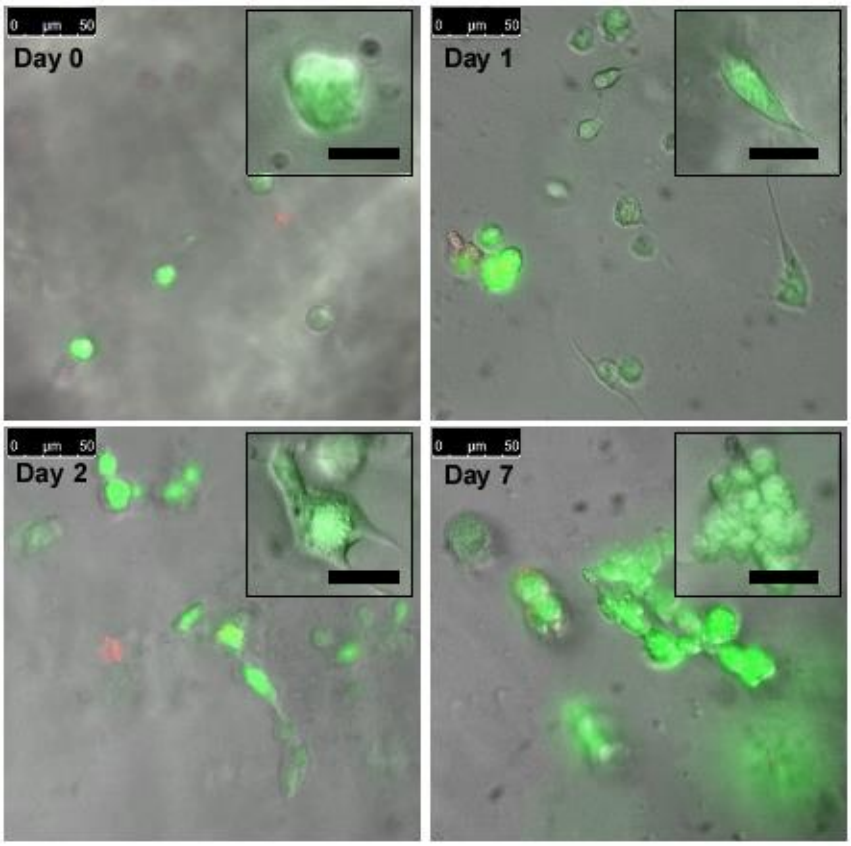

Figure 33 Fluorescent images of cells stained with Live/Dead assays in the hybrid hydrogel tubes after culturing for (A) 0 day, (B) 1 day, (C) 2 days and (D) 7 days. Inset: images of a single cell spreading with the culture time and forming into cell clusters in the hybrid hydrogel tubes.

3.5.6 Compensation between mechanical and biological property of hybrid hydrogel

In the current study, we developed Matrigel/agarose hybrid hydrogels and examined their rheological properties and 3D printability. Using human HCT116 cells in the printing hydrogels, cell growth and viability were evaluated. The desired mechanical properties of the hybrid hydrogel should firstly ensure a successful printing process and provide mechanical support for the printed structures. In addition, the mechanical properties of the hybrid hydrogel should not play a negative role in supporting cell growth. Furthermore, because Matrigel has been demonstrated for intestinal stem cells culture [70, 211], we expect the application of the developed hybrid Matrigel to benefit intestinal stem cells

culture in 3D-printed structures. Hence, this can contribute to the construction of *in vivo*-mimicking intestinal model systems.

Agarose performed outstanding mechanical features during construction of 3D architectures, however, it lacks essential proteins to which cells can adhere and develop cell-matrix interactions [66]. HCT116 cells cultured in the printed agarose exhibited spherical morphology (Figure 26) and failed to generate tensions against the 3D matrix to exhibit critical spindle-like morphology. This has been observed in protein-based hydrogels such as Matrigel and collagen [67, 212]. When Matrigel was added into the agarose matrix, HCT116 cells started to spread out and the number of spreading cells increased with the increase of volumetric fractions of Matrigel (Figure 29), indicating that adding Matrigel improves cell growth and adhesion in the 3D matrix. The percentage of spreading cells with spindle-like morphology in 50 % Matrigel was 37 % after 3 days of cell culturing. In fact, a previous study has shown that the growth of intestinal stem cells depends on the amount of Matrigel: the highest efficiency of colonoid formation (33±5 %) has been observed when 50 % Matrigel is used [196].

Adding excess Matrigel significantly affects the rheological performance and printability of agarose. It is known that when agarose solution (37 ^{o}C) is placed at room temperature (25 ^{o}C), G' increases with time due to the gelation of agarose at low temperature [213]. This is consistent with what we observed here (Figure 27A). The temperature drop due to the addition of Matrigel (4 ^{o}C) to agarose solution (37 ^{o}C) did not increase the G' of the hybrid hydrogel significantly; instead, G' decreased with the increase of volumetric fractions of Matrigel. Since solidified Matrigel has a relative low G' due to its high water content [214], it is likely that adding Matrigel dilutes the hybrid hydrogel

and compromises its elastic properties. Indeed, when the Matrigel/agarose was used to print tubes, 2 wt% agarose with 50% (v/v) Matrigel had the poorest printability (Figure 28C). In order to increase the printability of Matrigel/agarose bio-ink while maintaining the high percentage of Matrigel to support cell growth and spreading, the concentration of agarose stock solution was increased to 3 wt% while Matrigel was kept constant at 50 % (v/v). Because the volumetric fraction of Matrigel was kept constant, the increase of wt% of agarose did not affect the concentration of Matrigel in the mixture. The concentration of Matrigel in the hybrid hydrogel was 7.5, 15, and 50 µg/ml corresponding to 15 %, 30 % and 5 0% (v/v) Matrigel, respectively. As a result, not only was G' of 1250 Pa (G" ~ 60 Pa) obtained for the hybrid hydrogel (Figures 27) due to the increased wt% of agarose, but cell growth and cell-matrix interactions were improved. Stable tubular structure can therefore be printed and maintained (Figure 30). Although previous studies have shown the development of hybrid hydrogel for 3D printing [64, 215], our study shows the correlation between the formulation of hybrid hydrogels with their rheological properties and biocompatibility, and hence provides quantitative understanding of the material properties and biological activities of hybrid hydrogels for 3D bio-printing.

The results of culturing of HCT116 cells in 3D printed hydrogel constructs show that cells can spread and exhibit stretched non-spherical morphology during culture (Figure 31A, inset), indicating that the matrix supports cell adhesion and growth and cell-matrix interactions are established. The component of Matrigel also supports the cell growth with high viability in first 7 days. However, a decrease of cell viability and reduced percentage of spreading cells in the late stage of culture was observed, which may arise from the heterogeneous structures of the tube when printed without temperature control. Because

temperature of the hybrid hydrogel decreased with time, agarose would solidify during printing resulting in granular and non-uniform microstructures in the printed tube (Figures 23 and 24). The heterogonous structure could render a various physical properties such as stiffness at different locations of the tube and affect cellular behavior and direct cell fate [51, 98, 216]. In fact, our results show improved percentage of spreading cells and cell viability when cells are printed in more homogenous hybrid hydrogels. This indicates that homogeneous hydrogel matrix is supportive for cell growth and spreading. Note that it is also possible that the relative high modulus (G' ~ 1250 Pa) of the printed hybrid hydrogel negatively affects cell viability [217-219]. In addition, the diffusion length of oxygen and nutrient in hydrogel is around 150-200 μm [82], whereas the wall thickness of the tube is 2 mm. Although the entire hydrogel tube is immersed in a culture medium during cell culture, it is likely that the cells had insufficient uptake of nutrients and oxygen through the tube wall. Indeed, from the COMSOL simulation results (Figure 34), it can be found that the diffusion is inhibited by the thick tube wall that impaired the nutrient and oxygen delivery, which caused the diffusion of culture medium failed to cover the cells growing at whole tube structures. Therefore, our results highlight the much needed strategies for the development of physiologically relevant biomaterials and construction of vascular systems for 3D cell culture and tissue engineering, as shown by many recent efforts including results from our laboratory [55, 81, 108].

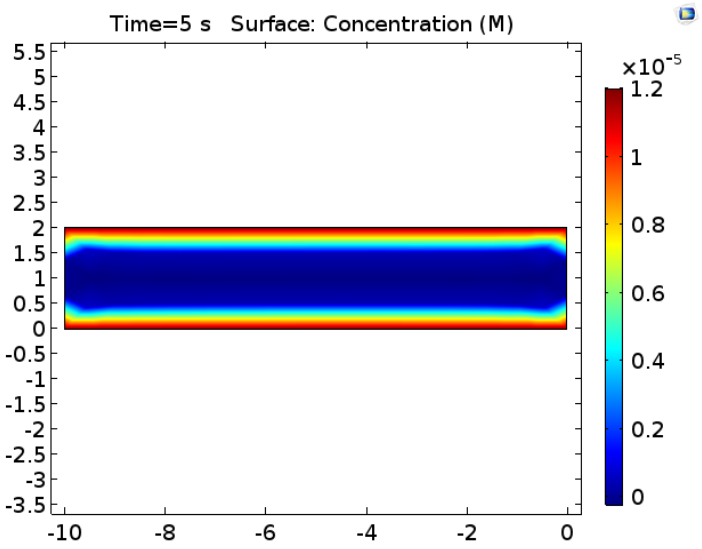

Figure 34 COMSOL simulation result shows the diffusion model in thick hydrogel construct.

3.5.7 HCT116 and Salmonella interaction in cell-laden agarose tube

We further investigated the HCT116 colon cancer cell and Salmonella bacteria interaction in such developed hydrogel culture system, which is expected to provide the knowledge of cell-bacteria communication and mechanism of bowel inflammation. In particular, Salmonella is a type of bacteria that can be found in the digestive tracts of humans and animals, especially reptiles, and it is well-known to cause illness including typhoid fever, paratyphoid fever and food poisoning [220]. Significantly, in recent decades, it has been proved that cells growing in digestive tracks could have strong intereaction with the local bacteria, in which critical communication is happened. For example, Salmonella was found to penetrate the intestinal barrier and interact with CD18-positive immune cells [221], during which toxins are usually released by bacteria that triggers the signaling tranduction of cells. In turns, the release of cytokine from cells, is then induced by such Salmonella infection [222], which could render inflammation that causes risks for developing chronic inflammation and may lead to tumor [223]. Indeed, bacterial infection was found to evade

the immune system or stimulate immune responses that plays defensive role in tumor formation, then causes carcinogenic changes through cytokines released by inflammatory cells, including such as interleukin-6 (IL-6), IL-8 [224], tumor necrosis factor-α (TNF- α) [222], reactive oxygen species (ROS) [225, 226], cyclooxygenase-2 (COX-2) [225] and nitric oxide (NO) [227]. On ther other hand, cytokines released by cells also play critical roles in activating immune system and suppressing bacterial growth and inflammation [228, 229]. The interaction between cells growing in disgestive tracks and bacteria, however, is still remaining elusive due to its complexity. Hence, in this part of the study, communication between HCT116 colorectal cancer cells and Salmonella is being exmained aiming to provide understainding of the mechanism behinds the bowel inflammation disease.

As shown in Figure 35, cell-laden agarose tubes constructed by 3D printing were firstly being examined due to its robustness for bearing flow condition. The tubes were culutred for various duration before Salmonella infection, so called pre-culture. The purpose of pre-culture is to let cells become more adapatable to the 3D environments and start to proceed their metabolism, including morphology adjustment, modification of surrounding matrix and trigger signaling pathways. Such pre-culture is expected to influence the cellular response during bactrial infetion, because longer pre-culture time will render the cells become more preparable for the interaction and hence more cytokines could be released in response to the infection. Then bacterial infection was conducted by injecting Salmonella suspension through the lumen of cell-laden tube for 30 min at different flow rates, 0 (control), 63, 126 and 413 µl/min, in which flow conditions were applied to mimic the physiological bowel environment. After the infection, Salmonella were removed by

washing and the cell-laden tubes were cultured for extra 30 min for fully responding to the infection, which is called post-culture. Finally, medium in post-culture were collected for analyzing cytokine released by cells and cells were collected for detecting the RNA changes.

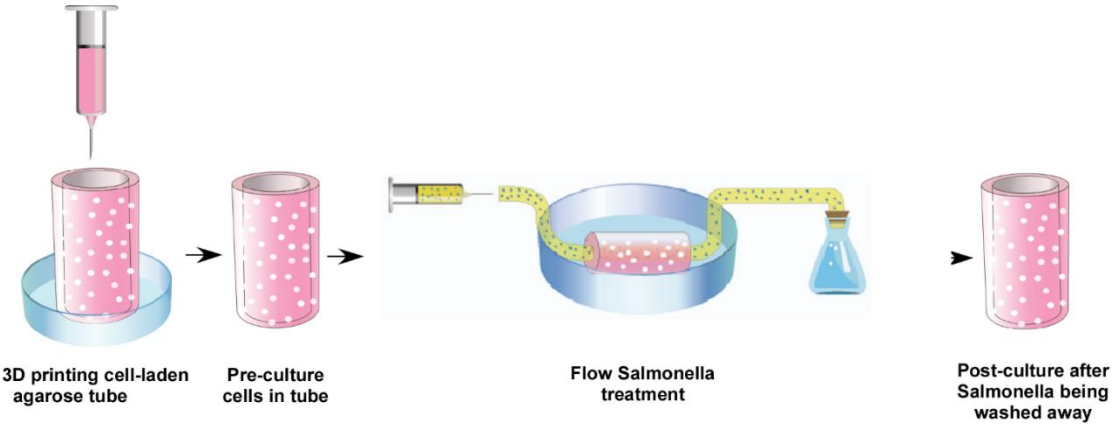

Figure 35 Schematics of experimental process, including 3D printing cell-laden tube, pre-culture tube, Salmonella infection and post-culture for sample collection.

Salmonella suspension was incorporated into the 3D printing cell-laden system, which is on the purpose to trigger the release of cytokine from HCT116 cells that growing in 3D environments, because the toxins secreted from Salmonella are expected to diffuse through the hydrogel barrier and stimulate the cells. On the other hand, after the secretion of cytokines from cells induced by bacterial infection, the released cytokines are expected to attract more Salmonella to this area, which forms a cycle. This expected phenomenon will explain how the HCT116 colorectal cancer cells communicate with the bacterial environment when grow in 3D conditions [187, 188]. As a results, bacterial adhesion was found to be significantly increased by prolonging pre-culture time, indicating pre-culture indeed played a positive role in letting cells become more adaptable to the 3D environments and respond to the infection more actively (Figures 36 and 38). On the other hand,

comparing to the static condition (0 µl/min), when cell-laden tubes were treated with Salmonella bacterial flow, the bacterial adhesion was dropped significantly (Figures 36 and 38). The adhesion was found to be decreased with the increasing flow rates, indicating the flow played inhibited roles in cell-bacteria communication. This observation could be explained by two factors. The first reason for the decrease could be the flow took the toxins or cytokines away from the system, which impaired the communication between cell and bacteria. The second possible explanation is the shear flow exerted on the wall of the tube inhibited the bacteria to attach. Hence the bacteria adhesion was found to drop with increasing flow rates.

Meanwhile, we run a control experiment with exact same condition apart from without cell seeding, which could be helpful to rule out the effect of agarose tubes (Figure 37). Results show when there were no cells growing in the agarose tubes, the bacterial adhesion was significantly dropped comparing to the conditions with cell seeding, and it did not change too much with the pre-culture, suggesting pre-culture time has no effect on promoting bacterial adhesion (Figure 38). This phenomenon indicates that the presence of cells enhanced the bacterial adhesion due to the communication at molecular level. On the other hand, it demonstrates the pre-culture indeed only facilitated cells to interact with bacteria during the infection. Also, similar observation was found when flow condition was incorporated. The bacterial adhesion was reduced with increasing flow rates. It should be noted that high flow rate 413 µl/min caused low adhesion for both experiment, implies the shear condition is too high for the cells and bacteria to communicate with each other.

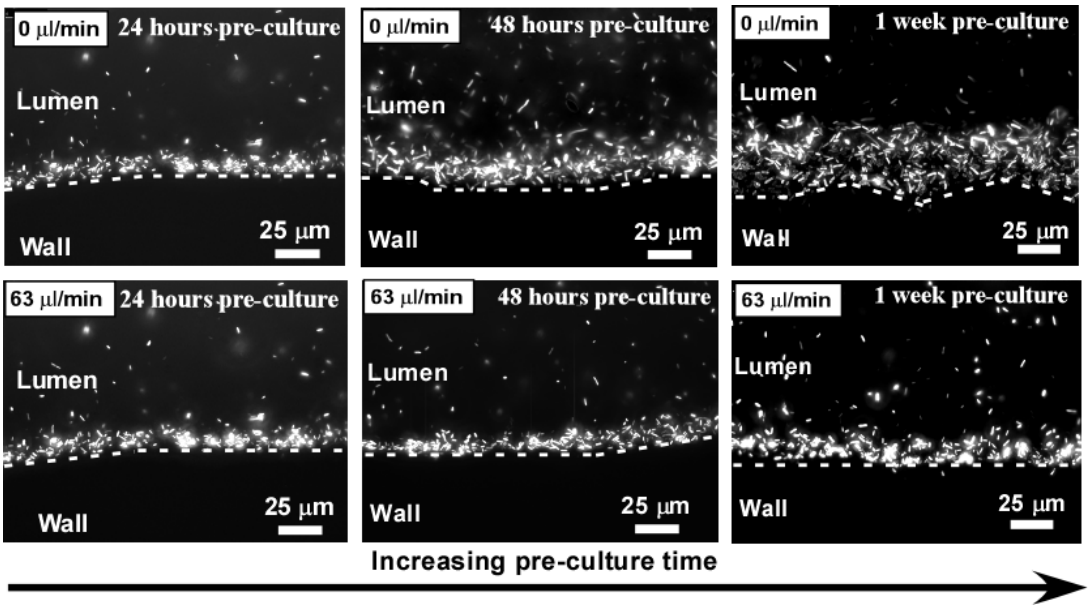

Figure 36 Fluorescent images of Salmonella bacterial adhesion at the lumen of agarose tube when HCT116 colorectal cancer cells were encapsulated. While dot line indicates the wall of tube lumen.

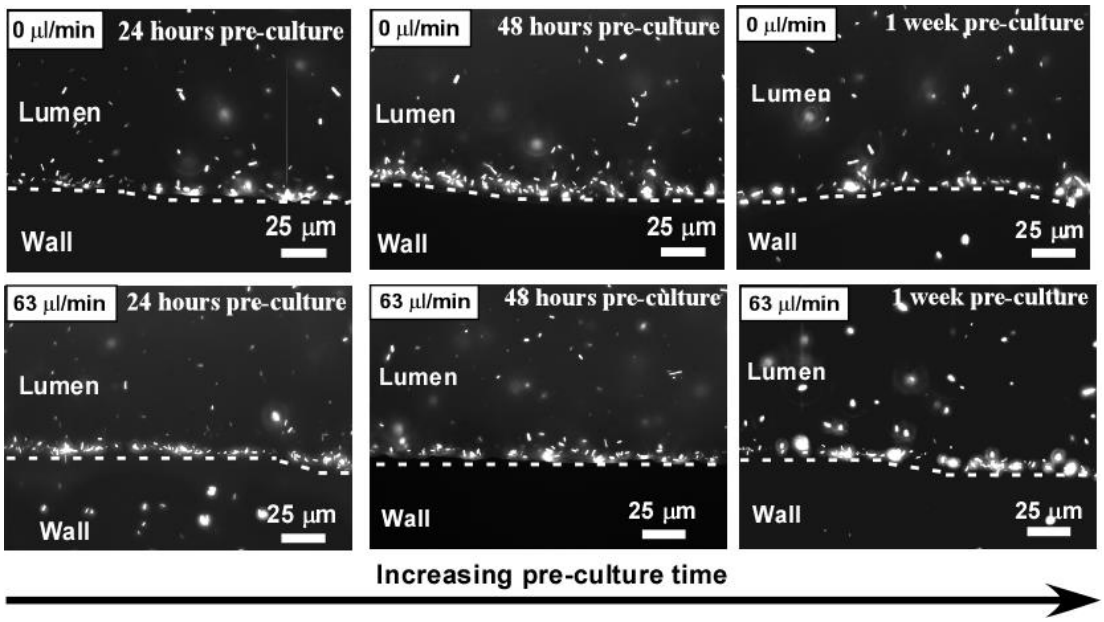

Figure 37 Fluorescent images of Salmonella bacterial adhesion at the lumen of agarose tube when there were no HCT116 colorectal cancer cells seeded. The while dot line indicates the wall of tube lumen.

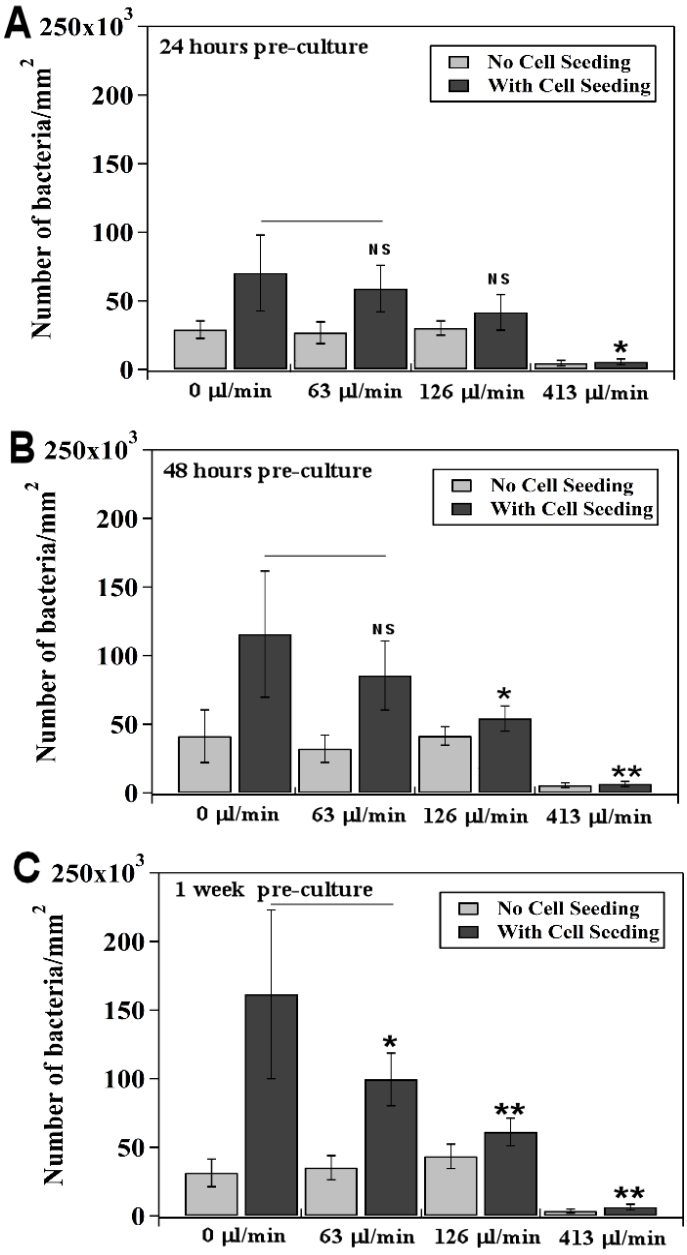

Figure 38 Bacterial adhesion changes with flow condition and pre-culture time when cells were seeded and not seeded in the agarose tube respectively. Agarose tubes were pre-cultured for (A) 24 h, (B) 48 h and (C) 1 week before infection.

3.5.8 Salmonella treatment of cell-laden hybrid hydrogel tube

Cell laden agarose tubes were tested by the Salmonella infection at flow condition due to its robustness, however, it is still concerned that agarose failed to provide a physiologically relevant condition for cell growth and cellular function, which may be failed to let the cells fully realize its communication to bacteria. Therefore, we applied the hybrid hydrogel cell-laden tube to test the Salmonella infection. After printing, cell-laden hybrid hydrogel tubes were pre-cultured for 1 week to fully adapt the cells into 3D culture environments and promote its cell dynamics. Then same protocol was followed to test the cell response during Salmonella bacterial infection. As a result, in control experiment where there is no cell seeding in the tube, a decreasing trend of bacterial adhesion was observed with increasing flow rates, but cell adhesion was increased by two-fold comparing to 3D agarose system shown in previous section (Figure 39A), indicating Matrigel is capable of improving the cell-bacterial interaction due to its possible essential component.

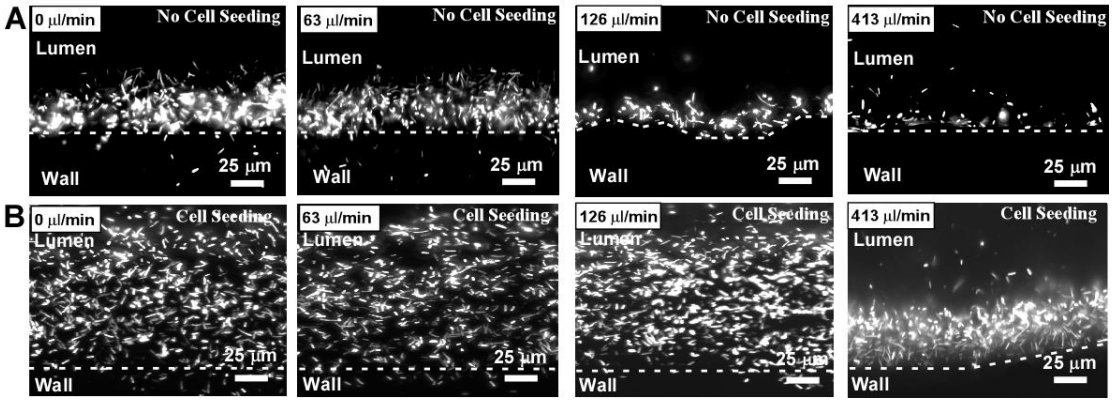

Figure 39 Fluorescent images of Salmonella bacterial adhesion at the lumen of hybrid hydrogel tube when there were (A) no cell seeding and (B) with cell seeding respectively. The while dot line indicates the wall of tube lumen.

When cells were seeded into the hybrid hydrogel, however, significant increase of bacterial adhesion was exhibited (Figure 39B). The bacterial adhesion was found to increase by two-fold comparing to 3D agarose condition (Figure 40), suggesting the Matrigel served as a critical role in facilitating cell dynamics, proceeding signaling transduction and molecular expression, and hence could interfere with bacterial in a more effective manner. In addition, the regulatory role of flow in bacterial adhesion was found being non-significant when flow rate was increased from 0 to 126 μl/min, indicating the interaction between HCT116 cells seeded in hybrid hydrogel tube and Salmonella was significantly enhanced and became strong to overcome the negative regulation from shear flow. Therefore, the hybrid hydrogel with incorporation of Matrigel component has been proved again for not only promoting cell growth and cell dynamics in 3D culture environments, but also providing a potential effective platform to investigate cell-bacteria interactions, which is critically helpful for disease model and drug testing.

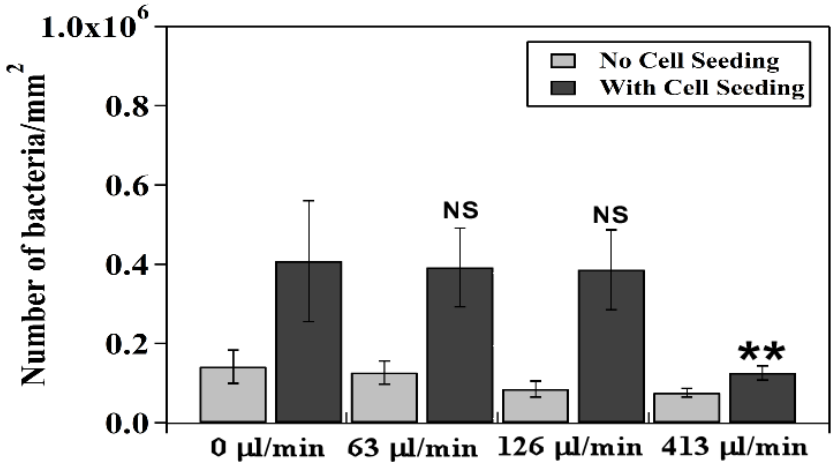

Figure 40 Bacterial adhesion changes with flow condition when cells were seeded and not seeded in the hybrid hydrogel tube respectively. Hybrid hydrogel tubes were pre-cultured for 1 week before infection.

3.6 Conclusion for Chapter 3

In this study, 3D printing technique has been applied successfully to construct the tubular structures for mimicking the human bowel environment. Comparing to other approaches such as biological film and microfluidics, 3D printing method brings well-controlled manners in both designing and constructing process. Complex structures could be created with extraordinary resolution and cells could be distributed homogenously in the whole tube through the accurate deposition. Disadvantages including the shear rate arises from the printing process that may influence the cell viability, and the blockage of printing head may occur from the gelation of bioink should be considered, but could be overcame by using a nozzle with relative large size.

On the other hand, Matrigel/agarose hybrid hydrogel has been developed with desired rheological properties for both 3D bio-printing and culturing human intestinal epithelial cells. The elasticity of the hybrid hydrogels increases with gelation time but decreases when the volumetric concentration of Matrigel increases. An optimized formulation of hybrid hydrogel with 50 % (v/v) Matrigel and 3 wt% agarose was identified to be 3D printable and showed the ability to support cell growth and adhesion. It is important that both cell spreading and cell viability were significantly improved when printing was performed at a constant temperature (37 ^{o}C).

In addition, the developed system has been employed successfully to test the interaction between HCT116 cells and Salmonella. Bacterial adhesion was found to be enhanced with prolonging pre-culture time and incorporating Matrigel, but impaired by increasing flow rate. It should be noted that there is a part of study about the analysis of cytokine level released by cells and Salmonella regulation in RNA expression of cells

during the infection still in progress by our collaborator at University of Illinois at Chicago, and will be proceeded in the future. Therefore, such developed system enables to mimic several critical factors in the physiological bowel condition for studying cell dynamics, and also provides useful guideline to develop Matrigel-based hydrogels for 3D printing and tissue engineering.

Chapter 4. Leaf-inspired Artificial Microvascular Networks (LIAMN) for Three-dimensional Cell Culture

Construction of vascular architecture capable of distributing oxygen and nutrients is critically important for 3D cell culture, tissue engineering, and the development of functional living organs. However, controlled engineering complex, hierarchical vascular structures that could address critical factors including the degree of branching, capillary density, and connecting microvascular networks with large vascular vessels still remains challenging. In previous section, cells growing 3D hydrogel constructs are subjected to the lack of nutrient supply due to the missing of vascular delivering system, which resulted in hindering long-term cell culture. Here, we construct an effective leaf-mimicking vascular system for 3D cell culture through applying leaf skeletal structures, which shows significant supportive roles for cell growth in 3D environments. On the other hand, we demonstrate a concept of leaf-inspired artificial microvascular networks (LIAMN) that artificially developed a hierarchical vascular structure for serving as an effective perfusion system for 3D cell culture in hydrogel. Because cell-containing hydrogel constructs with desired thickness can be constructed using embedded LIAMN layers, our strategy paves a new avenue to engineer effective vascular transport system for 3D cell culture, understand cell dynamics and the development of functional artificial organs.

4.1 Introduction

Effective vascularization in engineered tissues is critical to the development of living organs and remains one of the highest priorities in tissue engineering [143, 144, 230, 231]. Without a vascular network, for example, the maximal thickness of an engineered tissue is approximately 150-200 μm due to the limited oxygen diffusion [232]. As a result, large three-dimensional (3D) engineered tissue constructs quickly develop necrotic regions [151]. Hence, an effective transport system including both large vascular vessels and microvascular networks is required to sustain the biomimetic functions of thick, complex tissue constructs. To date, tissue engineered large and small blood vessels have been demonstrated by using porous scaffolds [233] and cell sheet technology [234] However, controlled formation of complex, hierarchical microvascular networks, such as the degree of branching, capillary density, and connecting microvascular networks with large vascular vessels is challenging.

The rapid development of micro-fabrication technology has realized the fabrication of microvascular networks in tissue constructs. Controlled engineering of vascularized structures in various bio-substrates, in which endothelial cells are growing into monolayer, has been reported to be realized by microfluidic-based systems [235]. Recent advances in biodegradable microfluidics and 3D vascularized microfluidic scaffolds pave new avenue for achieving implantable 3D microfluidic tissue constructs [236]. On the other hand, generation of vascular networks in engineered tissues has been accomplished by using 3D printing filament networks of carbohydrate glass [55] and agarose template fibers [111] as cytocompatible sacrificial templates. Such systems enable the improvement of mass transport, cell viability and differentiation when cells are seeded in 3D tissue construct.

Moreover, 3D printing technique, as a popular tool in recent years, has been emerged rapidly as an effective bottom-up approach to fabricate vascularized 3D tissue constructs [157, 237]. A rapid prototyping bioprinting method for scaffold-free small diameter vascular reconstruction has been demonstrated for the fabrication of single- and double-layered small diameter vascular tubes (OD ranging from 0.9 to 2.5 mm) [108]. Vascularized cell-laden tissue constructs have also been fabricated by 3D printing a fugitive ink (Pluronic F127) in cell-containing gelatin methacrylate hydrogels [110]. In addition, formations of microvascular architectures using methods such as direct writing [164] and electrical discharge [162, 238] have been demonstrated.

4.2 Motivation

Evolutionary innovations in the venation patterns of leaves, on the other hand, allow the effective transport of water, nutrients and carbon throughout the entire leaf [239, 240], and thus might provide an alternative approach to overcome the supplying difficulties in 3D cell culture and enable an effective distribution of nutrient and oxygen. Indeed, hydraulic analysis of water flow through leaves of sugar maple (*Acer saccharum*) and red oak (*Quercus rubra*) has shown that the hydraulic architecture of leaves minimizes construction costs relative to hydraulic capacity [241]. Venation patterns of leaves also have an optimized vein density [242]. Furthermore, studies of the isotopic composition of leaf water have demonstrated the presence of hydraulic capacitance in the ground tissues of vein ribs and a lateral exchange of water from veins [243], suggesting that major veins serve as high-capacity supply lines to minor vein system. All these characteristics of

venation patterns of leaves including minimized construction costs, optimized vein density, and hierarchical connection of microvascular vein with large vessels are ideal features of microvascular networks for 3D cell culture [244]. Furthermore, the presence of the diversification of low-order vein architecture and the commonness of reticulate, hierarchical leaf venation provides tolerances to hydraulic disruption through wounding [244], highlighting the advantages of leaf vascular architecture in hydraulic (or nutrient) transport. Thus, over 400 million years evolution, the hydraulic system of leaves has been evolved as such transport system that no portion of the leaf is under-supplied, and therefore, is likely be able to act as an effective microvascular perfusion system for 3D cell culture.

4.3 Objective

The objective of this study is to propose an innovative but effective principle to offer solution of delivering problem in 3D solid matrix that enables supporting long-term cell growth and formation of tissue structures. In particular, a concept of leaf-inspired artificial microvascular networks (LIAMN) will be proposed and the feasibility and advantages of the LIAMN will be validated for 3D cell culture. This will be shown by developing both leaf-mimicking (Figure 41A) and leaf-inspired (Figure 41B) microfluidic perfusion systems to support the growth of HCT116 colon cancer cells in a 3D hydrogel matrix. In addition, approach for fabricating thick hydrogel construct with vascular structures embedded and its supportive role in cell growth is going to be demonstrated. Therefore, our approach is expected to opens a new avenue that enables the efficacious engineering

of vascular networks in thick hydrogel constructs and provides a novel conceptual and experimental framework for vascular tissue engineering.

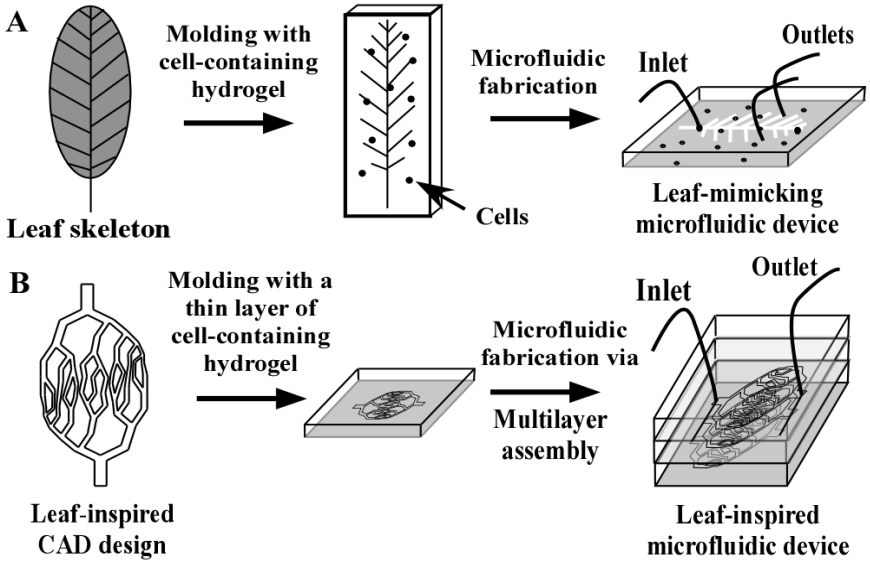

Figure 41 Schematics of the fabrication of leaf-mimicking and leaf-inspired microfluidic devices for 3D cell culture. Fabrication process of (A) leaf-mimicking microfluidic device and (B) multilayer leaf-inspired microfluidic device.

4.4 Design and fabrication

4.4.1 Cell culture and maintenance

HCT116 human colon cancer cells were cultured in DMEM (Life Technologies, CA) containing 10 % (v/v) fetal bovine serum (Life Technologies) and 1 % (v/v) penicillin/streptomycin (Life Technologies). The cells were maintained in a T-25 culture flask and incubated in an incubator at 37 °C with 5 % CO_2. To prepare cells for culturing in agarose, cells cultured in the T-25 culture flask were washed by PBS solution and trypsinized for 5 min to detach cells from the culture flask. The cell suspension was then centrifuged and re-dispersed in a DMEM culture medium for further experimental use (1 ×

10^8/ml). Because dead cells were not attached on the culture flask and were washed away by PBS solution, the viability of cells in the suspension is approximately the same for all experiments. To image cells under a confocal microscope, cells were stained by nucleus-blue (Life Technologies) and/or actin-green (Life Technologies) fluorescent dye following the manufacturer's protocol.

4.4.2 PDMS-based leaf-mimicking microfluidic device

Poly(dimethysiloxane) (PDMS) (Sylgard 184, Dow Corning) was poured to the leaf skeleton of *Hevea Brasiliensis* (Nature Bounty Supply) at the ratio of 10 : 1 for elastomer base and curing agent. After heated at 85 ºC for 1 hour, the PDMS replica was peeled off from the leaf skeleton and punched with holes as inlets and outlets. The PDMS replica was then bound to a clean microscopy glass slide using oxygen plasma treatment and fabricated into the leaf-mimicking microfluidic device (Figure 42A). The inlet of the leaf-mimicking microfluidic device was always located at the petiole of the original leaf (main vein, $d \approx$ 700 μm), whereas outlets were located at either the end of the main vein, the 1st order branch ($d \approx$ 300 μm), or the networks between the 1st order branches ($d \approx$ 50 μm) (Figure 42B).

4.4.3 Agarose-based leaf-mimicking microfluidic device

Agarose solution was prepared by dissolving agarose powder (Sigma) in DI-water at 2 wt%, and then mixed with HCT116 cells in DMEM (Life Technologies) dispersion (1×10^8/ml). Leaf skeleton of *Hevea Brasiliensis* (Nature Bounty Supply) was used as template and sterilized by exposing to UV light for 5 min before use. Agarose-cell mixture solution was poured onto the leaf skeleton and gelled at room temperature for 1 hour. The agarose

replica was then peeled off from the leaf skeleton and holes were punched at the main petiole (inlet) and the network area (outlets). The agarose matrix was placed on a glass slide and DMEM was injected into the device from a syringe (Norm-Ject) by using a syringe pump (Harvard Apparatus, PHD, Ultra). The device was then immersed in 2 ml DMEM in a petri dish and cultured at 37 °C in an incubator (Binder) for 24 hours. Cell viability was determined by using Live/Dead fluorescent assay (Life Technologies) on an inverted Leica fluorescence microscope (Leica Microsystems, DMI 6000). Each set of experiment was repeated by at least three times, and error bar presented as standard deviation of all trials. Note that, cell growth and viability were determined by cells growing within 200 μm to the branches, which was measured by microscope.

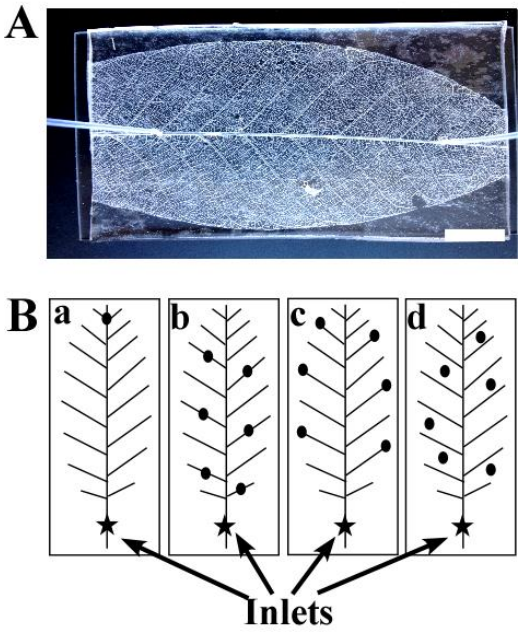

Figure 42 Analysis of the hydraulic transport efficiency of leaf-mimicking PDMS microfluidic devices. (A) Image of a typical leaf-mimicking PDMS microfluidic device. Scale bar: 2 cm. (B) Schematics of positions of inlets and outlets in the leaf-mimicking PDMS microfluidic devices

.

4.4.4 Agarose-based leaf-inspired microfluidic device

Leaf-inspired microfluidic master was fabricated using established soft lithography technique. In particular, 3 inches wafers were purchased from UniverstiyWafer and cleaned by using acetone and isopropyl alcohol (IPA). Then photoresist SU-8 (MicroChem) was deposited on the silicon wafer by spin coating following recipe. 2 min soft bake at 95 °C was conducted to remove the parts of the solvents and promote the adhesion between substrate and resist. Lithography mask was then aligned on the silicon wafer with SU-8 coating and exposed to UV light following protocol. After the UV exposure, silicon wafer was post baked at 105 °C for 2 min, in order to remove parts of the solvent and improve the resist sidewall profile by reducing the effect of standing waves. The photoresist coated on the silicon wafer was next developed by using SU-8 developer (MicroChem) and rinsed by acetone. Finally, wafer was baked at 115 °C for 2 min to improve the mechanical robustness of the resist for subsequence process and measured the dimension of pattern by using profilometer. In this study, the height of the microchannel is 37 μm everywhere.

HCT116 cell-containing agarose mixture was then prepared as described above and poured onto the microfluidic master to form a single layer of agarose hydrogel replica at room temperature. The thickness of agarose replica was controlled by adjusting the volume of agarose mixture solution being used and measured under a microscope. To assemble the 3D LIAMN, three pieces of agarose replica were aligned and stacked together. The assembled device was placed under room temperature for additional 30 min so that the agarose became slightly dry and adhered better to each layer. Inlet and outlet holes were then punched throughout the three-layer construct. The inlet and outlet tubing, however, were only inserted at the top layer. The assembled device that was continuously supplied

by DMEM through the embedded perfusion channels was then immersed in 5 mL DMEM and cultured in an incubator. Cell growth, viability, morphology, and distribution were measured under an inverted Leica fluorescence microscope or confocal microscope (Leica Microsystems).

4.4.5 Statistical analysis

Hydraulic transport efficiency of leaf-mimicking microfluidic device was characterized by measuring water coverage when inlets were punched at different location. Water coverage was characterized by the ratio of the water-covered area of the device to the total area of the device. Images were took before and after the water injection, and analyzed by using Image J and Matlab software. On the other hand, the viability of the cells growing in 3D construct was measured based on using Live/Dead fluorescent assay, microscopic image and time-lapse video, and was then characterized by $N/N_0 \times 100$ %, where N is the number of living cells measured every day by counting, and N_0 is the number of living cells at Day 0. To determine significant differences of data between experimental parameters, Student's *t*-test was performed where $P<0.05$ was considered significant. Each set of experiment was conducted for more than three times. The data was expressed as mean +/- standard deviation. Plots were prepared by using Igor software, whereas figures were drew by Canvas software.

4.5 Results and discussion

4.5.1 Hydraulic measurement of leaf-mimicking microfluidic device

To develop leaf-mimicking microfluidic devices, we used the skeleton of leaves with pinnate venation, e.g., rubber tree leaves (*Hevea Brasiliensis*), as the template. Pinnate venation has a main vein that extends from the bottom to the tip of the leaf, from which small veins are branching off. The main vein can serve as the high-capacity supply lines for fast, long-distance water transport [245], whereas the hierarchical structure derived along the central axis into higher order branches (network area) can carry out local dispersion. In addition, pinnate-veined leaves (with an elliptic shape) have a high density of minor veins comparing to parallel- or palmate-veined leaves [246], and thus are expected to have a better hydraulic conductance [247]. We then fabricated PDMS-based leaf-mimicking microfluidic devices and studied the hydraulic conductance in such devices.

To study the hydraulic transport efficiency of the leaf-mimicking PDMS microfluidic device, water were injected into the device by applying pressure to a water-containing syringe (Norm-Ject), which was connected to the device via a polyethylene tubing (0.015" (0.38 mm) I.D. × 0.043" (1.09 mm) O.D.). A gas regulator with precision of 0.1 psi (Omega) was used to control the applied pressure. The pressure at which water started to flow out of the device through the outlets is recorded as the input pressure. Devices with outlets located at the main vein required the lowest input pressure, whereas devices with outlets located at the 1st order branches and networks required relatively high input pressure (Figure 43A).

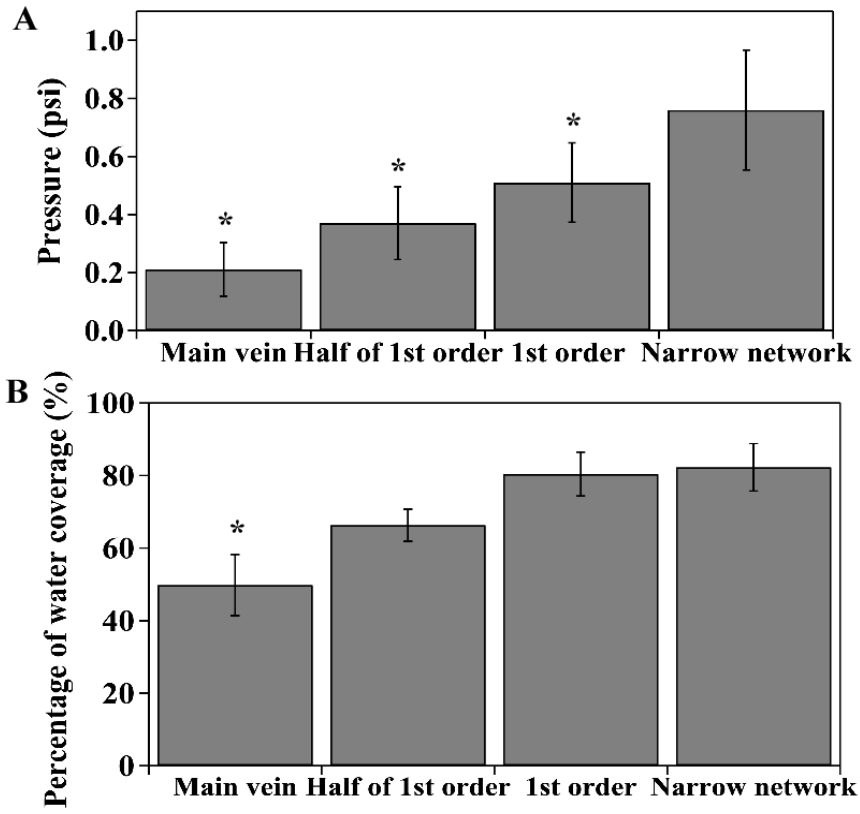

Figure 43 Analysis of hydraulic transport in leaf-mimicking microfluidic device. (A) Effect of position of outlets on the input pressure. (B) Dependence of fluid coverage on the position of outlets in leaf-mimicking PDMS microfluidic devices.

Most importantly, devices that have outlets at the 1st order branch and networks had 80% area covered with water, while only 50 % and 63 % water coverage was obtained when outlets were located at the main vein and at the half of the 1st order branch, respectively (Figure 43B). Therefore, the results show that, given a relatively high input pressure, high water coverage can be obtained when the outlets of the device are located at the network area replicated from the original leaf. Because we are interested in the development of perfusion systems for 3D cell culture where a high coverage of culture medium in the device is desired, the outlets of the devices in the following studies are always located at the network area.

4.5.2 Agarose-based leaf-mimicking microfluidic device for 3D cell culture

We next fabricated the leaf-mimicking microfluidic devices using cell-containing agarose and examined the growth of HCT116 colon cancer cells in such devices (Figure 44A). Briefly, agarose (2 wt%) was mixed with HCT116 cells in a DMEM culture medium (1×10^8/ml) and used as the hydrogel matrix to fabricate the agarose-based leaf-mimicking microfluidic device. After the device was fabricated, it was then immersed in a 2 ml DMEM culture medium and cultured for 24 hours. In addition, a continuous supply of culture medium through the leaf-mimicking microfluidic channel was applied. We then examined the viability of cells within 200 μm to the channel and found that after 24 hours, cells located at the network area, near the 1st order branches and main vein had a viability of 97 %, 91 %, and 90 %, respectively (Figure 44B). In contrast, cells died rapidly in agarose constructs without the leaf-mimicking microfluidic channels: the overall cell viability dropped to 40 % after 24 hours. Because diffusion-based medium delivery in both devices is approximately the same, the enhanced cell viability in the leaf-mimicking devices suggests that a continuous supply of culture medium and oxygen [244] through the leaf-mimicking microfluidic channel is essential to maintain the cell homeostasis in hydrogel. In addition, the high viability of cells located at different locations of the leaf-mimicking devices implies a relatively homogeneous distribution of culture medium in the hydrogel construct, and thus shows the advantages of leaf-based microvascular network for 3D cell culture. It should be noted, however, that because the leaf used here has approximately a two-dimensional structure, e.g., the thickness of the leaf is much smaller than that of its size, leaf-mimicking microfluidic devices are marginally effective to deliver culture medium in thick hydrogel constructs.

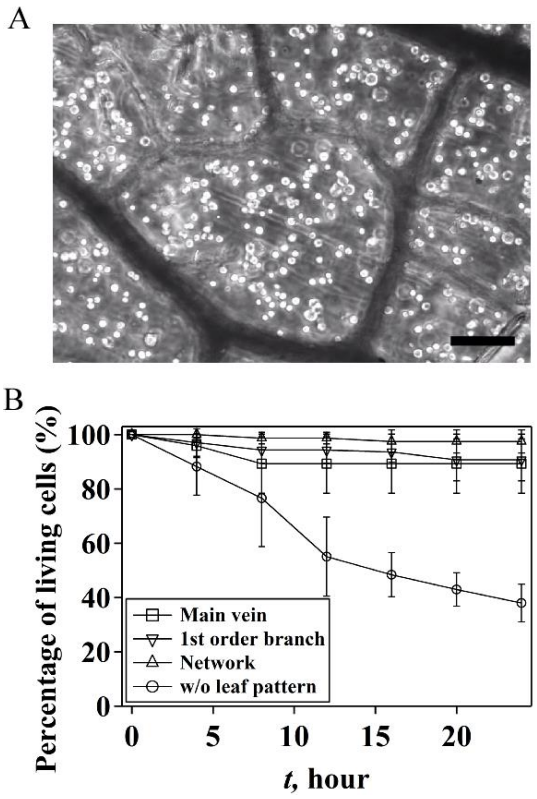

Figure 44 HCT116 colon cancer cells in agarose-based leaf-mimicking microfluidic devices. (A) Image of cultured HCT116 cells in the network area of the leaf-mimicking agarose microfluidic devices. Scale bar: 100 μm. (B) Viability of HCT116 cells cultured near the main vein, the 1st order branch, and the network area.

4.5.3 Theories for developing leaf-inspired artificial microvascular networks

In order to improve the feasibility and controllability of leaf-based microvascular structures for 3D cell culture, we further develop a leaf-inspired artificial microvascular networks (LIAMN). We combine the Murray's law, area preserving assumption, volume filling assumption, and L-system to determine the key parameters that control the patterns of the leaf-inspired microfluidic devices. Specifically, the degree of branching of channels is determined by L-system, which has been primarily developed for description of the branching model of plants [248]. L-system translates generated strings into the derivation of alphabet symbols for illustrating the relationships between plant branches, and thus

allows the generation of complex models by using short numbers as input parameters. For example, a typical approach to generate branches in L-system is ($A \rightarrow AB$) and ($B \rightarrow A$). ($A \rightarrow AB$) means that the parent branch A bifurcates into daughter branches A and B leading to the 1th order of the level increase. ($B \rightarrow A$) indicates that daughter branch B returns to branch A for further bifurcation, without addition of the order level. By repeating the process, complex branching structures with high orders of levels can be generated [248].

The radius of branches at different levels, on the other hand, is determined by the Murray's law and area preserving assumption. Most of branching vasculatures including leaf venations and mammalian circulatory and respiratory systems obey the Murray's law, because maximum flow efficiency is found to occur when the law is obeyed [249, 250]. When flow is laminar and the volumetric flow rate is conserved, Murray's law equalizes the sum of the radii cubed between the parent and bifurcated daughter branches, $\frac{\sum r_{daughter}^3}{\sum r_{parent}^3} = 1$, where $r_{daughter}$ is the radius of daughter branches, and r_{parent} is the radius of parent branches. However, large branches with diameter greater than 1 mm follow closely to the area preserving assumption [251, 252], which states that the sum of the square of the radii of the daughter branches ($r_{daughter}$) equals the square of the radius of the parent vessels (r_{parent}), $\frac{\sum r_{daughter}^2}{\sum r_{parent}^2} = 1$. Area preserving assumption has also been verified by studying the transport efficiency in larger hydraulic architecture like xylem, canopy area, and branches derived from trunk. Therefore, in our study, the area preserving assumption is used when the branch diameter is larger than 1 mm, whereas the Murray's law is applied only for small branches. Last, to determine the length of each branches, we utilize the volume filling assumption, which states that the product of the number of daughter branches and the cube

of their length equals the product of their parent branches, $N_k \times L_k^3 = N_{k+1} \times L_{k+1}^3$, where N_k and N_{k+1} is the number of branches at level k and level k+1, while the L_k and L_{k+1} are their branch length respectively. Assuming the network is composed of identical tubes of equal length, volume filling assumption ensures each of the branch would receive equal supply from the parent branch, and meanwhile maintain a constant flow [253]. This assumption has been found well-fit in trees and shrubs, particularly Angiosperms and Conifers [253, 254].

Based on the principles discussed above, we have constructed a leaf-inspired microfluidic network with five levels of branches (n = 5). The radius (d) and length (l) of each branch (channel) at specific levels are calculated accordingly (Figure 45A and Table 1). In addition, two leaf-inspired microfluidic networks are combined together by connecting channels at the 5th order of the network and form a single microfluidic perfusion system, in which two main veins from each network serve as the inlet and outlet respectively (Figure 45A). Transport efficiency is examined by running the COMSOL simulation, which indicates the flow is not compromised by the designed structures (Figure 46). A single layer of cell-containing agarose replica with thickness of 300 ± 52 μm is then developed using the leaf-inspired microfluidic perfusion system as template. By assembling three pieces of such agarose replica, we are able to construct 3D multi-layer agarose constructs with a thickness about 1 mm (Figure 45B). Bright field image of the cross-sectional area of the constructs shows the microfluidic channels at each layer (Figure 45C).

Although some of the channels are partially collapsed (presumably due to the cutting process), aqueous solution such as fluorescein sodium salt solution can be delivered

throughout the whole construct (Figure 45B). Indeed, when fluorescein sodium salt solution is injected into the 3D construct, we find that not only does the dye solution flow through the vascular structure laterally, diffusion between agarose layers is also observed, e.g., the appearance of blurred fluorescence between layers (Figure 45B). This phenomenon has not been observed in PDMS devices where diffusion of fluorescein into PDMS is negligible (Figure 45D). Because cells encapsulated in the middle of the agarose layer is approximately 150 µm apart from the perfusion channel located at the upper and lower agarose layers, cells can receive oxygen and nutrient from the perfusion channel by diffusion. To verify the diffusion efficiency in such system, a COMSOL simulation was run that proving the culture medium can be delivered through layers and cover the whole structures (Figure 47).

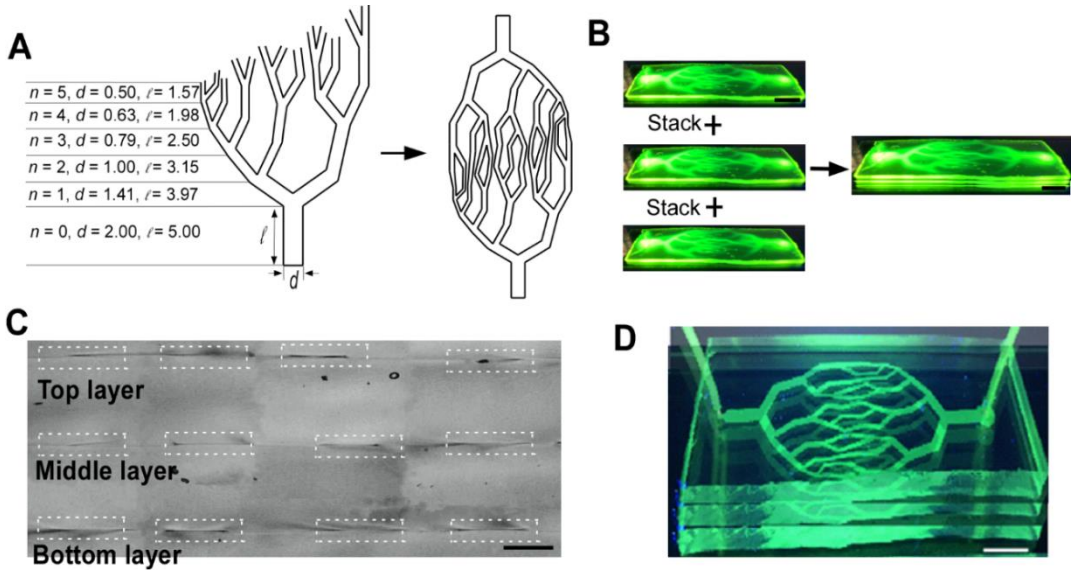

Figure 45 Leaf-inspired microfluidics for 3D cell culture. (A) Schematic of the design of leaf-inspired microfluidics. Unit: mm. (B) Assembly of a three-layer agarose microfluidic device. Scale bar: 2 mm. (C) Image of the cross-sectional view of the assembled three-layer agarose microfluidic device. Scale bar: 200 µm. (D) Image of a three-layer PDMS microfluidic device when fluorescein solution is flowing through the device. Scale bar: 3 mm.

Level (*n*)	Diameter (*d*, mm)	Length (*l*, mm)
0 (main vein)	2.00	5.00
1	1.41	3.97
2	1.00	3.15
3	0.79	2.50
4	0.63	1.98
5	0.50	1.57

Table 1 Calculated parameters of the leaf-inspired branching system. Note that the distances between the smallest branches (5^{th} order branches) are from 400 to 500 μm.

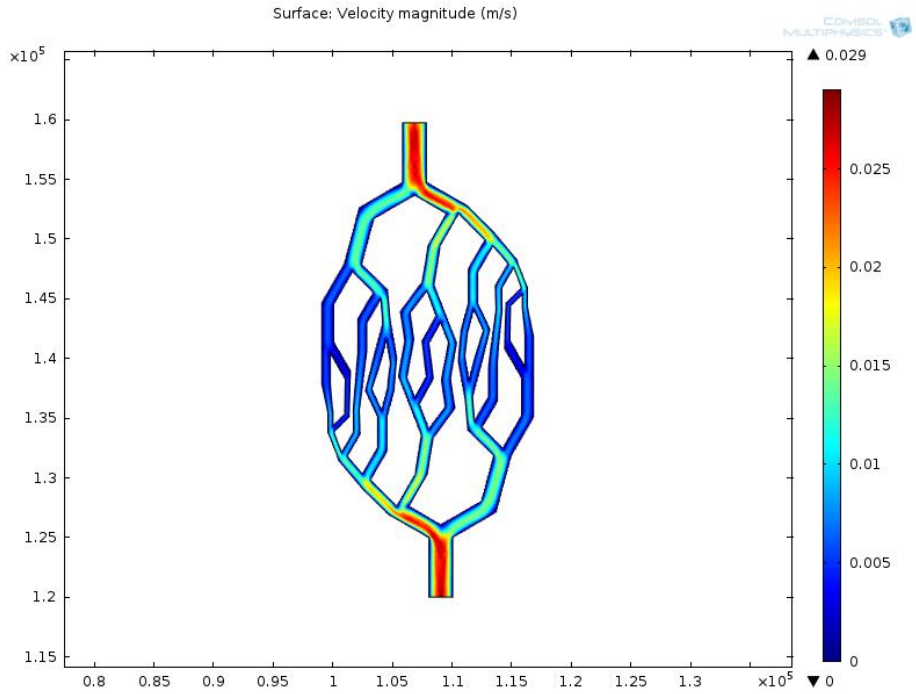

Figure 46 COMSOL simulation of fluid velocity through the LIAMN structures.

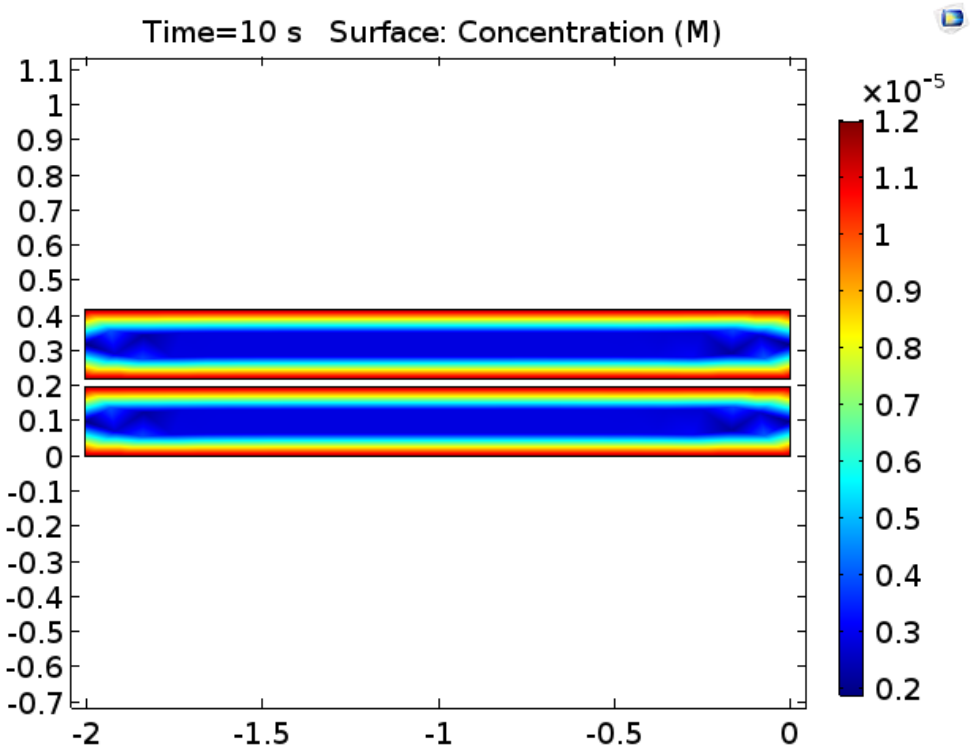

Figure 47 COMSOL simulation of the diffusion model in the thick vascularized hydrogel construct that realized by LIAMN.

4.5.4 Short-term culture of cells in leaf-inspired microfluidic device

As a result, cells cultured in the entire 3D agarose construct will receive supplies by either lateral flow or vertical diffusion. When HCT116 cells are encapsulated in each agarose layer (Figure 48A) and cultured for 24 hours in the stacked agarose constructs, for example, the viability of cells is 72%, 80% and 85% for top, middle, and bottom layer, respectively (Figure 48B), implying that the perfusion system is able to effectively deliver the culture medium to cells at each layer. Note that the cell viability is measured in the area of 3rd-5th order branches but throughout the entire hydrogel construct.

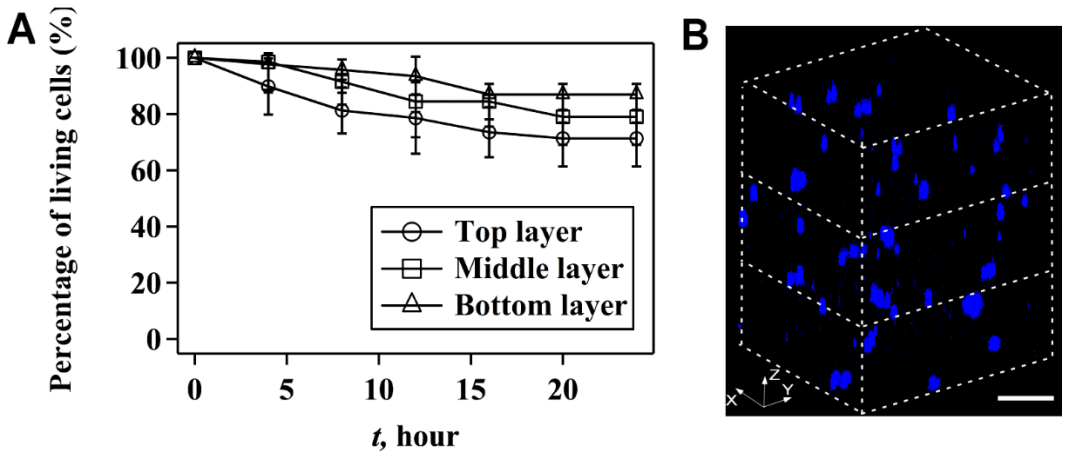

Figure 48 Cell growth in a short-term manner in leaf-inspired microfluidic device. (A) 3D construction of confocal images of HCT116 cells in the three-layer agarose microfluidic device. Cells are stained by nucleus-blue fluorescent dye. Scale bar: 200 µm. (B) Viability of HCT 116 cells cultured in the three-layer agarose matrix.

4.5.5 Long-term culture of cells in leaf-inspired microfluidic device

To examine the feasibility of the developed LIAMN for long-term cell culture, we have monitored the growth of cells inside the 3D agarose constructs for 14 days. Figure 49A shows the distribution of cells in the 3D agarose constructs at the beginning of the culture (day 1). After three days, most of the cells start to divide for proliferation, which can be observed by the increased fluorescent intensity of living cells on day 3 and 9 (Figure 49B and C). Notably, formation of cell spheroids has been observed at day 9 (Figure 49C). Figure 49D shows the cell spheroids stained by actin-green and nucleus-blue. Evidently, nucleus forms cluster whereas secreted actin are mostly surrounding at the edge of the spheroid. Because actin is involved in many cellular processes, such as cell motility, cell division, and maintenance of cell shape [255], the abundant secretion of actin suggests an active cellular response to the 3D environment. At day 14, however, dead cells start to appear, presumably due to the nature of the agarose matrix [210]. Nevertheless, the developed LIAMN system has realized the superiority of microfluidics for nutrient supply

and removal of metabolic waste through the embedding vascular systems and provides a new approach to obtain long-term spheroid culture.

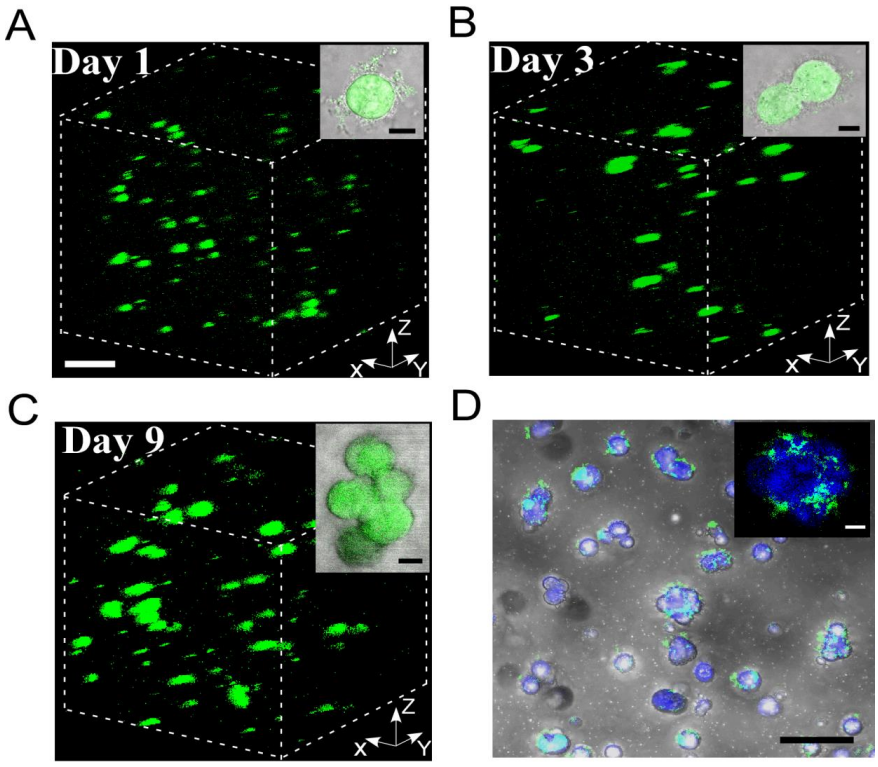

Figure 49 Growth of HCT116 cells in the developed three-layer leaf-inspired agarose matrix. 3D construction of confocal images of HCT116 cells stained with cell Live/Dead assay at day 1 (A), 3 (B), and 9 (C) of culture. Scale bar: 200 µm. Inset: Merged bright-field and fluorescent images of cells at the single cell level. Scale bar: 5 µm. (D) Merged bright-field and fluorescent image of cell spheroids stained with actin-green and nucleus-blue fluorescent dye. Scale bar: 100 µm. Inset: Fluorescent image of a single spheroid. Scale bar: 10 µm.

4.6 Conclusion for Chapter 4

In summary, we have introduced microfluidic approaches of exploiting direct replication of leaf venation and LIAMN for the construction of complex and hierarchical microvascular networks for solving the delivering problem for cell culture in 3D solid matrix. Our approach begins with leaf-mimicking microfluidic perfusion system fabricated via direct replication of leaf venation structures and shows that such perfusion system can maintain high cell viability for short-term 3D cell culture. We subsequently incorporate the

framework of branching models to construct the leaf-inspired microfluidic perfusion systems that support cell growth in 3D hydrogel constructs for at least two weeks. Comparing to the majority approaches of 3D cell culture where highly porous scaffolds have to be used to ensure the diffusion of nutrients to embedded cells, LIAMN not only maintains a high cell viability in less porous agarose gel, but also exhibits desired mechanical property to support hydrogel constructs, which is critical for the construction of artificial organs. Because hydrogel constructs with desired thickness embedded with LIAMN can be constructed by assembling multiple LIAMN hydrogel layers, our strategy using LIAMN as a perfusion system paves a new way to engineering effective vascular transport system for 3D cell culture and the development of functional artificial organs.

Chapter 5. Circulatory Shear Flow Regulates the Viability and Proliferation of Circulating Colon Cancer Cells

Cell dynamics in 3D culture environments not only refer to solid matrix, but can be liquid condition. In this chapter, cell dynamics in 3D flow condition is investigated for understanding the cancer metastasis. In particular, circulating tumor cells constantly experience hemodynamic shear stress in the circulation. Previous efforts have been contributed to investigate the cell dynamics under shear stimulation and general understanding of cell metabolism under shear condition has been acquired. Most of the system being used for testing cell dynamics in shear condition, however, failed to represent the physiological condition, which may cause bias for the knowledge achieved from the studies. Here, a microfluidic approach has been developed to establish a circulatory microenvironment for studying circulating human colon cancer HCT116 cells in response to a variety of magnitude of shear stress and circulating time. The developed microsystem enables addressing several critical factors to mimic the physiological circulatory environment for studying cancer metastasis, including driving force, fluidic pattern, shear stress magnitude and cell status. Cellular responses at both behavioral and molecular level to circulatory shear stimulation are discussed in this chapter. This study provides a new insight to the roles of shear stress in cellular responses of circulating tumor cells in a physiologically relevant model, and hence will be of interest for the study of cancer cell mechano-sensing and cancer metastasis.

5.1 Introduction

Cancer metastasis, a multistep process in which cancer cells migrate or flow from the primary tumor site to a distal location, causes over 90% of cancer-related deaths [201, 256]. Over 50% patients with colorectal cancer, for example, develop distant metastasis, making the colorectal cancer the second leading cause of cancer deaths in the United States [201]. During metastasis, circulating tumor cells (CTCs) are transported through the blood circulatory system and are subjected to hemodynamic forces [257]. Although it is known that fluid shear-forces resulted from the bloodstream cause destructions of CTCs and only a small fraction of CTCs can survive and generate metastasis [256, 258, 259], the effect of circulatory shear flow on the viability and proliferation of CTCs remains elusive.

Recent studies have employed a variety of techniques aiming to understand the cell dynamics under shear condition. In particular, it has been found that shear stress mediates intracellular signaling pathways that are essential to the homeostasis of colon cancer cells. β-catenin/Wnt signaling pathway, which is associated with cell proliferation and cancer development, for example, is inhibited by shear stress [260]. On the other hand, when laminar shear stress is applied to SW480 and HT29 colon cancer cells adhered to a flow channel, the expression of *β-catenin* is inhibited [260]. The inhibition of *β-catenin*, in turn, suppresses cell proliferation and induces cell apoptosis [261, 262]. Similar effects have also been observed in adhered SW620 colon cancer cells [260, 263]. Moreover, the expression of α6β4 integrin, which serves as a mechanosensor in SW620 colon cancer cells, is increased by shear flow [264]. The increased expression of α6β4 integrin activates the PI 3-kinase activity, causing the up-regulation of *Rac 1* expression and the depletion of the active β-catenin [260, 265]. In addition, phosphorylation of *p38*, which is the third

branch of the mitogen-activated protein kinase (MAPK) family and participates in cell shape change and migration [266, 267], increases in SW620 (and SW480) upon laminar shear stress [260]. The activation of p38 results in reorganization of the actin cytoskeleton and induces a robust increase of Dickkopf-1 (DKK1) expression, which is a well-known negative regulator of Wnt signaling [268]. Furthermore, the gene of *GADD45b*, an inhibitor of β-catenin dephosphorylation, is up-regulated by shear stress and induces inhibition of β-catenin signaling [269].

5.2 Motivation

Progress has been made to understand the mechanism of shear stress in the regulation of cancer cells. However, the majority of studies investigate the effects of shear on cells that are immobilized in micro-wells or adhered to microchannels [270-272]. The effect of shear on circulating cancer cells in suspension, however, remains less understood. Approaches, such as cone-and-plate viscometer and stirring bath, have been developed to study the effect of shear on cell suspensions [263, 273, 274]. However, the shear conditions are less physiologically relevant, and thus are marginally effective to evaluate the effect of circulatory shear stress on CTCs. Most importantly, previous studies have mainly focused on cell viability after shear stimulation [270, 273, 275], the proliferation of cells that are survived from shear, which plays an important role in the development of secondary tumors, remains unknown.

5.3 Objective

In this study, a microfluidic circulatory system to study the effect of shear stress on the viability and proliferation of circulating HCT116 human colon cancer cells will be presented. The microfluidic circulatory platform is a close-loop circulating system that consists of a peristaltic pump, connecting tubing, and a microfluidic channel embedded with a constriction. When HCT116 cells are flowing in the developed microfluidic circulating system, they experience periodically low wall shear stresses in the connecting tubing but increased wall shear stress in the microfluidic channel, mimicking the circulation of CTCs in the blood vascular system composed of large vessels and arterioles. By using such system, the viability of HCT116 cells after circulating at different magnitudes of wall shear stress and circulating time will be investigated. The proliferation of HCT116 cells that were survived from the circulation and the expression of critical genes related to the β-catenin signaling, a key regulator of cell proliferation are going to be discussed**.** This study is expected to offer a new insight into the effect of circulatory shear stress on circulating tumor cells in a physiologically relevant model and essential understanding to the core knowledge of cancer metastasis.

5.4 Design and fabrication

5.4.1 Cell culture and maintenance

Human colon cancer HCT 116 cells were cultured in a T-25 culture flask supplied with DMEM (Life Technologies) containing 10% (v/v) fetal bovine serum (FBS) (Life

Technologies) and 1% (v/v) penicillin/streptomycin (Life Technologies) under 37 °C and 5 % CO_2. To prepare the cell suspension, cells were washed by a PBS solution (Life Technologies) and treated with Trypsin (Life Technologies) for 5 min to detach the cell from the culture flask. The cell suspension was then centrifuged and re-suspended in a fresh DMEM supplied with 10% FBS in a concentration of 1×10^8/ml. Because dead cells did not attach on the surface of the culture flask and were washed away by PBS, the viability of cells in the suspension was approximately the same for all experiments.

5.4.2 Microfluidic fabrication and circulation of HCT116 colon cancer cells

The microfluidic circulatory system is shown in Figure 50A, which composed of microfluidic device, tubing, and peristaltic pump. The microfluidic device was fabricated by using the standard soft lithography technique in poly(dimethysiloxane) (PDMS) (Sylgard 184, Dow Corning) as described in previous section. The microfluidic device contains a wide straight channel with 100 μm width and a constriction channel with 800 μm length and 20 μm width (Figure 50B), comparable to the typical size of arterioles [276]. The height of the microchannel is 37 μm everywhere. Two polyethylene tubing (Scientific Commodities Inc, 0.015" (0.38 mm) I.D. × 0.043" (1.09 mm) O.D.) were inserted into the inlet and outlet of the microfluidic device, respectively. A large silicone tubing (Tygon, 0.031" I.D. × 0.094" O.D.) was connected to the ends of polyethylene tubing through adaptors (Qosina) to establish a close-loop circulatory system (Figure 50A). Last, the silicone tubing was wrapped on the rollers of a peristaltic pump that drove the circulation by squeezing the silicone tubing via rotating rollers.

All tubing and microfluidic devices were sterilized by 70% ethanol (Sigma) for 10 min and washed by PBS for all experiments. Air bubbles in the microfluidic system were

removed during the washing steps using ethanol and PBS. The peristaltic pump was sterilized and placed into the incubator with the microfluidic device. No specific channel treatment was conducted in the experiment. 1.5 mL HCT116 cell suspension (1×10^8/ml) was injected into the microfluidic circulatory system through the polyethylene tubing connected with the inlet of the microfluidic device. The flow rate of circulation was controlled by changing the rotating speed (revolution per minute (rpm)) of the roller in the peristaltic pump. A peristaltic speed of 0.1, 0.5 or 1.0 rpm was used. The calculation of shear stress at each location in this microfluidic circulatory system is shown in Table 2.

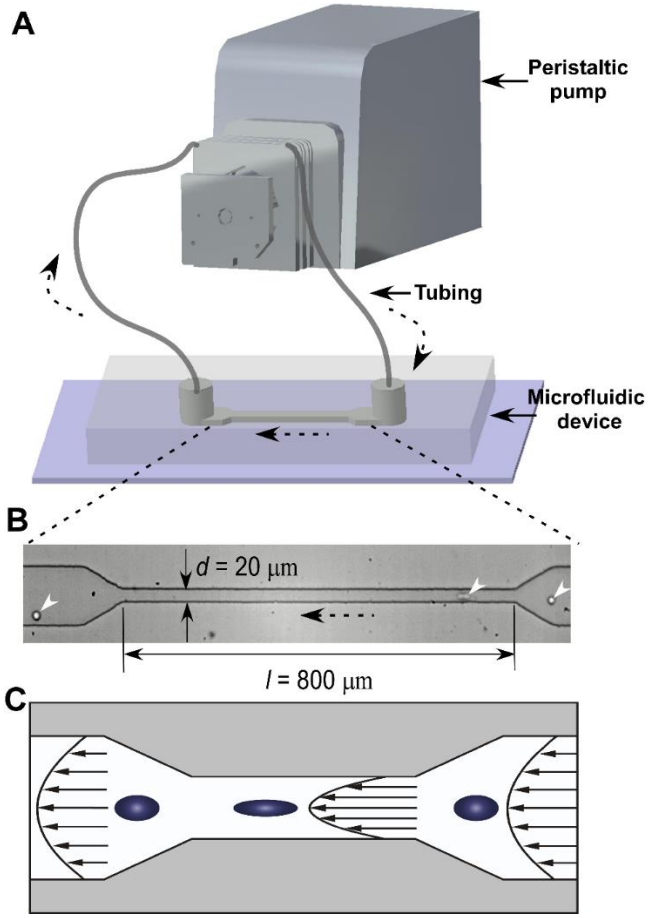

Figure 50 Circulation of cells in microfluidic platform. (A) Schematic of the microfluidic facility for cell circulation. (B) A typical microscopic image of cells flowing through the constriction in the microfluidic device. (C) Schematic illustration of the elongation of circulating cancer cells when passing through the constriction due to increased shear stress.

Calculating parameter	Value
Viscosity (μ)	$1 \times 10^{-3}\text{Pa} \cdot \text{s}$
Volume flow rate (Q) for 0.1 rpm	$2.5 \times 10^{-10}\ \text{m}^3/\text{min}$
Volume flow rate (Q) for 0.5 rpm	$1.9 \times 10^{-9}\ \text{m}^3/\text{min}$
Volume flow rate (Q) for 1.0 rpm	$4.3 \times 10^{-9}\ \text{m}^3/\text{min}$
Width of the constriction channel (w)	20×10^{-6} m
Height of the constriction channel (h)	30×10^{-6} m
Width of the wide microchannel (w)	100×10^{-6} m
Height of the wide microchannel (h)	30×10^{-6} m
Inner diameter of the tubing (d)	3.8×10^{-4} m
Approximate average shear stress in the constriction channel	
(τ_c)	$3.5\ \text{dyn}/\text{cm}^2$
0.1 rpm	$26.9\ \text{dyn}/\text{cm}^2$
0.5 rpm	$60.5\ \text{dyn}/\text{cm}^2$
1.0 rpm	
Approximate average shear stress in the wide microchannel	$0.46\ \text{dyn}/\text{cm}^2$
(τ_w)	$3.56\ \text{dyn}/\text{cm}^2$
0.1 rpm	$8\ \text{dyn}/\text{cm}^2$
0.5 rpm	
1.0 rpm	$0.0077\ \text{dyn}/\text{cm}^2$
Approximate average shear stress in the tubing (τ_t)	$0.06\ \text{dyn}/\text{cm}^2$
0.1 rpm	$0.13\ \text{dyn}/\text{cm}^2$
0.5 rpm	
1.0 rpm	

Table 2 Calculation of average wall shear stress in the microfluidic system. Note that τ_c and τ_w are calculated based on the equation $\tau = \frac{\mu Q}{w^2 \times h}$, whereas τ_t is calculated based on the equation $\tau = \frac{32\,\mu Q}{\pi d^3}$.

5.4.3 Determination of cell viability and growth after circulation

To analyze cell viability immediately after circulation, we collected cells from the microfluidic circulatory system and allowed cells to sediment to the surface of petri dish (~1 hour). Cell viability was then determined by using the Live/Dead assays (Life Technologies) following the manufacture's protocol. Images of cells stained with Live/Dead assays were analyzed using a confocal microscope (Leica Microscope, SP5). To monitor the growth of cells that were survived after circulation, cells were collected in a petri dish supplied with a DMEM culture medium and allowed to settle for 2 hours in an on-stage incubator with 37 °C and 5% CO_2. Cells that were survived after circulation could adhere on the surface of the petri dish. The growth of survived cells was recorded by a camera (C10600-10B-H, Hamamatsu) mounted on a fluorescence microscope (Leica Microsystems, DMI 6000) for 16 hours. Time-lapse videos of adhered cells were used to analyze the rate of cell growth. The number of cells was measured every 2 hours.

5.4.4 Quantitative real-time PCR

Total RNA was extracted from circulated cells using TRIzol reagent (Invitrogen, Grand Island, NY, USA). The RNA integrity was verified by electrophoresis. RNA reverse transcription was performed using the iScript cDNA synthesis kit (Bio-Rad, Hercules, CA, USA) according to the manufacturer's protocol. The RT cDNA reaction products were subjected to quantitative real-time PCR using CTFX 96 Real-time system (Bio-Rad, Hercules, CA, USA) and SYBR green supermix (Bio-Rad, Hercules, CA, USA) according to the manufacturer's protocol. The primers are listed in Table 3. All expression levels were normalized to β-actin levels of the same sample. Percent expression was calculated as the

ratio of the normalized value of each sample to that of the corresponding untreated control cells. All real-time PCR reactions were performed in triplicate.

Gene name	Primers
β-actin F	AGAGCAAGAGAGGCATCCTC
β-actin R	CTCAAACATGATCTGGGTCA
β-catenin F	AAAATGGCAGTGCGTTTAG
β-catenin R	TTTGAAGGCAGTCTGTCGTA
Bmi 1 F	AGCAGAAATGCATCGAACAA
Bmi 1 R	CCTAACCAGATGAAGTTGCTGA
c-myc F	ACAGCTACGGAACTCTTGTGC
c-myc R	GCCCAAAGTCCAATTTGAGGC
GSK-3β F	GGAACTCCAACAAGGGAGCA
GSK-3β R	TTCGGGGTCGGAAGACCTTA
P53 F	CCCAAGCAATGGATGATTTGA
P53 R	GGCATTCTGGGAGCTTCATCT

Table 3 Primers used in real-time PCR measurement.

5.4.5 Statistical analysis

Each set of the experiment was repeated for at least three times with more than 100 cells being measured. The error bar was presented as the standard deviation of the mean for all trials. Data sets were plotted using the software of Igor Pro (Wave Metrics, Inc). A two-tailed paired *t*-test was used for the analysis of cell viability, cell proliferation and PCR results. The comparisons between two groups with $P<0.05$ are considered significant.

5.5 Results and discussion

5.5.1 Cell viability in response to shear stimulation

We developed a microfluidic system that was composed of a peristaltic pump, silicone tubing, and a microfluidic device with a constriction channel to study the effect of periodic circulatory shear stress on circulating HCT116 colon cancer cells (Figure 50A). Wall shear

stress was calculated based on the peristaltic speed of circulation and the geometry of microfluidic channel (Table 2). Particularly, cells circulating at 0.1 rpm were subjected to a wall shear stress of approximate 3.5 dyne/cm^2 at the constriction and 0.46 dyne/cm^2 in the wide channel (Figure 50C), which were close to the physiologically relevant shear conditions in venous circulation (0.5-4 dyne/cm^2) [277]. Circulation at 0.5 rpm provided a wall shear stress of 26.9 and 3.56 dyne/cm^2 for the constriction and wide channel respectively, close to the wall shear stress in arterial circulation (4-30 dyne/cm^2) [277]. The speed of 1.0 rpm, generated relatively high wall shear stresses at both of the constriction (60.5 dyne/cm^2) and wide channel (8 dyne/cm^2). It should be noted that due to the complex pulsatile three-dimensional flow in the microfluidic circulatory system, quantitative identification of local shear stresses near single circulating cells is experimentally challenging [278]. The calculated wall shear stress thus represents approximate average shear values in flow and cannot be treated as definitive shear stress experienced by single cells.

To study the effect of shear and circulating time on the viability of HCT116 colon cancer cells, we circulated the cells in the microfluidic circulatory system at different peristaltic speeds (rpm) and circulating time. The results showed that, at a constant peristaltic speed, cell viability decreased with the increase of circulating time (Figure 51A). 2 min circulation at 1.0 rpm, for example, barely affected the cell viability (Figure 51B), whereas significant cell death was found when cells were circulated for 20 h (Figure 51C). The results are consistent with previous studies in which cell viability decreases with increased duration of applied shear [275, 279]. On the other hand, when the circulating time was kept constant, the effect of peristaltic speed on cell viability (comparing to

control) was not significant for circulating time of 2 min and 10 min (P>0.05, Student's t-test, except rpm = 0.5 for circulating time 10 min). When the circulating time increased to 1 h, 2.5 h and 20 h, however, cell viability increased with the increase of peristaltic speed.

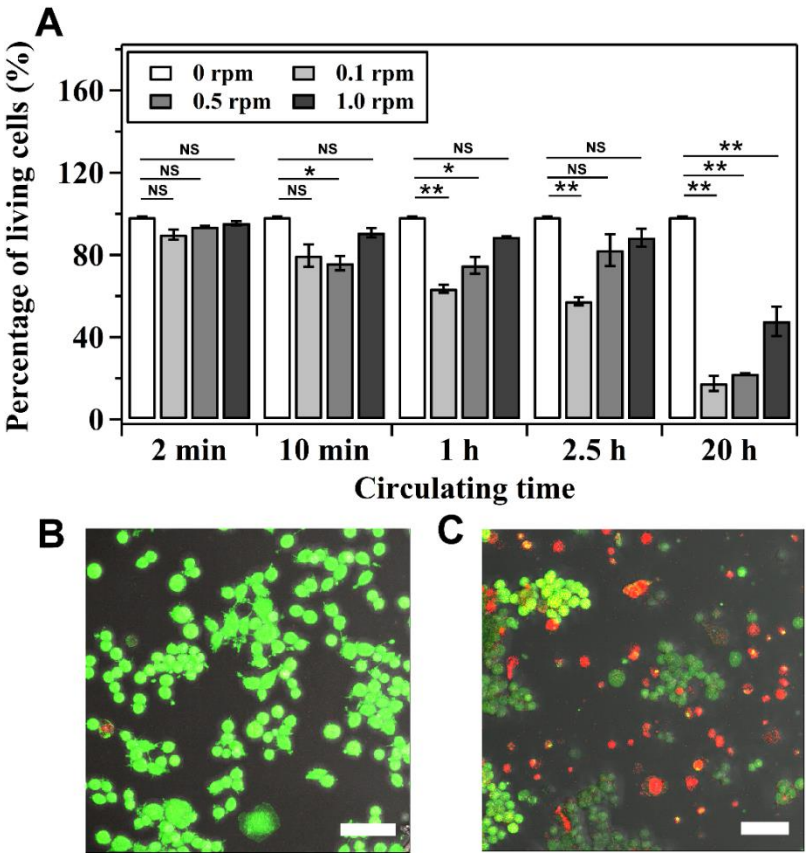

Figure 51 Effect of shear on the viability of circulating HCT116 cells. (A) Percentage of living cells in various shear conditions in the microfluidic circulatory system. Fluorescent images of cells stained with Live/Dead assay after circulation at flow rate of 1.0 rpm for (B) 2 min and (C) 20 h, respectively. Scale bar: 50 μm.

5.5.2 Cell proliferation in response to shear stimulation

Next, we cultured cells that were survived from the microfluidic circulatory system for 16 hours and monitored the cell growth. The effect of circulating time on cell growth was studied using cells that were circulated at a constant peristaltic speed (0.1 rpm) (Figure

52A). Comparing to the viability of control cells (145%), viability of cells circulated for 2 min and 10 min was not significantly different with control (cell viability was 133% and 125% for cells circulated for 2 and 10 min respectively, $P>0.05$). The results suggested that, for a short duration of applied shear stress, cell proliferation was not compromised significantly. Cells experienced 1 h and 2.5 h circulation showed the viability of 106 % and 94 % respectively, indicating that cell proliferation was affected by the circulation. Long-term circulation (20 h), however, resulted in a significant ($P<0.01$) decrease of cell viability (65 %).

When the circulating time was constant (1 h), the proliferation of survived cells was also negatively affected by the peristaltic speed. The percentages of living cells after 16 h culture, for example, were 106 % and 123 % for cells treated with 0.1 and 0.5 rpm respectively (Figure 52B). Significant ($P<0.01$) decrease of the cell proliferation (38 %) was observed when cells were treated with 1.0 rpm circulation. Thus, cell proliferation decreased with the increasing peristaltic speed, although high cell viability at increased peristaltic speed was observed in Figure 51A.

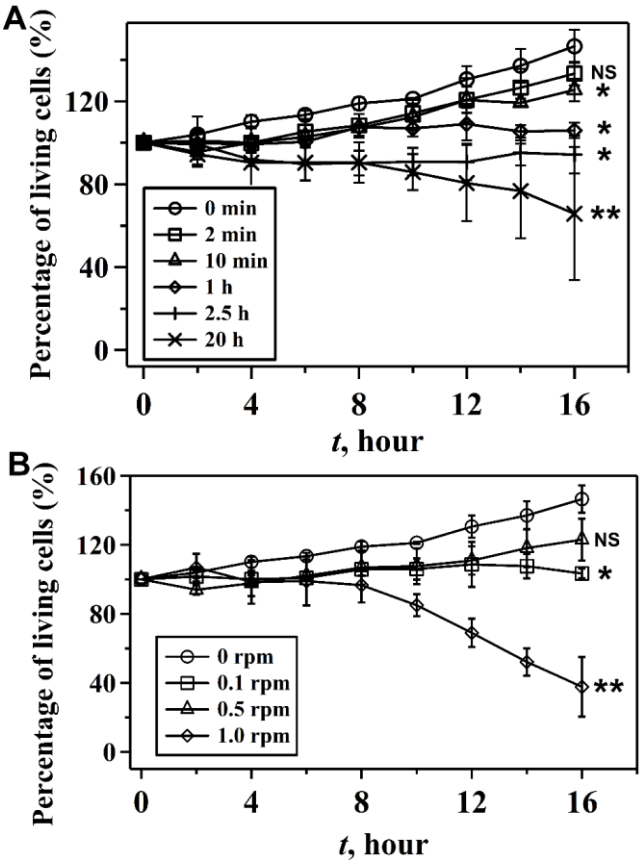

Figure 52 Effect of shear on the proliferation of survived HCT116 cells after circulation for (A) different durations and (B) shear conditions.

5.5.3 Expression of critical genes related to β-catenin signaling in response to shear stimulation

Because β-catenin plays significant roles in cell cycle, proliferation and apoptosis [280], we further studied the expression of β-catenin at the mRNA level in response to shear stimulation (Figure 53A). The real-time PCR results showed that, comparing to control, shear stress always induced increased mRNA expression of β-catenin. Long time (20 h) circulation at constant wall shear stresses decreased or did not affect significantly the expression of β-catenin comparing to that of short term circulation (2.5 h). At a constant circulation time, β-catenin expression increased with the increase of the magnitude of wall

shear stress. The increased expression of β-catenin with shear was opposite to previous studies where β-catenin/Wnt signaling pathway was inhibited by shear stress when cells were immobilized on surfaces [260, 263].

To further understand the effects and regulation of β-catenin expression, we measured the expression of Bmi1, c-myc, and glycogen synthase kinase 3β (GSK-3β), as the regulator of β-catenin's stability. Our results showed that significant ($P<0.05$) increase of expression of both Bmi1 and c-myc was observed at high wall shear stress (Figure 53B). Because Bmi1 and c-myc were known as the downstream targets of the β-catenin signaling pathway, increased expression of β-catenin led to the increased expression of both Bmi1 and c-myc at high magnitude of wall shear stress. On the other hand, GSK-3β is responsible for the degradation of β-catenin and negatively regulates β-catenin expression [281]. In our experiments, expression of GSK-3β was ($P<0.05$) promoted by high wall shear stress. P53 is also known to regulate cell apoptosis, proliferation and responses to stresses [282]. However, no significant ($P>0.05$) effect of high shear on the expression of p53 was observed (Figure 53C).

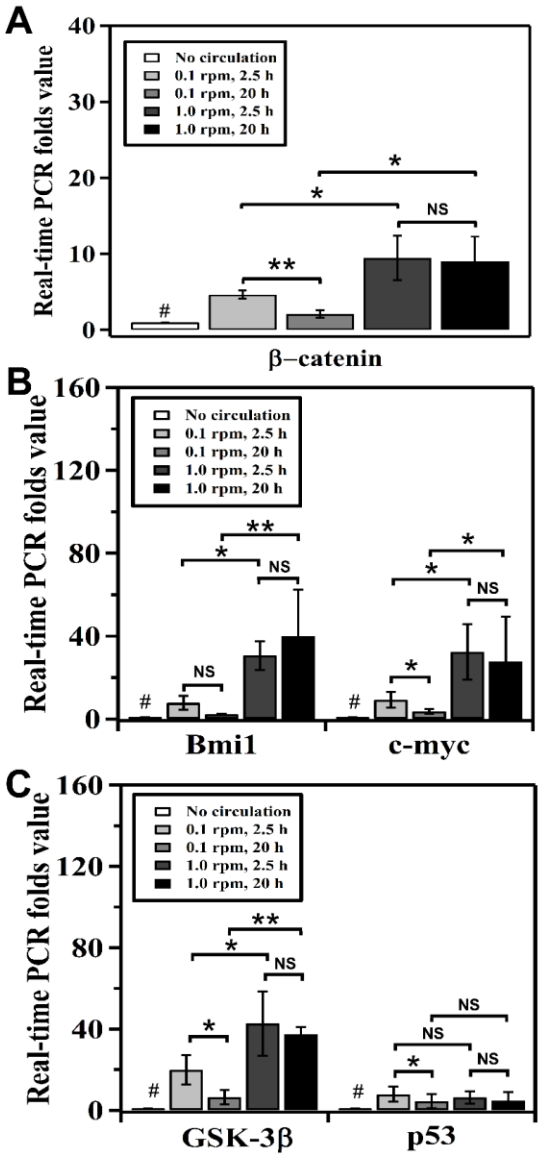

Figure 53 Effect of shear on the mRNA expression level of (A) β-catenin, (B) Bmi1 and c-myc, and (C) GSK-3β and p53 mRNA in HCT116 cells circulated at speeds of 0.1 and 1.0 rpm for 2.5 h and 20 h respectively.

5.5.4 Correlation between cellular behavior and gene expression

Although the influence of shear stress on the growth of adhered colon cancer cells has been reported previously [270-272], the effect of shear stress on circulating colon cancer cells remains less understood. Here, we demonstrated a microfluidic circulatory system to closely mimic the physiologically relevant shear conditions in circulation and showed that

the viability, proliferation, and gene expression of circulating HCT116 cells depended significantly on the circulatory wall shear stress and circulating time.

We showed that when wall shear stress was kept constant, cell viability decreased with increasing circulating time (Figure 51A). The results were consistent with previous studies on other cell lines [283, 284] and can be explained by the observed expression of β-catenin in Figure 53A, in which the expression of β-catenin decreased with increased circulating time (from 2.5 h to 20 h). Remarkably, HCT116 colon cancer cells had high cell viability when experiencing high magnitude of wall shear stress (Figure 51A) and the expression of β-catenin was also increased with shear (Figure 53A).

The results of increased cell viability and β-catenin expression at high shear, however, are surprising because previous studies showed that the viability of cells (such as SW480, HT29, and SW620 colon cancer cells) decreased with increased shear and β-catenin expression was inhibited upon shear stimulation [260, 261, 264, 265, 267-269]. These studies, however, were based on cells that were adhered on surfaces and, thus, the shear condition in which cells were experienced was different with our current setup. This may cause different regulation mechanisms in terms of intracellular signaling. During circulation in suspension, for example, the role of adhesive molecule, such as α6β4 integrin that was promoted by shear flow in adhered SW620 colon cancer cells [260],[264], became not significant. Because α6β4 was able to activate the expression of p53 that enhanced the degradation of β-catenin, the non-activated expression of p53 due to the lack of activation of α6β4 would not be able to degrade β-catenin [285]. Indeed, our data showed that p53 expression was not significantly affected by wall shear stress (Figure

53C). We speculate that β-catenin expression was not compromised by shear stimulation in our experiments (Figure 53A).

In addition, the circulation in our microfluidic system generated a periodic non-constant shear stress, which was known to be able to affect cellular behavior and intracellular signaling differently, compared to constant laminar shear stress [286-288]. From the investigation of osteocytic cells, for example, periodic shear stress was found to be able to activate the secretion of Prostaglandin E_2 (PGE2) in a more effective manner than constant flow [289]. Enhancement of PGE2 signaling could then promote the Akt-mediated phosphorylation of GSK-3β, improving the translocation of β-catenin to nucleus. In addition, when human umbilical vein endothelial cells were treated by periodic flow conditions, the vasodilator nitric oxide synthase mRNA was found to be significantly up-regulated comparing with steady shear stress at the same magnitude[290]. Therefore, it was also possible that the expression of β-catenin in HCT116 colon cancer cells preferred a periodic non-constant shear condition to a constant flow. In fact, we showed an increased expression of Bmi1 and c-myc at high circulatory shear stress that was known to enhance the nucleus translocation of β-catenin. However, it should be noted that although we observed high cell viability at high shear, proliferation of survived cell decreased with the increase of shear, suggesting that intracellular functions regulated by the β-catenin signaling pathway were significantly disrupted by the shear stimulation. Note that concentration of circulating cells did not affect significantly cell viability immediately after circulation but had an influence on the proliferation of survived cells (Figure 54). Nevertheless, HCT116 cells were still able to survive in circulation at 0.1 and 0.5 rpm that

had physiologically relevant shear conditions (wall shear stress ≈ 4-30 dyne/cm^2) for at least 1 hour and proliferate. The underlying mechanisms remain to be determined.

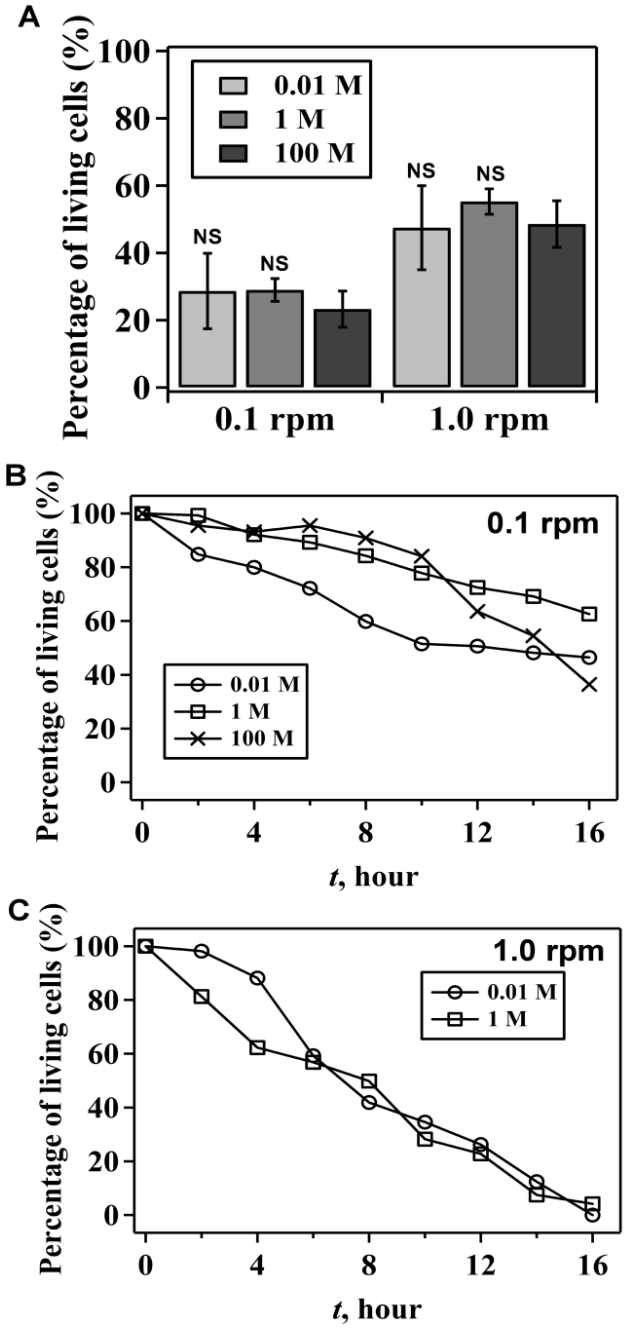

Figure 54 Effect of concentration of circulation cells on cell viability and proliferation. (A) Immediate cell viability after cells circulated for 20 h with an initial cell concentration of 0.01, 1, or 100 M cells/ml. The circulation speeds were 0.1 and 1.0 revolution per minute (rpm). (B) and (C) are proliferation of cells survived from 20 h circulation at 0.1 rpm and 1.0 rpm respectively.

5.6 Conclusion for Chapter 5

In summary, a microfluidic system has been developed to study the cell dynamics in 3D liquid flow condition and the effect of periodic circulatory shear stress on circulating HCT116 cells. Cell viability decreased at long circulating time but increased at high magnitude of wall shear stress. We showed that the expression of β-catenin increased at high wall shear stress. The increased expression of β-catenin and cell viability was probably due to the circulatory shear conditions that could lead to different intracellular signaling pathways comparing to constant laminar shear stress experienced by adhered cells. Proliferation of cells survived from circulation could be maintained when cells were circulated at physiologically relevant conditions, but decreased at increasing wall shear stress and circulating time. The current study thus revealed a previously unrecognized role of circulatory shear stress on CTCs and contributed to the acquaintance of shear stimulation on CTCs *in vivo*. In addition, the developed microfluidic approach that could create physiologically relevant microenvironments of CTCs in circulation offered potential techniques to develop model systems for the study of attachment and invasion of CTCs during circulation and cancer metastasis.

Chapter 6. Conclusion and Future Opportunities

3D artificial biological architecture becomes a remarkable platform for cell biology and biological applications. The 3D culture system is desirable to compose of cell culture zone, 3D surrounding matrix, delivering system, and addition of necessary factors, such as gradient zone, growth factors, and cellular cross-communication. It was demonstrated that formation of tissue structures, cellular communication and drug orientation can be accomplished through using developed 3D culture platform. In addition, organ-on-chip technology could be researched based on the knowledge acquired from 3D cell culture. In order to obtain understanding of cell dynamics, this research is aiming to create a physiologically relevant environment to investigate cell dynamics in 3D culture environments including solid and liquid matrix. The developed 3D culture system employed lithography, microfluidics, 3D printing technique, hydrogel system and bacteria to fully mimic the *in vivo* cell growth environment, which enables cells performing physiological structure and functions. This chapter summarizes the present research on 3D culture environment for understanding cell dynamics and contributions of the development of long-term sustained cell culture and potential platform for drug development. The chapter also concludes the dissertation by highlighting some future opportunities.

6.1 Research Summary

The increasing utilization of 3D system for cell culture has turned the development of artificial physiologically relevant culture system into a necessary task to complete, because it provides new perspective to understand the cell dynamics, opens new avenue to tissue engineering and cell biology. On the other hand, the advance in 3D culture environment enables research to reveal the knowledge behind the disease and cancer, and thus contributes to the biomedical therapeutics. By incorporating multifunctional technologies, in this research, construction of 3D artificial physiologically relevant culture system that could address critical *in vivo* influencing factors was introduced for investigating cell dynamics and cancer mechanism at both cell behavioral and molecular level. The developed 3D culture system can overcome the limitations of conventional method for addressing multifunctional factors and enables sustaining 3D cell culture with realization of cell proliferation, formation of spheroid and reaction to stimulator.

The current development of cell culture has been reviewed in Chapter 1, leading to the motivation behind this dissertation and the objective to develop physiologically relevant culture systems for cell biology and biomedical applications. This dissertation aims to contribute the filling of the gap of the knowledge, and provides effective alternatives to achieve tissue engineering and the development of artificial organs.

In Chapter 2, production of 3D cell-laden hydrogel microparticles through microfluidics was accomplished in an oil-free environment using a PFP oil system and an evaporation approach. Cell dynamics was investigated without oil influence and showed differences from 2D culture environments regarding to cell cycle, survival and response to inflammatory treatment. Comparing to a 2D monolayer culture system, cell cycle was

found to be prolonged in 3D microparticles and cells became more susceptible to the TNF-α stimulation, emphasizing the necessary role of 3D matrix in realizing *in vivo*-like cell dynamics. This study is also believed to provide a better alternative to generate cell-laden microparticles, which could be used as micro-bioreactors to test drug efficacy, multi-type of cell communication and tumor development.

A significant improvement of the 3D culture environments was exhibited in Chapter 3, where a 3D printing hydrogel tubular structure was created to mimic the physiological bowel environment for studying colon cancer cell dynamics in 3D solid matrix. This study emphasizes the role of biomaterials in building 3D structures and maintaining cell dynamics. Different types of hydrogel were characterized with their mechanical properties and biocompatibility for supporting cell dynamics. Different aspects of cell dynamics including cell cycle, cell survival and cell interaction with 3D matrix and bacterial were revealed and the necessary role of vascular delivering system was highlighted.

Chapter 4 presents a novel study for creating an effective delivery system with hierarchical structures in 3D solid culture environments, inspired by leaf skeletal architectures. Microfluidic technique was involved to fabricate the leaf-mimicking device using a real leaf, in which improved cell growth was observed. On the other hand, leaf-inspired artificial microvascular network model was designed through applying Murray's law, Volume filling assumption and L-system, which determine the parameter of the vascular structures. Vascularized thick hydrogel constructs could be built and effective delivery of fluid was observed in such system. Sustained cell culture and formation of spheroid structures were achieved during the long-term culture test. The present study

overcomes the limitation of delivering function in conventional 3D culture method that may lead to cell necrosis, and serves as a novel and effective platform to explore long-term tissue culture and drug delivery and toxicity characterization.

Apart from investigating the cell dynamics in 3D solid matrix, cell metabolism in 3D liquid environment was studied in Chapter 5. An artificial circulatory system was created by using microfluidics and cell dynamics responding to circulatory shear stimulation was exhibited. Cell survival, cell cycle and gene expression were found being significantly regulated by shear stress, and a previously unrecognized role of shear stress was revealed due to the physiologically relevant condition of blood circulation, which is believed to contribute to the core knowledge of cancer metastasis.

In summary, cell dynamics in 3D culture environments, including solid matrix and liquid matrix, was investigated, in which physiological conditions in human body were mimicked. Improvement of biological system and approach has been achieved, in which critical *in vivo* influencing factors have been addressed to understand the cell dynamics in different environments. Various aspects of cell dynamics, including cell survival, cell cycle, formation of spheroid and gene expression responding to external stimulation have been revealed.

6.2 Key contributions

This dissertation is aiming to develop artificial *in vitro* biological toolboxes that could closely mimic the physiological *in vivo* environment for 3D cell culture. In Chapter 2, we developed 3D cell-laden hydrogel microaprticles without the negative effect of the

remaining oil on cell dynamics and identified the roles of 3D matrix in regulating cell cycle, survival and sensitivity to inflammatory environment. Such cell-laden hydrogel microparticles could serve as a basic unit to study tissue growth, tumor formation and the testing of drug efficacy. Each cell-laden particle works as a single bio-reactor and can provide the feedback during biological testings. Moreover, the cell-laden particles could also be applied as the building blocks for a bottom-up approach, such as 3D printing, to construct a well-controlled 3D system in both micro- and macro conditions. Therefore, the complex structures for mimicking organs could be created while maintaining a well-controlled microenvironment inside the cell-laden particles.

We also developed a 3D hybrid hydrogel cell-laden tube system via 3D printing to mimic human bowel environment (Chapter 3). 3D printing approach is more advantageous over other methods, because it can provides extraordinary controllability during the structure design, distributing cells, and bioink deposition. The system developed in this study not only satisfies the mechanical requirement for building 3D tube structures, but also meets the biological needs for realizing cell dynamics. A broader understanding of 3D bioprinting, hydrogel constructs, and cell-matrix interaction is acquired, providing the knowledge for engineering physiologically relevant systems. Interaction between cell and Salmonella bacterial uncovers the knowledge behind the bowel inflammation. Moreover, this 3D printed hydrogel system possesses effective 3D matrix interactions, spatial orientation and structural properties and could serve as the cornerstone to study the mechanism of ISCs and intestinal tissue. Such research will be promising to both engineering and biomedical strategies that will allow the construction of artificial colon organ.

In Chapter 4, a top-bottom approach is developed for engineering the vascular delivering system in 3D culture environment, using leaf vein structures. Results showed that the hydraulic transport of such vascular system was efficient and water could be distributed throughout the whole construct. An artificial vascular network, LIAMN, is also designed to mimic the leaf vein and blood vessel structure for feeding the cells in 3D environments. However, this approach is not typical top-bottom, because it take advantages of the hierarchical structures of leaf vein to engineer a vascularized hydrogel construct. A strong supportive role in long-term 3D cell growth is revealed, indicating this approach is an effective alternative to solve the delivering problem in 3D cell culture. Apart from the contribution to tissue engineering and artificial organ construction in future opportunity, this system could also be explored for the drug testing platform.

Last, the severity of cancer metastasis has been recognized by clinical study, but the mechanism of cancer transport has not been fully understood. The study shown in Chapter 5 creates a bottom-up approach by using microfluidics. An artificial circulatory system is constructed to closely mimic the blood circulation in human body and investigate the cancer circulation in a well-controlled manner. Several key factors of blood circulation, including periodic change of non-constant shear condition, physiological level of shear stress and cell transport in suspension have been simulated. Cell dynamics in 3D liquid flow environment, such as cell cycle, survival and gene expression responding to shear stimulation has been revealed in comparison with other works, and previously un-recognized role of shear stress in regulating cell dynamics is discussed in Chapter 5. Such developed system not only uncovers the knowledge of cancer metastasis, but can be

explored for understanding the dynamics of red blood cells, sickle cells, mechanism of ATP realizing and blood-related diseases.

6.3 Future opportunities

The present research in this dissertation provide fundamental knowledge and strategies of creating physiologically relevant environment for 3D cell culture mainly by using microfluidics and 3D printing technique, based on which the following directions could be followed up.

6.3.1 3D Bioprinting ICSs for the development of a functional colon

In human intestine, a crypt-villus structure is presented with the cover of an intestinal mucosa layer, which is composed of an epithelium layer of cells, the lamina propria, and the muscularis mucosae[6, 291]. The cells of the epithelial layer joined with each other through tight junctions, forming a contiguous and relatively impermeable membrane. Such structure serves as an intestinal barrier that protects the intestinal tissues from external stimulation including shear flow, bacterial and mechanical impact, as well as ensures the proper nutrient uptakes. The function of intestine is maintained through the continuous renewal of the epithelial layer, which is arise from the intestinal stem cells (ISCs).

ISCs in intestinal crypts play a critical role in maintaining the vigorous proliferation of intestinal epithelium [202, 203]. Impaired activity of ICSs was found to correlated with colorectal cancer [204, 205]. Acquisition of the ability to modulate ISCs in a well-controlled microenvironment becomes attractive for both fundamental research of stem

cells and clinical applications. Development of *in vitro* culture systems to sustain the growth and differentiation of ISCs, however, is challenging and in part is because of the loss of physiologically relevant 3D architecture of the tissue and preservation of epithelial viability is difficult [206, 207].

Because 3D printing is a bottom-up approach and provides extraordinary spatial control over the position of cells along printed structures, and effective 3D culture system has been validated in this dissertation. Hybrid hydrogel tube is 3D printed for creating a stable intestinal structure-like system, while realizing a proper cell dynamics. Therefore, the 3D constructs that closely mimic the *in vivo* microenvironments of ISCs niche can be potentially produced via 3D printing ISCs-laden hydrogel. Possible vascular structures embedded in the 3D construct could be possible to create, which is expected to delineate the regulatory roles in the homeostasis of ISCs and construct an intestinal epithelial lining. In such system, proliferation and differentiation of ISCs in 3D hydrogel construct is available to be characterized, and hence setting the stage for clinical testing of such therapeutic strategies.

The successful completion of this opportunities will contribute a missing, fundamental element to our basic knowledge of ISCs, without which the long-term culture of ISCs for tissue engineering and ISCs-based therapy can hardly be achieved. Therefore, a fundamental colon epithelial lining could be expected to be produced in a well-controlled manner, resulting in a new and innovative approach to study intestinal function and the treatment of digestive diseases. Such study are expected to have a critical impact, because in addition to fundamentally advancing the fields of stem cell and cancer cell research, the proposed study is highly likely to provide new approaches for therapeutic interventions.

6.3.2 Microfluidically 3D printing construct composed of cell-laden microparticles

Microfluidics is known as its extraordinary controllability over fluid and generation of cell-laden microparticles, whereas 3D printing provides excellent spatial control over the 3D construction. In order to engineer a well-controlled system at both macro- and microenvironment for accomplishing tissue culture and organ assembling, combining the advances of microfluidics with the advantages of 3D printing techniques could be a promising alternative. In such system, cell unit could be patterned into precise location and express cellular function in each micro-bioreactors, whereas the whole architectures could be constructed to mimic the organ structures. Hence, a physiologically relevant condition is expected to be created at both macro- and microenvironments, which has not been reported at current stage.

The possible method to accomplish this opportunity is using the cell-laden microparticles generated from microfluidics as bioinks for 3D printing, which could be realized by mounting the microfluidic device on the printing head of 3D printer. Such experimental setup would enable producing cell-laden microparticles at high throughput rate for generating bioinks, while printing the cell-laden microparticles into 3D architectures with extraordinary spatial control for mimicking organ structures. Because cells encapsulated into microparticels are physically isolated from surrounding environment and serve as a basic biological unit for cell proliferation, differentiation and formation of tissue or tumor. The capability of encapsulating cells in microparticles and cell dynamics in such environment have been discussed in previous section, which has already provide fundamental technology to achieve this idea. On the other hand, HCT116 colorectal cancer cell-laden tubular structures have been demonstrated to be printed by 3D

printer through using hybrid hydrogel, in which cells performed *in vivo* structures and functions. The printing techniques, rheology testing of hybrogel, cell dynamics and bacterial interaction have been characterized that provides fundamental knowledge to proceed to further step. Therefore, it is possible to accomplish the construction of artificial functional organ through using the developed techniques.

Chapter 7. References

[1] L. Vermeulen and H. J. Snippert, "Stem cell dynamics in homeostasis and cancer of the intestine," *Nature Reviews Cancer,* vol. 14, pp. 468-480, 2014.

[2] B. N. Kholodenko, "Cell-signalling dynamics in time and space," *Nature reviews Molecular cell biology,* vol. 7, pp. 165-176, 2006.

[3] D. G. Spiller, C. D. Wood, D. A. Rand, and M. R. H. White, "Measurement of single-cell dynamics," *Nature,* vol. 465, pp. 736-745, 2010.

[4] S. J. Elledge, "Cell cycle checkpoints: preventing an identity crisis," *Science,* vol. 274, p. 1664, 1996.

[5] T. Weber, M. K. Corbett, L. M. Chow, M. B. Valentine, S. J. Baker, and J. Zuo, "Rapid cell-cycle reentry and cell death after acute inactivation of the retinoblastoma gene product in postnatal cochlear hair cells," *Proceedings of the National Academy of Sciences,* vol. 105, pp. 781-785, 2008.

[6] H. Clevers, "The intestinal crypt, a prototype stem cell compartment," *Cell,* vol. 154, pp. 274-284, 2013.

[7] K. Vermeulen, D. R. Van Bockstaele, and Z. N. Berneman, "The cell cycle: a review of regulation, deregulation and therapeutic targets in cancer," *Cell proliferation,* vol. 36, pp. 131-149, 2003.

[8] S. Even-Ram and K. M. Yamada, "Cell migration in 3D matrix," *Current opinion in cell biology,* vol. 17, pp. 524-532, 2005.

[9] D. E. Ingber, "Cellular mechanotransduction: putting all the pieces together again," *The FASEB journal,* vol. 20, pp. 811-827, 2006.

[10] E. Hadjipanayi, V. Mudera, and R. A. Brown, "Guiding cell migration in 3D: a collagen matrix with graded directional stiffness," *Cell motility and the cytoskeleton,* vol. 66, pp. 121-128, 2009.

[11] M. Ni, W. H. Tong, D. Choudhury, N. A. A. Rahim, C. Iliescu, and H. Yu, "Cell culture on MEMS platforms: a review," *International journal of molecular sciences,* vol. 10, pp. 5411-5441, 2009.

[12] J. B. Kim, R. Stein, and M. J. O'hare, "Three-dimensional in vitro tissue culture models of breast cancer-a review," *Breast cancer research and treatment,* vol. 85, pp. 281-291, 2004.

[13] F. Mannello and G. A. Tonti, "Concise review: no breakthroughs for human mesenchymal and embryonic stem cell culture: conditioned medium, feeder layer, or feeder-free; medium with fetal calf serum, human serum, or enriched plasma; serum-free, serum replacement nonconditioned medium, or ad hoc formula? All that glitters is not gold!," *Stem cells,* vol. 25, pp. 1603-1609, 2007.

[14] J. W. Haycock, "3D cell culture: a review of current approaches and techniques," *3D Cell Culture: Methods and Protocols,* pp. 1-15, 2011.

[15] A. Abbott, "Cell culture: biology's new dimension," *Nature,* vol. 424, pp. 870-872, 2003.

[16] R. I. Freshney, *Culture of specific cell types*: Wiley Online Library, 2005.

[17] F. Pampaloni, E. G. Reynaud, and E. H. Stelzer, "The third dimension bridges the gap between cell culture and live tissue," *Nature reviews Molecular cell biology,* vol. 8, pp. 839-845, 2007.
[18] G. D. Prestwich, "Simplifying the extracellular matrix for 3 - D cell culture and tissue engineering: A pragmatic approach," *Journal of cellular biochemistry,* vol. 101, pp. 1370-1383, 2007.
[19] P. Roy, D. Kim, K. Lee, E. Spiecker, and P. Schmuki, "TiO2 nanotubes and their application in dye-sensitized solar cells," *Nanoscale,* vol. 2, pp. 45-59, 2010.
[20] H. Liu and K. Roy, "Biomimetic three-dimensional cultures significantly increase hematopoietic differentiation efficacy of embryonic stem cells," *Tissue engineering,* vol. 11, pp. 319-330, 2005.
[21] N. T. Elliott and F. Yuan, "A review of three-dimensional in vitro tissue models for drug discovery and transport studies," *Journal of pharmaceutical sciences,* vol. 100, pp. 59-74, 2011.
[22] G. D. Nicodemus and S. J. Bryant, "Cell encapsulation in biodegradable hydrogels for tissue engineering applications," *Tissue Engineering Part B: Reviews,* vol. 14, pp. 149-165, 2008.
[23] C. Fischbach, R. Chen, T. Matsumoto, T. Schmelzle, J. S. Brugge, P. J. Polverini, and D. J. Mooney, "Engineering tumors with 3D scaffolds," *Nature methods,* vol. 4, pp. 855-860, 2007.
[24] C. Godugu, A. R. Patel, U. Desai, T. Andey, A. Sams, and M. Singh, "AlgiMatrix™ based 3D cell culture system as an in-vitro tumor model for anticancer studies," *PLoS One,* vol. 8, p. e53708, 2013.
[25] R. Fan, K. Naqvi, K. Patel, J. Sun, and J. Wan, "Evaporation-based microfluidic production of oil-free cell-containing hydrogel particles," *Biomicrofluidics,* vol. 9, p. 052602, 2015.
[26] M.-H. Wu, S.-B. Huang, and G.-B. Lee, "Microfluidic cell culture systems for drug research," *Lab on a Chip,* vol. 10, pp. 939-956, 2010.
[27] Y.-C. Tung, A. Y. Hsiao, S. G. Allen, Y.-s. Torisawa, M. Ho, and S. Takayama, "High-throughput 3D spheroid culture and drug testing using a 384 hanging drop array," *Analyst,* vol. 136, pp. 473-478, 2011.
[28] L. A. Kunz-Schughart, J. P. Freyer, F. Hofstaedter, and R. Ebner, "The use of 3-D cultures for high-throughput screening: the multicellular spheroid model," *Journal of biomolecular screening,* vol. 9, pp. 273-285, 2004.
[29] Y. Yan, X. Wang, Y. Pan, H. Liu, J. Cheng, Z. Xiong, F. Lin, R. Wu, R. Zhang, and Q. Lu, "Fabrication of viable tissue-engineered constructs with 3D cell-assembly technique," *Biomaterials,* vol. 26, pp. 5864-5871, 2005.
[30] D. Huh, G. A. Hamilton, and D. E. Ingber, "From 3D cell culture to organs-on-chips," *Trends in cell biology,* vol. 21, pp. 745-754, 2011.
[31] K. Louekari, "Status and prospects of in vitro tests in risk assessment," *Alternatives to laboratory animals: ATLA,* vol. 32, pp. 431-435, 2004.
[32] E. J. Suuronen, H. Sheardown, K. D. Newman, C. R. McLaughlin, and M. Griffith, "Building in vitro models of organs," *International review of cytology,* vol. 244, pp. 137-173, 2005.
[33] E. Cukierman, R. Pankov, D. R. Stevens, and K. M. Yamada, "Taking cell-matrix adhesions to the third dimension," *Science,* vol. 294, pp. 1708-1712, 2001.

[34] K. Wrzesinski, M. C. Magnone, L. V. Hansen, M. E. Kruse, T. Bergauer, M. Bobadilla, M. Gubler, J. Mizrahi, K. Zhang, and C. M. Andreasen, "HepG2/C3A 3D spheroids exhibit stable physiological functionality for at least 24 days after recovering from trypsinisation," *Toxicology Research,* vol. 2, pp. 163-172, 2013.

[35] B. M. Baker and C. S. Chen, "Deconstructing the third dimension-how 3D culture microenvironments alter cellular cues," *J Cell Sci,* vol. 125, pp. 3015-3024, 2012.

[36] F. Wang, V. M. Weaver, O. W. Petersen, C. A. Larabell, S. Dedhar, P. Briand, R. Lupu, and M. J. Bissell, "Reciprocal interactions between β1-integrin and epidermal growth factor receptor in three-dimensional basement membrane breast cultures: a different perspective in epithelial biology," *Proceedings of the National Academy of Sciences,* vol. 95, pp. 14821-14826, 1998.

[37] A. S. Meshel, Q. Wei, R. S. Adelstein, and M. P. Sheetz, "Basic mechanism of three-dimensional collagen fibre transport by fibroblasts," *Nature cell biology,* vol. 7, pp. 157-164, 2005.

[38] C. Roskelley, P. Desprez, and M. Bissell, "Extracellular matrix-dependent tissue-specific gene expression in mammary epithelial cells requires both physical and biochemical signal transduction," *Proceedings of the National Academy of Sciences,* vol. 91, pp. 12378-12382, 1994.

[39] B. Knight, C. Laukaitis, N. Akhtar, N. A. Hotchin, M. Edlund, and A. R. Horwitz, "Visualizing muscle cell migration in situ," *Current Biology,* vol. 10, pp. 576-585, 2000.

[40] T. Sun, S. Jackson, J. W. Haycock, and S. MacNeil, "Culture of skin cells in 3D rather than 2D improves their ability to survive exposure to cytotoxic agents," *Journal of biotechnology,* vol. 122, pp. 372-381, 2006.

[41] F. Grinnell, "Fibroblast biology in three-dimensional collagen matrices," *Trends in cell biology,* vol. 13, pp. 264-269, 2003.

[42] S. Umar, "Intestinal stem cells," *Current gastroenterology reports,* vol. 12, pp. 340-348, 2010.

[43] T. Vanuytsel, S. Senger, A. Fasano, and T. Shea-Donohue, "Major signaling pathways in intestinal stem cells," *Biochimica et Biophysica Acta (BBA)-General Subjects,* vol. 1830, pp. 2410-2426, 2013.

[44] T. J. Webster, R. W. Siegel, and R. Bizios, "Osteoblast adhesion on nanophase ceramics," *Biomaterials,* vol. 20, pp. 1221-1227, 1999.

[45] S. Ozawa and S. Kasugai, "Evaluation of implant materials (hydroxyapatite, glass-ceramics, titanium) in rat bone marrow stromal cell culture," *Biomaterials,* vol. 17, pp. 23-29, 1996.

[46] S. P. Massia and J. Hubbell, "Human endothelial cell interactions with surface‐coupled adhesion peptides on a nonadhesive glass substrate and two polymeric biomaterials," *Journal of biomedical materials research,* vol. 25, pp. 223-242, 1991.

[47] A. R. Vancha, S. Govindaraju, K. V. Parsa, M. Jasti, M. González-García, and R. P. Ballestero, "Use of polyethyleneimine polymer in cell culture as attachment factor and lipofection enhancer," *BMC biotechnology,* vol. 4, p. 23, 2004.

[48] T. Takezawa, Y. Mori, and K. Yoshizato, "Cell culture on a thermo-responsive polymer surface," *Nature Biotechnology,* vol. 8, pp. 854-856, 1990.

[49] G. Zhao, Z. Schwartz, M. Wieland, F. Rupp, J. Geis‐Gerstorfer, D. Cochran, and B. Boyan, "High surface energy enhances cell response to titanium substrate microstructure," *Journal of Biomedical Materials Research Part A*, vol. 74, pp. 49-58, 2005.

[50] W. Vrouwenvelder, C. Groot, and K. De Groot, "Histological and biochemical evaluation of osteoblasts cultured on bioactive glass, hydroxylapatite, titanium alloy, and stainless steel," *Journal of biomedical materials research*, vol. 27, pp. 465-475, 1993.

[51] N. Huebsch, P. R. Arany, A. S. Mao, D. Shvartsman, O. A. Ali, S. A. Bencherif, J. Rivera-Feliciano, and D. J. Mooney, "Harnessing traction-mediated manipulation of the cell/matrix interface to control stem-cell fate," *Nature materials*, vol. 9, pp. 518-526, 2010.

[52] J. Lötters, W. Olthuis, P. Veltink, and P. Bergveld, "The mechanical properties of the rubber elastic polymer polydimethylsiloxane for sensor applications," *Journal of Micromechanics and Microengineering*, vol. 7, p. 145, 1997.

[53] K. A. Simon, K. M. Park, B. Mosadegh, A. B. Subramaniam, A. D. Mazzeo, P. M. Ngo, and G. M. Whitesides, "Polymer-based mesh as supports for multi-layered 3D cell culture and assays," *Biomaterials*, vol. 35, pp. 259-268, 2014.

[54] Z. Liu, Q. Lin, Y. Sun, T. Liu, C. Bao, F. Li, and L. Zhu, "Spatiotemporally Controllable and Cytocompatible Approach Builds 3D Cell Culture Matrix by Photo‐Uncaged‐Thiol Michael Addition Reaction," *Advanced Materials*, vol. 26, pp. 3912-3917, 2014.

[55] J. S. Miller, K. R. Stevens, M. T. Yang, B. M. Baker, D.-H. T. Nguyen, D. M. Cohen, E. Toro, A. A. Chen, P. A. Galie, and X. Yu, "Rapid casting of patterned vascular networks for perfusable engineered three-dimensional tissues," *Nature materials*, vol. 11, pp. 768-774, 2012.

[56] C. Piconi, W. Burger, H. Richter, A. Cittadini, G. Maccauro, V. Covacci, N. Bruzzese, G. Ricci, and E. Marmo, "Y-TZP ceramics for artificial joint replacements," *Biomaterials*, vol. 19, pp. 1489-1494, 1998.

[57] E. Serra, A. Tucci, L. Esposito, and C. Piconi, "Volumetric determination of the wear of ceramics for hip joints," *Biomaterials*, vol. 23, pp. 1131-1137, 2002.

[58] C.-T. Ho, R.-Z. Lin, R.-J. Chen, C.-K. Chin, S.-E. Gong, H.-Y. Chang, H.-L. Peng, L. Hsu, T.-R. Yew, and S.-F. Chang, "Liver-cell patterning lab chip: mimicking the morphology of liver lobule tissue," *Lab on a Chip*, vol. 13, pp. 3578-3587, 2013.

[59] S. Roohani-Esfahani, C. Dunstan, J. Li, Z. Lu, B. Davies, S. Pearce, J. Field, R. Williams, and H. Zreiqat, "Unique microstructural design of ceramic scaffolds for bone regeneration under load," *Acta biomaterialia*, vol. 9, pp. 7014-7024, 2013.

[60] M. Rinaudo, "Main properties and current applications of some polysaccharides as biomaterials," *Polymer International*, vol. 57, pp. 397-430, 2008.

[61] J.-K. F. Suh and H. W. Matthew, "Application of chitosan-based polysaccharide biomaterials in cartilage tissue engineering: a review," *Biomaterials*, vol. 21, pp. 2589-2598, 2000.

[62] A. Skardal, J. Zhang, and G. D. Prestwich, "Bioprinting vessel-like constructs using hyaluronan hydrogels crosslinked with tetrahedral polyethylene glycol tetracrylates," *Biomaterials*, vol. 31, pp. 6173-6181, 2010.

[63] S. Khalil and W. Sun, "Bioprinting endothelial cells with alginate for 3D tissue constructs," *Journal of biomechanical engineering,* vol. 131, p. 111002, 2009.
[64] B. Duan, L. A. Hockaday, K. H. Kang, and J. T. Butcher, "3D bioprinting of heterogeneous aortic valve conduits with alginate/gelatin hydrogels," *Journal of Biomedical Materials Research Part A,* vol. 101, pp. 1255-1264, 2013.
[65] M. W. Tibbitt and K. S. Anseth, "Hydrogels as extracellular matrix mimics for 3D cell culture," *Biotechnology and bioengineering,* vol. 103, pp. 655-663, 2009.
[66] H. A. Awad, M. Q. Wickham, H. A. Leddy, J. M. Gimble, and F. Guilak, "Chondrogenic differentiation of adipose-derived adult stem cells in agarose, alginate, and gelatin scaffolds," *Biomaterials,* vol. 25, pp. 3211-3222, 2004.
[67] F. Gelain, D. Bottai, A. Vescovi, and S. Zhang, "Designer self-assembling peptide nanofiber scaffolds for adult mouse neural stem cell 3-dimensional cultures," *PloS one,* vol. 1, p. e119, 2006.
[68] L. Chen, Z. Xiao, Y. Meng, Y. Zhao, J. Han, G. Su, B. Chen, and J. Dai, "The enhancement of cancer stem cell properties of MCF-7 cells in 3D collagen scaffolds for modeling of cancer and anti-cancer drugs," *Biomaterials,* vol. 33, pp. 1437-1444, 2012.
[69] Y. Nagamoto, K. Tashiro, K. Takayama, K. Ohashi, K. Kawabata, F. Sakurai, M. Tachibana, T. Hayakawa, M. K. Furue, and H. Mizuguchi, "The promotion of hepatic maturation of human pluripotent stem cells in 3D co-culture using type I collagen and Swiss 3T3 cell sheets," *Biomaterials,* vol. 33, pp. 4526-4534, 2012.
[70] T. Sato and H. Clevers, "Growing self-organizing mini-guts from a single intestinal stem cell: mechanism and applications," *Science,* vol. 340, pp. 1190-1194, 2013.
[71] F. Molina-Jimenez, I. Benedicto, V. L. D. Thi, V. Gondar, D. Lavillette, J. J. Marin, O. Briz, R. Moreno-Otero, R. Aldabe, and T. F. Baumert, "Matrigel-embedded 3D culture of Huh-7 cells as a hepatocyte-like polarized system to study hepatitis C virus cycle," *Virology,* vol. 425, pp. 31-39, 2012.
[72] R. G. Wells, "The role of matrix stiffness in regulating cell behavior," *Hepatology,* vol. 47, pp. 1394-1400, 2008.
[73] S. V. Murphy and A. Atala, "3D bioprinting of tissues and organs," *Nature biotechnology,* vol. 32, pp. 773-785, 2014.
[74] W. Hassan, Y. Dong, and W. Wang, "Encapsulation and 3D culture of human adipose-derived stem cells in an in-situ crosslinked hybrid hydrogel composed of PEG-based hyperbranched copolymer and hyaluronic acid," *Stem Cell Res Ther,* vol. 4, p. 32, 2013.
[75] P. R. Baraniak and T. C. McDevitt, "Scaffold-free culture of mesenchymal stem cell spheroids in suspension preserves multilineage potential," *Cell and tissue research,* vol. 347, pp. 701-711, 2012.
[76] A. P. Napolitano, D. M. Dean, A. J. Man, J. Youssef, D. N. Ho, A. P. Rago, M. P. Lech, and J. R. Morgan, "Scaffold-free three-dimensional cell culture utilizing micromolded nonadhesive hydrogels," *Biotechniques,* vol. 43, p. 494, 2007.
[77] A. Y. Hsiao, Y. C. Tung, X. Qu, L. R. Patel, K. J. Pienta, and S. Takayama, "384 hanging drop arrays give excellent Z-factors and allow versatile formation of co-culture spheroids," *Biotechnology and bioengineering,* vol. 109, pp. 1293-1304, 2012.

[78] E. Carletti, A. Motta, and C. Migliaresi, "Scaffolds for tissue engineering and 3D cell culture," *3D Cell Culture: Methods and Protocols*, pp. 17-39, 2011.
[79] S. R. Peyton, C. B. Raub, V. P. Keschrumrus, and A. J. Putnam, "The use of poly (ethylene glycol) hydrogels to investigate the impact of ECM chemistry and mechanics on smooth muscle cells," *Biomaterials*, vol. 27, pp. 4881-4893, 2006.
[80] C. B. Khatiwala, S. R. Peyton, and A. J. Putnam, "Intrinsic mechanical properties of the extracellular matrix affect the behavior of pre-osteoblastic MC3T3-E1 cells," *American Journal of Physiology-Cell Physiology*, vol. 290, pp. C1640-C1650, 2006.
[81] R. Fan, Y. Sun, and J. Wan, "Leaf-inspired artificial microvascular networks (LIAMN) for three-dimensional cell culture," *RSC Advances*, vol. 5, pp. 90596-90601, 2015.
[82] J. Liu, J. Hilderink, T. A. Groothuis, C. Otto, C. A. Blitterswijk, and J. Boer, "Monitoring nutrient transport in tissue-engineered grafts," *Journal of tissue engineering and regenerative medicine*, vol. 9, pp. 952-960, 2015.
[83] A. M. Kloxin, M. W. Tibbitt, and K. S. Anseth, "Synthesis of photodegradable hydrogels as dynamically tunable cell culture platforms," *Nat. Protocols*, vol. 5, pp. 1867-1887, 11//print 2010.
[84] D. Sun, J. Lu, Z. Chen, Y. Yu, and Y. Li, "A novel three-dimensional microfluidic platform for on chip multicellular tumor spheroid formation and culture," *Microfluidics and Nanofluidics*, vol. 17, pp. 831-842, 2014.
[85] I. Meyvantsson and D. J. Beebe, "Cell culture models in microfluidic systems," *Annu. Rev. Anal. Chem.*, vol. 1, pp. 423-449, 2008.
[86] X. Li, A. V. Valadez, P. Zuo, and Z. Nie, "Microfluidic 3D cell culture: potential application for tissue-based bioassays," *Bioanalysis*, vol. 4, pp. 1509-1525, 2012.
[87] Y.-C. Tan, K. Hettiarachchi, M. Siu, Y.-R. Pan, and A. P. Lee, "Controlled microfluidic encapsulation of cells, proteins, and microbeads in lipid vesicles," *Journal of the American Chemical Society*, vol. 128, pp. 5656-5658, 2006.
[88] A. Kumachev, J. Greener, E. Tumarkin, E. Eiser, P. W. Zandstra, and E. Kumacheva, "High-throughput generation of hydrogel microbeads with varying elasticity for cell encapsulation," *Biomaterials*, vol. 32, pp. 1477-1483, 2011.
[89] J. F. Edd, D. Di Carlo, K. J. Humphry, S. Köster, D. Irimia, D. A. Weitz, and M. Toner, "Controlled encapsulation of single-cells into monodisperse picolitre drops," *Lab on a Chip*, vol. 8, pp. 1262-1264, 2008.
[90] M. Chabert and J.-L. Viovy, "Microfluidic high-throughput encapsulation and hydrodynamic self-sorting of single cells," *Proceedings of the National Academy of Sciences*, vol. 105, pp. 3191-3196, 2008.
[91] S. K. Suh, K. W. Bong, T. A. Hatton, and P. S. Doyle, "Using stop-flow lithography to produce opaque microparticles: Synthesis and modeling," *Langmuir*, vol. 27, pp. 13813-13819, 2011.
[92] J. Clausell-Tormos, D. Lieber, J.-C. Baret, A. El-Harrak, O. J. Miller, L. Frenz, J. Blouwolff, K. J. Humphry, S. Köster, and H. Duan, "Droplet-based microfluidic platforms for the encapsulation and screening of mammalian cells and multicellular organisms," *Chemistry & biology*, vol. 15, pp. 427-437, 2008.
[93] T. Rossow, J. A. Heyman, A. J. Ehrlicher, A. Langhoff, D. A. Weitz, R. Haag, and S. Seiffert, "Controlled synthesis of cell-laden microgels by radical-free gelation in

droplet microfluidics," *Journal of the American Chemical Society,* vol. 134, pp. 4983-4989, 2012.
[94] T. Okuyama, H. Yamazoe, N. Mochizuki, A. Khademhosseini, H. Suzuki, and J. Fukuda, "Preparation of arrays of cell spheroids and spheroid-monolayer cocultures within a microfluidic device," *Journal of bioscience and bioengineering,* vol. 110, pp. 572-576, 2010.
[95] K. Kwapiszewska, A. Michalczuk, M. Rybka, R. Kwapiszewski, and Z. Brzózka, "A microfluidic-based platform for tumour spheroid culture, monitoring and drug screening," *Lab on a Chip,* vol. 14, pp. 2096-2104, 2014.
[96] S. J. Trietsch, G. D. Israëls, J. Joore, T. Hankemeier, and P. Vulto, "Microfluidic titer plate for stratified 3D cell culture," *Lab on a chip,* vol. 13, pp. 3548-3554, 2013.
[97] A. Tourovskaia, X. Figueroa-Masot, and A. Folch, "Differentiation-on-a-chip: a microfluidic platform for long-term cell culture studies," *Lab on a Chip,* vol. 5, pp. 14-19, 2005.
[98] Y. Luo and M. S. Shoichet, "A photolabile hydrogel for guided three-dimensional cell growth and migration," *Nature Materials,* vol. 3, pp. 249-253, Apr 2004.
[99] J. Y. Park, M. Morgan, A. N. Sachs, J. Samorezov, R. Teller, Y. Shen, K. J. Pienta, and S. Takayama, "Single cell trapping in larger microwells capable of supporting cell spreading and proliferation," *Microfluidics and nanofluidics,* vol. 8, pp. 263-268, 2010.
[100] A. Van der Meer, A. Poot, M. Duits, J. Feijen, and I. Vermes, "Microfluidic technology in vascular research," *BioMed Research International,* vol. 2009, 2009.
[101] B. Patra, Y.-H. Chen, C.-C. Peng, S.-C. Lin, C.-H. Lee, and Y.-C. Tung, "A microfluidic device for uniform-sized cell spheroids formation, culture, harvesting and flow cytometry analysis," *Biomicrofluidics,* vol. 7, p. 054114, 2013.
[102] B. G. Chung, L. A. Flanagan, S. W. Rhee, P. H. Schwartz, A. P. Lee, E. S. Monuki, and N. L. Jeon, "Human neural stem cell growth and differentiation in a gradient-generating microfluidic device," *Lab on a Chip,* vol. 5, pp. 401-406, 2005.
[103] S. Mao, D. Gao, W. Liu, H. Wei, and J.-M. Lin, "Imitation of drug metabolism in human liver and cytotoxicity assay using a microfluidic device coupled to mass spectrometric detection," *Lab on a chip,* vol. 12, pp. 219-226, 2012.
[104] H. Lipson and M. Kurman, *Fabricated: The new world of 3D printing*: John Wiley & Sons, 2013.
[105] A. Skardal, D. Mack, E. Kapetanovic, A. Atala, J. D. Jackson, J. Yoo, and S. Soker, "Bioprinted amniotic fluid-derived stem cells accelerate healing of large skin wounds," *Stem cells translational medicine,* vol. 1, p. 792, 2012.
[106] X. Cui, K. Breitenkamp, M. Finn, M. Lotz, and D. D. D'Lima, "Direct human cartilage repair using three-dimensional bioprinting technology," *Tissue Engineering Part A,* vol. 18, pp. 1304-1312, 2012.
[107] S. Michael, H. Sorg, C.-T. Peck, L. Koch, A. Deiwick, B. Chichkov, P. M. Vogt, and K. Reimers, "Tissue engineered skin substitutes created by laser-assisted bioprinting form skin-like structures in the dorsal skin fold chamber in mice," *PloS one,* vol. 8, p. e57741, 2013.

[108] C. Norotte, F. S. Marga, L. E. Niklason, and G. Forgacs, "Scaffold-free vascular tissue engineering using bioprinting," *Biomaterials*, vol. 30, pp. 5910-5917, 10// 2009.
[109] F. Xu, J. Celli, I. Rizvi, S. Moon, T. Hasan, and U. Demirci, "A three-dimensional in vitro ovarian cancer coculture model using a high-throughput cell patterning platform," *Biotechnology journal*, vol. 6, pp. 204-212, 2011.
[110] D. B. Kolesky, R. L. Truby, A. Gladman, T. A. Busbee, K. A. Homan, and J. A. Lewis, "3D bioprinting of vascularized, heterogeneous cell-laden tissue constructs," *Advanced Materials*, vol. 26, pp. 3124-3130, 2014.
[111] L. M. Bellan, S. P. Singh, P. W. Henderson, T. J. Porri, H. G. Craighead, and J. A. Spector, "Fabrication of an artificial 3-dimensional vascular network using sacrificial sugar structures," *Soft Matter*, vol. 5, pp. 1354-1357, 2009.
[112] R. Landers, U. Hübner, R. Schmelzeisen, and R. Mülhaupt, "Rapid prototyping of scaffolds derived from thermoreversible hydrogels and tailored for applications in tissue engineering," *Biomaterials*, vol. 23, pp. 4437-4447, 2002.
[113] B. Leukers, H. Gülkan, S. H. Irsen, S. Milz, C. Tille, M. Schieker, and H. Seitz, "Hydroxyapatite scaffolds for bone tissue engineering made by 3D printing," *Journal of Materials Science: Materials in Medicine*, vol. 16, pp. 1121-1124, 2005.
[114] B. A. Justice, N. A. Badr, and R. A. Felder, "3D cell culture opens new dimensions in cell-based assays," *Drug discovery today*, vol. 14, pp. 102-107, 2009.
[115] M. Wartenberg, F. Donmez, F. C. Ling, H. Acker, J. Hescheler, and H. Sauer, "Tumor-induced angiogenesis studied in confrontation cultures of multicellular tumor spheroids and embryoid bodies grown from pluripotent embryonic stem cells," *The FASEB Journal*, vol. 15, pp. 995-1005, 2001.
[116] B. Lieubeau-Teillet, J. Rak, S. Jothy, O. Iliopoulos, W. Kaelin, and R. S. Kerbel, "von Hippel-Lindau gene-mediated growth suppression and induction of differentiation in renal cell carcinoma cells grown as multicellular tumor spheroids," *Cancer research*, vol. 58, pp. 4957-4962, 1998.
[117] T. Takezawa, M. Yamazaki, Y. Mori, T. Yonaha, and K. Yoshizato, "Morphological and immuno-cytochemical characterization of a hetero-spheroid composed of fibroblasts and hepatocytes," *Journal of Cell Science*, vol. 101, pp. 495-501, 1992.
[118] H. Hwang, J. Park, C. Shin, Y. Do, and Y.-K. Cho, "Three dimensional multicellular co-cultures and anti-cancer drug assays in rapid prototyped multilevel microfluidic devices," *Biomedical microdevices*, vol. 15, pp. 627-634, 2013.
[119] K. H. Lee, S. J. Shin, Y. Park, and S. H. Lee, "Synthesis of cell-laden alginate hollow fibers using microfluidic chips and microvascularized tissue-engineering applications," *Small*, vol. 5, pp. 1264-1268, 2009.
[120] R. Z. Lin and H. Y. Chang, "Recent advances in three-dimensional multicellular spheroid culture for biomedical research," *Biotechnology journal*, vol. 3, pp. 1172-1184, 2008.
[121] L. Y. Wu, D. Di Carlo, and L. P. Lee, "Microfluidic self-assembly of tumor spheroids for anticancer drug discovery," *Biomedical microdevices*, vol. 10, pp. 197-202, 2008.

[122] A. Y. Hsiao, Y.-s. Torisawa, Y.-C. Tung, S. Sud, R. S. Taichman, K. J. Pienta, and S. Takayama, "Microfluidic system for formation of PC-3 prostate cancer co-culture spheroids," *Biomaterials,* vol. 30, pp. 3020-3027, 2009.
[123] K. K. Yap, A. M. Dingle, J. A. Palmer, R. S. Dhillon, Z. Lokmic, A. J. Penington, G. C. Yeoh, W. A. Morrison, and G. M. Mitchell, "Enhanced liver progenitor cell survival and differentiation in vivo by spheroid implantation in a vascularized tissue engineering chamber," *Biomaterials,* vol. 34, pp. 3992-4001, 2013.
[124] P. R. Baraniak, M. T. Cooke, R. Saeed, M. A. Kinney, K. M. Fridley, and T. C. McDevitt, "Stiffening of human mesenchymal stem cell spheroid microenvironments induced by incorporation of gelatin microparticles," *Journal of the mechanical behavior of biomedical materials,* vol. 11, pp. 63-71, 2012.
[125] M.-H. Wu, S.-B. Huang, Z. Cui, Z. Cui, and G.-B. Lee, "Development of perfusion-based micro 3-D cell culture platform and its application for high throughput drug testing," *Sensors and Actuators B: Chemical,* vol. 129, pp. 231-240, 2008.
[126] J. Friedrich, C. Seidel, R. Ebner, and L. A. Kunz-Schughart, "Spheroid-based drug screen: considerations and practical approach," *Nature protocols,* vol. 4, pp. 309-324, 2009.
[127] X. Zhang, W. Wang, W. Yu, Y. Xie, X. Zhang, Y. Zhang, and X. Ma, "Development of an in vitro multicellular tumor spheroid model using microencapsulation and its application in anticancer drug screening and testing," *Biotechnology progress,* vol. 21, pp. 1289-1296, 2005.
[128] J. Lee, G. D. Lilly, R. C. Doty, P. Podsiadlo, and N. A. Kotov, "In vitro toxicity testing of nanoparticles in 3D cell culture," *Small,* vol. 5, pp. 1213-1221, 2009.
[129] A. R. Aref, R. Y.-J. Huang, W. Yu, K.-N. Chua, W. Sun, T.-Y. Tu, J. Bai, W.-J. Sim, I. K. Zervantonakis, and J. P. Thiery, "Screening therapeutic EMT blocking agents in a three-dimensional microenvironment," *Integrative Biology,* vol. 5, pp. 381-389, 2013.
[130] N. Beißner, T. Lorenz, and S. Reichl, "Organ on Chip," in *Microsystems for Pharmatechnology*, ed: Springer, 2016, pp. 299-339.
[131] D. YoonáNo, "Spheroid-based three-dimensional liver-on-a-chip to investigate hepatocyte–hepatic stellate cell interactions and flow effects," *Lab on a Chip,* vol. 13, pp. 3529-3537, 2013.
[132] J. W. Allen, T. Hassanein, and S. N. Bhatia, "Advances in bioartificial liver devices," *Hepatology,* vol. 34, pp. 447-455, 2001.
[133] M. Yarmush, M. Toner, J. Dunn, A. Rotem, A. Hubel, and R. Tompkins, "Hepatic tissue engineering: Development of critical technologies," *Annals of the New York Academy of Sciences,* vol. 665, pp. 238-252, 1992.
[134] Y. Nahmias, F. Berthiaume, and M. L. Yarmush, "Integration of technologies for hepatic tissue engineering," in *Tissue Engineering II*, ed: Springer, 2006, pp. 309-329.
[135] H. A. Pohl and H. Pohl, *Dielectrophoresis: the behavior of neutral matter in nonuniform electric fields* vol. 80: Cambridge university press Cambridge, 1978.
[136] J. Schütte, B. Hagmeyer, F. Holzner, M. Kubon, S. Werner, C. Freudigmann, K. Benz, J. Böttger, R. Gebhardt, and H. Becker, "“Artificial micro organs”-a microfluidic device for dielectrophoretic assembly of liver sinusoids," *Biomedical microdevices,* vol. 13, pp. 493-501, 2011.

[137] A. Blouin, R. P. Bolender, and E. R. Weibel, "Distribution of organelles and membranes between hepatocytes and nonhepatocytes in the rat liver parenchyma. A stereological study," *The Journal of cell biology,* vol. 72, pp. 441-455, 1977.
[138] A. Gressner, N. Krull, and M. Bachem, "Regulation of proteoglycan expression in fibrotic liver and cultured fat-storing cells," *Pathology-Research and Practice,* vol. 190, pp. 864-882, 1994.
[139] Y.-L. Park, B.-R. Chen, and R. J. Wood, "Design and fabrication of soft artificial skin using embedded microchannels and liquid conductors," *Sensors Journal, IEEE,* vol. 12, pp. 2711-2718, 2012.
[140] B. Andrée, K. Bela, T. Horvath, M. Lux, R. Ramm, L. Venturini, A. Ciubotaru, R. Zweigerdt, A. Haverich, and A. Hilfiker, "Successful re-endothelialization of a perfusable biological vascularized matrix (BioVaM) for the generation of 3D artificial cardiac tissue," *Basic research in cardiology,* vol. 109, pp. 1-13, 2014.
[141] S. Bose, S. Vahabzadeh, and A. Bandyopadhyay, "Bone tissue engineering using 3D printing," *Materials Today,* vol. 16, pp. 496-504, 2013.
[142] I. Wagner, E.-M. Materne, S. Brincker, U. Süßbier, C. Frädrich, M. Busek, F. Sonntag, D. A. Sakharov, E. V. Trushkin, and A. G. Tonevitsky, "A dynamic multi-organ-chip for long-term cultivation and substance testing proven by 3D human liver and skin tissue co-culture," *Lab on a chip,* vol. 13, pp. 3538-3547, 2013.
[143] F. A. Auger, L. Gibot, and D. Lacroix, "The pivotal role of vascularization in tissue engineering," *Annual review of biomedical engineering,* vol. 15, pp. 177-200, 2013.
[144] R. Y. Kannan, H. J. Salacinski, K. Sales, P. Butler, and A. M. Seifalian, "The roles of tissue engineering and vascularisation in the development of micro-vascular networks: a review," *Biomaterials,* vol. 26, pp. 1857-1875, 2005.
[145] Y.-C. Lu, W. Song, D. An, B. J. Kim, R. Schwartz, M. Wu, and M. Ma, "Designing compartmentalized hydrogel microparticles for cell encapsulation and scalable 3D cell culture," *Journal of Materials Chemistry B,* vol. 3, pp. 353-360, 2015.
[146] R. M. Sutherland, "Cell and environment interactions in tumor microregions: the multicell spheroid model," *Science,* vol. 240, pp. 177-184, 1988.
[147] M. Gou, X. Qu, W. Zhu, M. Xiang, J. Yang, K. Zhang, Y. Wei, and S. Chen, "Bio-inspired detoxification using 3D-printed hydrogel nanocomposites," *Nature communications,* vol. 5, 2014.
[148] J. Jia, D. J. Richards, S. Pollard, Y. Tan, J. Rodriguez, R. P. Visconti, T. C. Trusk, M. J. Yost, H. Yao, and R. R. Markwald, "Engineering alginate as bioink for bioprinting," *Acta biomaterialia,* vol. 10, pp. 4323-4331, 2014.
[149] K. Shalumon, S. Deepthi, M. Anupama, S. Nair, R. Jayakumar, and K. Chennazhi, "Fabrication of poly (l-lactic acid)/gelatin composite tubular scaffolds for vascular tissue engineering," *International journal of biological macromolecules,* vol. 72, pp. 1048-1055, 2015.
[150] J. Folkman and M. Hochberg, "SELF-REGULATION OF GROWTH IN THREE DIMENSIONS," *The Journal of Experimental Medicine,* vol. 138, pp. 745-753, 05/30/received 1973.
[151] K. Alessandri, B. R. Sarangi, V. V. Gurchenkov, B. Sinha, T. R. Kießling, L. Fetler, F. Rico, S. Scheuring, C. Lamaze, and A. Simon, "Cellular capsules as a tool for multicellular spheroid production and for investigating the mechanics of tumor

progression in vitro," *Proceedings of the National Academy of Sciences,* vol. 110, pp. 14843-14848, 2013.

[152] E. Benrashid, C. C. McCoy, L. M. Youngwirth, J. Kim, R. J. Manson, J. C. Otto, and J. H. Lawson, "Tissue engineered vascular grafts: Origins, development, and current strategies for clinical application," *Methods,* 2015.

[153] B. M. Baker, B. Trappmann, S. C. Stapleton, E. Toro, and C. S. Chen, "Microfluidics embedded within extracellular matrix to define vascular architectures and pattern diffusive gradients," *Lab on a chip,* vol. 13, pp. 3246-3252, 2013.

[154] C. J. Bettinger, E. J. Weinberg, K. M. Kulig, J. P. Vacanti, Y. Wang, J. T. Borenstein, and R. Langer, "Three-Dimensional Microfluidic Tissue-Engineering Scaffolds Using a Flexible Biodegradable Polymer," *Advanced Materials,* vol. 18, pp. 165-169, 2006.

[155] X. Zhao, Š. Selimović, G. Camci-Unal, M. R. Dokmeci, L. Yildirimer, N. Annabi, and A. Khademhosseini, "Microfabrication of Three-Dimensional Vascular Structures," *Vascularization: Regenerative Medicine and Tissue Engineering,* p. 143, 2014.

[156] B. Guillotin and F. Guillemot, "Cell patterning technologies for organotypic tissue fabrication," *Trends Biotechnol,* vol. 29, pp. 183-90, Apr 2011.

[157] V. Mironov, R. P. Visconti, V. Kasyanov, G. Forgacs, C. J. Drake, and R. R. Markwald, "Organ printing: Tissue spheroids as building blocks," *Biomaterials,* vol. 30, pp. 2164-2174, 4// 2009.

[158] D. B. Kolesky, R. L. Truby, A. S. Gladman, T. A. Busbee, K. A. Homan, and J. A. Lewis, "3D Bioprinting of Vascularized, Heterogeneous Cell-Laden Tissue Constructs," *Advanced Materials,* vol. 26, pp. 3124-3130, 2014.

[159] J. S. Miller, K. R. Stevens, M. T. Yang, B. M. Baker, D.-H. T. Nguyen, D. M. Cohen, E. Toro, A. A. Chen, P. A. Galie, X. Yu, R. Chaturvedi, S. N. Bhatia, and C. S. Chen, "Rapid casting of patterned vascular networks for perfusable engineered three-dimensional tissues," *Nat Mater,* vol. 11, pp. 768-774, 09//print 2012.

[160] W. Wu, A. DeConinck, and J. A. Lewis, "Omnidirectional Printing of 3D Microvascular Networks," *Advanced Materials,* vol. 23, pp. H178-H183, Jun 24 2011.

[161] J.-H. Huang, J. Kim, N. Agrawal, A. P. Sudarsan, J. E. Maxim, A. Jayaraman, and V. M. Ugaz, "Rapid Fabrication of Bio-inspired 3D Microfluidic Vascular Networks," *Advanced Materials,* vol. 21, pp. 3567-3571, 2009.

[162] J.-H. Huang, J. Kim, Y. Ding, A. Jayaraman, and V. M. Ugaz, "Embedding synthetic microvascular networks in poly (lactic acid) substrates with rounded cross-sections for cell culture applications," *PLoS One,* vol. 8, p. e73188, 2013.

[163] T. C. Lim, M. F. Leong, H. Lu, C. Du, S. Gao, A. C. Wan, and J. Y. Ying, "Follicular dermal papilla structures by organization of epithelial and mesenchymal cells in interfacial polyelectrolyte complex fibers," *Biomaterials,* vol. 34, pp. 7064-7072, 2013.

[164] W. Wu, A. DeConinck, and J. A. Lewis, "Omnidirectional printing of 3D microvascular networks," *Advanced Materials,* vol. 23, 2011.

[165] M. Guvendiren and J. A. Burdick, "Engineering synthetic hydrogel microenvironments to instruct stem cells," *Current opinion in biotechnology,* vol. 24, pp. 841-846, 2013.
[166] C. Yang, M. W. Tibbitt, L. Basta, and K. S. Anseth, "Mechanical memory and dosing influence stem cell fate," *Nature materials,* vol. 13, p. 645, 2014.
[167] S.-A. Lee, D. Y. No, E. Kang, J. Ju, D.-S. Kim, and S.-H. Lee, "Spheroid-based three-dimensional liver-on-a-chip to investigate hepatocyte-hepatic stellate cell interactions and flow effects," *Lab on a Chip,* vol. 13, pp. 3529-3537, 2013.
[168] A. M. Gressner and R. Weiskirchen, "Modern pathogenetic concepts of liver fibrosis suggest stellate cells and TGF-beta as major players and therapeutic targets," *J Cell Mol Med,* vol. 10, pp. 76-99, Jan-Mar 2006.
[169] C.-T. Kuo, H.-K. Liu, G.-S. Huang, C.-H. Chang, C.-L. Chen, K.-C. Chen, R. Y.-J. Huang, C.-H. Lin, H. Lee, and C.-S. Huang, "A spatiotemporally defined in vitro microenvironment for controllable signal delivery and drug screening," *Analyst,* vol. 139, pp. 4846-4854, 2014.
[170] G. Orive, S. K. Tam, J. L. Pedraz, and J.-P. Hallé, "Biocompatibility of alginate-poly-l-lysine microcapsules for cell therapy," *Biomaterials,* vol. 27, pp. 3691-3700, 2006.
[171] M. Serra, C. Correia, R. Malpique, C. Brito, J. Jensen, P. Bjorquist, M. J. Carrondo, and P. M. Alves, "Microencapsulation technology: a powerful tool for integrating expansion and cryopreservation of human embryonic stem cells," *PLoS One,* vol. 6, p. e23212, 2011.
[172] M. B. Oliveira and J. F. Mano, "Polymer ‐ based microparticles in tissue engineering and regenerative medicine," *Biotechnology progress,* vol. 27, pp. 897-912, 2011.
[173] A. Murua, M. de Castro, G. Orive, R. M. Hernández, and J. L. Pedraz, "In Vitro Characterization and In Vivo Functionality of Erythropoietin-Secreting Cells Immobilized in Alginate-Poly-l-Lysine-Alginate Microcapsules," *Biomacromolecules,* vol. 8, pp. 3302-3307, 2007.
[174] A. Oliveira, T. Moretti, C. Boschini, J. Baliero, L. Freitas, O. Freitas, and C. Favaro-Trindade, "Microencapsulation of B. lactis (BI 01) and L. acidophilus (LAC 4) by complex coacervation followed by spouted-bed drying," *Drying Technology*, vol. 25, pp. 1687-1693, 2007.
[175] T. Kobayashi, Y. Aomatsu, H. Kanehiro, M. Hisanaga, and Y. Nakajima, "Protection of NOD islet isograft from autoimmune destruction by agarose microencapsulation," in *Transplantation proceedings,* 2003, pp. 484-485.
[176] T. Kong, L. Wang, H. M. Wyss, and H. C. Shum, "Capillary micromechanics for core–shell particles," *Soft Matter,* vol. 10, pp. 3271-3276, 2014.
[177] A. Kumachev, E. Tumarkin, G. C. Walker, and E. Kumacheva, "Characterization of the mechanical properties of microgels acting as cellular microenvironments," *Soft Matter,* vol. 9, pp. 2959-2965, 2013.
[178] J. Wan, A. Bick, M. Sullivan, and H. A. Stone, "Controllable Microfluidic Production of Microbubbles in Water-in-Oil Emulsions and the Formation of Porous Microparticles," *Advanced Materials,* vol. 20, pp. 3314-3318, 2008.

[179] J. Li, Y. Wang, H. Chen, and J. Wan, "Electrowetting-on-dielectrics for manipulation of oil drops and gas bubbles in aqueous-shell compound drops," *Lab on a Chip,* vol. 14, pp. 4334-4337, 2014.
[180] A. Van Soom, A. Mahmoudzadeh, A. Christophe, M. Ysebaert, and A. De Kruif, "Silicone oil used in microdrop culture can affect bovine embryonic development and freezability," *Reproduction in Domestic Animals,* vol. 36, pp. 169-176, 2001.
[181] L. Ricci-Vitiani, D. G. Lombardi, E. Pilozzi, M. Biffoni, M. Todaro, C. Peschle, and R. De Maria, "Identification and expansion of human colon-cancer-initiating cells," *Nature,* vol. 445, pp. 111-115, 2007.
[182] J. Sun, M. E. Hobert, Y. Duan, A. S. Rao, T.-C. He, E. B. Chang, and J. L. Madara, "Crosstalk between NF-κB and β-catenin pathways in bacterial-colonized intestinal epithelial cells," *American Journal of Physiology-Gastrointestinal and Liver Physiology,* vol. 289, pp. G129-G137, 2005.
[183] D. C. Duffy, J. C. McDonald, O. J. Schueller, and G. M. Whitesides, "Rapid prototyping of microfluidic systems in poly (dimethylsiloxane)," *Analytical chemistry,* vol. 70, pp. 4974-4984, 1998.
[184] A. R. Abate, T. Hung, P. Mary, J. J. Agresti, and D. A. Weitz, "High-throughput injection with microfluidics using picoinjectors," *Proceedings of the National Academy of Sciences,* vol. 107, pp. 19163-19166, 2010.
[185] G. Raeber, M. Lutolf, and J. Hubbell, "Mechanisms of 3-D migration and matrix remodeling of fibroblasts within artificial ECMs," *Acta biomaterialia,* vol. 3, pp. 615-629, 2007.
[186] J. A. Green and K. M. Yamada, "Three-dimensional microenvironments modulate fibroblast signaling responses," *Advanced drug delivery reviews,* vol. 59, pp. 1293-1298, 2007.
[187] D. C. Rubin, A. Shaker, and M. S. Levin, "Chronic intestinal inflammation: inflammatory bowel disease and colitis-associated colon cancer," *Frontiers in immunology,* vol. 3, p. 107, 2012.
[188] S. F. van EEDEN, W. C. Tan, T. Suwa, H. Mukae, T. Terashima, T. Fujii, D. Qui, R. Vincent, and J. C. Hogg, "Cytokines involved in the systemic inflammatory response induced by exposure to particulate matter air pollutants (PM10)," *American journal of respiratory and critical care medicine,* vol. 164, pp. 826-830, 2001.
[189] P. Wang, W. Qiu, C. Dudgeon, H. Liu, C. Huang, G. Zambetti, J. Yu, and L. Zhang, "PUMA is directly activated by NF-κB and contributes to TNF-α-induced apoptosis," *Cell Death & Differentiation,* vol. 16, pp. 1192-1202, 2009.
[190] D. A. Turner, P. Paszek, D. J. Woodcock, D. E. Nelson, C. A. Horton, Y. Wang, D. G. Spiller, D. A. Rand, M. R. White, and C. V. Harper, "Physiological levels of TNFα stimulation induce stochastic dynamics of NF-κB responses in single living cells," *J Cell Sci,* vol. 123, pp. 2834-2843, 2010.
[191] K. M. Yamada and E. Cukierman, "Modeling tissue morphogenesis and cancer in 3D," *Cell,* vol. 130, pp. 601-610, 2007.
[192] L. G. Griffith and M. A. Swartz, "Capturing complex 3D tissue physiology in vitro," *Nature reviews Molecular cell biology,* vol. 7, pp. 211-224, 2006.
[193] Y. Tan, D. J. Richards, T. C. Trusk, R. P. Visconti, M. J. Yost, M. S. Kindy, C. J. Drake, W. S. Argraves, R. R. Markwald, and Y. Mei, "3D printing facilitated

scaffold-free tissue unit fabrication," *Biofabrication,* vol. 6, pp. 024111-024111, 2014.
[194] L. E. Bertassoni, J. C. Cardoso, V. Manoharan, A. L. Cristino, N. S. Bhise, W. A. Araujo, P. Zorlutuna, N. E. Vrana, A. M. Ghaemmaghami, and M. R. Dokmeci, "Direct-write bioprinting of cell-laden methacrylated gelatin hydrogels," *Biofabrication,* vol. 6, pp. 024105-024105, 2014.
[195] N. E. Fedorovich, H. M. Wijnberg, W. J. Dhert, and J. Alblas, "Distinct tissue formation by heterogeneous printing of osteo- and endothelial progenitor cells," *Tissue Engineering Part A,* vol. 17, pp. 2113-21, 2011.
[196] A. A. Ahmad, Y. Wang, A. D. Gracz, C. E. Sims, S. T. Magness, and N. L. Allbritton, "Optimization of 3-D organotypic primary colonic cultures for organ-on-chip applications," *Journal of biological engineering,* vol. 8, p. 1, 2014.
[197] B. Radotra and D. McCormick, "Glioma invasion in vitro is mediated by CD44-hyaluronan interactions," *The Journal of pathology,* vol. 181, pp. 434-438, 1997.
[198] S.-H. Lee, J. J. Moon, and J. L. West, "Three-dimensional micropatterning of bioactive hydrogels via two-photon laser scanning photolithography for guided 3D cell migration," *Biomaterials,* vol. 29, pp. 2962-2968, 2008.
[199] J.-H. Shim, J. Y. Kim, M. Park, J. Park, and D.-W. Cho, "Development of a hybrid scaffold with synthetic biomaterials and hydrogel using solid freeform fabrication technology," *Biofabrication,* vol. 3, p. 034102, 2011.
[200] E. M. Ahmed, "Hydrogel: Preparation, characterization, and applications: A review," *Journal of Advanced Research,* vol. 6, pp. 105-121, 2015.
[201] A. Jemal, R. Siegel, E. Ward, Y. Hao, J. Xu, T. Murray, and M. J. Thun, "Cancer statistics, 2008," *CA: a cancer journal for clinicians,* vol. 58, pp. 71-96, 2008.
[202] B. D. Simons and H. Clevers, "Stem cell self-renewal in intestinal crypt," *Experimental cell research,* vol. 317, pp. 2719-2724, 2011.
[203] C. Crosnier, D. Stamataki, and J. Lewis, "Organizing cell renewal in the intestine: stem cells, signals and combinatorial control," *Nature Reviews Genetics,* vol. 7, pp. 349-359, 2006.
[204] F. Radtke and H. Clevers, "Self-renewal and cancer of the gut: two sides of a coin," *Science,* vol. 307, pp. 1904-1909, 2005.
[205] N. Barker, R. A. Ridgway, J. H. van Es, M. van de Wetering, H. Begthel, M. van den Born, E. Danenberg, A. R. Clarke, O. J. Sansom, and H. Clevers, "Crypt stem cells as the cells-of-origin of intestinal cancer," *Nature,* vol. 457, pp. 608-611, 2009.
[206] J. Strater, U. Wedding, T. Barth, K. Koretz, C. Elsing, and P. Moller, "Rapid onset of apoptosis in vitro follows disruption of beta 1-integrin/matrix interactions in human colonic crypt cells," *Gastroenterology,* vol. 110, pp. 1776-1784, 1996.
[207] N. Perreault and J.-F. Beaulieu, "Primary cultures of fully differentiated and pure human intestinal epithelial cells," *Experimental cell research,* vol. 245, pp. 34-42, 1998.
[208] S. Lang, R. Sharrard, M. Stark, J. Villette, and N. Maitland, "Prostate epithelial cell lines form spheroids with evidence of glandular differentiation in three-dimensional Matrigel cultures," *British journal of cancer,* vol. 85, p. 590, 2001.
[209] K. Takayama, K. Kawabata, Y. Nagamoto, K. Kishimoto, K. Tashiro, F. Sakurai, M. Tachibana, K. Kanda, T. Hayakawa, and M. K. Furue, "3D spheroid culture of

hESC/hiPSC-derived hepatocyte-like cells for drug toxicity testing," *Biomaterials*, vol. 34, pp. 1781-1789, 2013.
[210] S. M. O'Connor, D. A. Stenger, K. M. Shaffer, and W. Ma, "Survival and neurite outgrowth of rat cortical neurons in three-dimensional agarose and collagen gel matrices," *Neuroscience letters*, vol. 304, pp. 189-193, 2001.
[211] Y. G. Zhang, S. Wu, Y. Xia, and J. Sun, "Salmonella-infected crypt-derived intestinal organoid culture system for host-bacterial interactions," *Physiological reports*, vol. 2, p. e12147, 2014.
[212] J. He, L. Zhu, Y. Liu, D. Li, and Z. Jin, "Sequential assembly of 3D perfusable microfluidic hydrogels," *Journal of Materials Science: Materials in Medicine*, vol. 25, pp. 2491-2500, 2014.
[213] J.-Y. Xiong, J. Narayanan, X.-Y. Liu, T. K. Chong, S. B. Chen, and T.-S. Chung, "Topology evolution and gelation mechanism of agarose gel," *The Journal of Physical Chemistry B*, vol. 109, pp. 5638-5643, 2005.
[214] N. Iyer, K. Cooper, J. Yang, and F. Zenhausern, "Measuring Elastic Properties of Thin Biological Films Using Capillary Wrinkling," in *IV INTERNATIONAL CONFERENCE TIMES OF POLYMERS (TOP) AND COMPOSITES*, 2008, pp. 41-43.
[215] S. Hong, D. Sycks, H. F. Chan, S. Lin, G. P. Lopez, F. Guilak, K. W. Leong, and X. Zhao, "3D printing of highly stretchable and tough hydrogels into complex, cellularized structures," *Advanced Materials*, vol. 27, pp. 4035-4040, 2015.
[216] M. P. Lutolf, P. M. Gilbert, and H. M. Blau, "Designing materials to direct stem-cell fate," *Nature*, vol. 462, pp. 433-441, 2009.
[217] A. Balgude, X. Yu, A. Szymanski, and R. Bellamkonda, "Agarose gel stiffness determines rate of DRG neurite extension in 3D cultures," *Biomaterials*, vol. 22, pp. 1077-1084, 2001.
[218] Y. S. Pek, A. C. Wan, and J. Y. Ying, "The effect of matrix stiffness on mesenchymal stem cell differentiation in a 3D thixotropic gel," *Biomaterials*, vol. 31, pp. 385-391, 2010.
[219] M. Ehrbar, A. Sala, P. Lienemann, A. Ranga, K. Mosiewicz, A. Bittermann, S. Rizzi, F. Weber, and M. Lutolf, "Elucidating the role of matrix stiffness in 3D cell migration and remodeling," *Biophysical journal*, vol. 100, pp. 284-293, 2011.
[220] K. J. Ryan and C. G. Ray, "Medical microbiology," *McGraw Hill*, vol. 4, p. 370, 2004.
[221] A. Haraga, M. B. Ohlson, and S. I. Miller, "Salmonellae interplay with host cells," *Nature Reviews Microbiology*, vol. 6, pp. 53-66, 2008.
[222] F. Galdiero, G. C. de l'Ero, N. Benedetto, M. Galdiero, and M. Tufano, "Release of cytokines induced by Salmonella typhimurium porins," *Infection and immunity*, vol. 61, pp. 155-161, 1993.
[223] A. J. Lax and W. Thomas, "How bacteria could cause cancer: one step at a time," *Trends in microbiology*, vol. 10, pp. 293-299, 2002.
[224] J. Biarc, I. S. Nguyen, A. Pini, F. Gossé, S. Richert, D. Thiersé, A. Van Dorsselaer, E. Leize-Wagner, F. Raul, and J.-P. Klein, "Carcinogenic properties of proteins with pro-inflammatory activity from Streptococcus infantarius (formerly S. bovis)," *Carcinogenesis*, vol. 25, pp. 1477-1484, 2004.

[225] S. F. Schoppmann, P. Birner, J. Stöckl, R. Kalt, R. Ullrich, C. Caucig, E. Kriehuber, K. Nagy, K. Alitalo, and D. Kerjaschki, "Tumor-associated macrophages express lymphatic endothelial growth factors and are related to peritumoral lymphangiogenesis," *The American journal of pathology,* vol. 161, pp. 947-956, 2002.
[226] S.-C. Baik, H.-S. Youn, M.-H. Chung, W.-K. Lee, M.-J. Cho, G.-H. Ko, C.-K. Park, H. Kasai, and K.-H. Rhee, "Increased oxidative DNA damage in Helicobacter pylori-infected human gastric mucosa," *Cancer Research,* vol. 56, pp. 1279-1282, 1996.
[227] E. E. Mannick, L. E. Bravo, G. Zarama, J. L. Realpe, X.-J. Zhang, B. Ruiz, E. T. Fontham, R. Mera, M. J. Miller, and P. Correa, "Inducible nitric oxide synthase, nitrotyrosine, and apoptosis in Helicobacter pylori gastritis: effect of antibiotics and antioxidants," *Cancer Research,* vol. 56, pp. 3238-3243, 1996.
[228] L. Eckmann and M. F. Kagnoff, "Cytokines in host defense against Salmonella," *Microbes and Infection,* vol. 3, pp. 1191-1200, 2001.
[229] P. Mastroeni, "Immunity to systemic Salmonella infections," *Current molecular medicine,* vol. 2, pp. 393-406, 2002.
[230] E. C. Novosel, C. Kleinhans, and P. J. Kluger, "Vascularization is the key challenge in tissue engineering," *Advanced drug delivery reviews,* vol. 63, pp. 300-311, 2011.
[231] R. P. Visconti, V. Kasyanov, C. Gentile, J. Zhang, R. R. Markwald, and V. Mironov, "Towards organ printing: engineering an intra-organ branched vascular tree," *Expert opinion on biological therapy,* vol. 10, pp. 409-420, 2010.
[232] J. Folkman and M. Hochberg, "Self-regulation of growth in three dimensions," *Journal of Experimental Medicine,* vol. 138, pp. 745-753, 1973.
[233] S. L. Dahl, A. P. Kypson, J. H. Lawson, J. L. Blum, J. T. Strader, Y. Li, R. J. Manson, W. E. Tente, L. DiBernardo, and M. T. Hensley, "Readily available tissue-engineered vascular grafts," *Science translational medicine,* vol. 3, pp. 68ra9-68ra9, 2011.
[234] R. Gauvin, T. Ahsan, D. Larouche, P. Lévesque, J. Dubé, F. A. Auger, R. M. Nerem, and L. Germain, "A novel single-step self-assembly approach for the fabrication of tissue-engineered vascular constructs," *Tissue Engineering Part A,* vol. 16, pp. 1737-1747, 2010.
[235] A. D. van der Meer, V. V. Orlova, P. ten Dijke, A. van den Berg, and C. L. Mummery, "Three-dimensional co-cultures of human endothelial cells and embryonic stem cell-derived pericytes inside a microfluidic device," *Lab on a Chip,* vol. 13, pp. 3562-3568, 2013.
[236] J. T. Borenstein, E. J. Weinberg, B. K. Orrick, C. Sundback, M. R. Kaazempur-Mofrad, and J. P. Vacanti, "Microfabrication of three-dimensional engineered scaffolds," *Tissue engineering,* vol. 13, pp. 1837-1844, 2007.
[237] B. Guillotin and F. Guillemot, "Cell patterning technologies for organotypic tissue fabrication," *Trends in biotechnology,* vol. 29, pp. 183-190, 2011.
[238] J. H. Huang, J. Kim, N. Agrawal, A. P. Sudarsan, J. E. Maxim, A. Jayaraman, and V. M. Ugaz, "Rapid Fabrication of Bio‐inspired 3D Microfluidic Vascular Networks," *Advanced Materials,* vol. 21, pp. 3567-3571, 2009.
[239] J. S. Boyer, "Water transport," *Annual Review of Plant Physiology,* vol. 36, pp. 473-516, 1985.

[240] C. K. Boyce, "Patterns of segregation and convergence in the evolution of fern and seed plant leaf morphologies," *Paleobiology,* vol. 31, pp. 117-140, 2005.
[241] L. Sack, C. M. Streeter, and N. M. Holbrook, "Hydraulic analysis of water flow through leaves of sugar maple and red oak," *Plant Physiology,* vol. 134, pp. 1824-1833, 2004.
[242] X. Noblin, L. Mahadevan, I. Coomaraswamy, D. A. Weitz, N. M. Holbrook, and M. A. Zwieniecki, "Optimal vein density in artificial and real leaves," *Proceedings of the National Academy of Sciences,* vol. 105, pp. 9140-9144, 2008.
[243] K. S. Gan, S. C. Wong, J. W. H. Yong, and G. D. Farquhar, "18O spatial patterns of vein xylem water, leaf water, and dry matter in cotton leaves," *Plant Physiology,* vol. 130, pp. 1008-1021, 2002.
[244] T.-Y. Kang, J. M. Hong, J. W. Jung, J. J. Yoo, and D.-W. Cho, "Design and assessment of a microfluidic network system for oxygen transport in engineered tissue," *Langmuir,* vol. 29, pp. 701-709, 2012.
[245] A. Roth-Nebelsick, D. Uhl, V. Mosbrugger, and H. Kerp, "Evolution and function of leaf venation architecture: a review," *Annals of Botany,* vol. 87, pp. 553-566, 2001.
[246] Ü. Niinemets, A. Portsmuth, and M. Tobias, "Leaf shape and venation pattern alter the support investments within leaf lamina in temperate species: a neglected source of leaf physiological differentiation?," *Functional Ecology,* vol. 21, pp. 28-40, 2007.
[247] A. D. McKown, H. Cochard, and L. Sack, "Decoding leaf hydraulics with a spatially explicit model: principles of venation architecture and implications for its evolution," *The American Naturalist,* vol. 175, pp. 447-460, 2010.
[248] P. Prusinkiewicz, P. Federl, R. Karwowski, and R. Mech, "L-systems and beyond," *Course notes from SIGGRAPH,* vol. 5, pp. 70-82, 2003.
[249] W. Wu, C. J. Hansen, A. M. Aragón, P. H. Geubelle, S. R. White, and J. A. Lewis, "Direct-write assembly of biomimetic microvascular networks for efficient fluid transport," *Soft Matter,* vol. 6, pp. 739-742, 2010.
[250] T. F. Sherman, "On connecting large vessels to small. The meaning of Murray's law," *The Journal of general physiology,* vol. 78, pp. 431-453, 1981.
[251] C. A. Price, S.-J. C. Knox, and T. J. Brodribb, "The influence of branch order on optimal leaf vein geometries: Murray's Law and area preserving branching," *PLoS One,* vol. 8, p. e85420, 2013.
[252] Y. Huo and G. S. Kassab, "Intraspecific scaling laws of vascular trees," *Journal of The Royal Society Interface,* vol. 9, pp. 190-200, 2012.
[253] G. B. West, J. H. Brown, and B. J. Enquist, "A general model for the origin of allometric scaling laws in biology," *Science,* vol. 276, pp. 122-126, 1997.
[254] C. A. Price and B. J. Enquist, "Scaling of mass and morphology in plants with minimal branching: an extension of the WBE model," *Functional Ecology,* vol. 20, pp. 11-20, 2006.
[255] G. J. Doherty and H. T. McMahon, "Mediation, modulation, and consequences of membrane-cytoskeleton interactions," *Annu. Rev. Biophys.,* vol. 37, pp. 65-95, 2008.
[256] C. L. Chaffer and R. A. Weinberg, "A perspective on cancer cell metastasis," *Science,* vol. 331, pp. 1559-1564, 2011.

[257] V. K. Chivukula, B. L. Krog, J. T. Nauseef, M. D. Henry, and S. C. Vigmostad, "alterations in cancer cell mechanical properties after fluid shear stress exposure: a micropipette aspiration study," *Cell health and cytoskeleton,* vol. 7, p. 25, 2015.
[258] G. P. Gupta and J. Massagué, "Cancer metastasis: building a framework," *Cell,* vol. 127, pp. 679-695, 2006.
[259] D. Wirtz, K. Konstantopoulos, and P. C. Searson, "The physics of cancer: the role of physical interactions and mechanical forces in metastasis," *Nature Reviews Cancer,* vol. 11, pp. 512-522, 2011.
[260] C. L. Avvisato, X. Yang, S. Shah, B. Hoxter, W. Li, R. Gaynor, R. Pestell, A. Tozeren, and S. W. Byers, "Mechanical force modulates global gene expression and β-catenin signaling in colon cancer cells," *Journal of cell science,* vol. 120, pp. 2672-2682, 2007.
[261] P. J. Morin, "β‐catenin signaling and cancer," *Bioessays,* vol. 21, pp. 1021-1030, 1999.
[262] P. Polakis, "Wnt signaling and cancer," *Genes & development,* vol. 14, pp. 1837-1851, 2000.
[263] V. Thamilselvan, A. Patel, J. v. d. Voort van Zyp, and M. D. Basson, "Colon cancer cell adhesion in response to Src kinase activation and actin‐cytoskeleton by non‐laminar shear stress," *Journal of cellular biochemistry,* vol. 92, pp. 361-371, 2004.
[264] E. Hintermann, M. Bilban, A. Sharabi, and V. Quaranta, "Inhibitory role of α6β4-associated erbB-2 and phosphoinositide 3-kinase in keratinocyte haptotactic migration dependent on α3β1 integrin," *The Journal of cell biology,* vol. 153, pp. 465-478, 2001.
[265] L. M. Shaw, I. Rabinovitz, H. H.-F. Wang, A. Toker, and A. M. Mercurio, "Activation of phosphoinositide 3-OH kinase by the α6β4 integrin promotes carcinoma invasion," *Cell,* vol. 91, pp. 949-960, 1997.
[266] J. C. Hedges, M. A. Dechert, I. A. Yamboliev, J. L. Martin, E. Hickey, L. A. Weber, and W. T. Gerthoffer, "A role for p38MAPK/HSP27 pathway in smooth muscle cell migration," *Journal of Biological Chemistry,* vol. 274, pp. 24211-24219, 1999.
[267] S. Rousseau, F. Houle, J. Landry, and J. Huot, "p38 MAP kinase activation by vascular endothelial growth factor mediates actin reorganization and cell migration in human endothelial cells," *Oncogene,* vol. 15, pp. 2169-2177, 1997.
[268] B. Mao, W. Wu, G. Davidson, J. Marhold, M. Li, B. M. Mechler, H. Delius, D. Hoppe, P. Stannek, and C. Walter, "Kremen proteins are Dickkopf receptors that regulate Wnt/β-catenin signalling," *Nature,* vol. 417, pp. 664-667, 2002.
[269] J. Hildesheim, G. I. Belova, S. D. Tyner, X. Zhou, L. Vardanian, and A. J. Fornace, "Gadd45a regulates matrix metalloproteinases by suppressing ΔNp63α and β-catenin via p38 MAP kinase and APC complex activation," *Oncogene,* vol. 23, pp. 1829-1837, 2004.
[270] N. Porquet, A. Poirier, F. Houle, A.-L. Pin, S. Gout, P.-L. Tremblay, É. R. Paquet, R. Klinck, F. A. Auger, and J. Huot, "Survival advantages conferred to colon cancer cells by E-selectin-induced activation of the PI3K-NFκB survival axis downstream of Death receptor-3," *BMC cancer,* vol. 11, p. 285, 2011.
[271] C.-W. Luo, C.-C. Wu, and H.-J. Ch'ang, "Radiation sensitization of tumor cells induced by shear stress: The roles of integrins and FAK," *Biochimica et Biophysica Acta (BBA)-Molecular Cell Research,* vol. 1843, pp. 2129-2137, 2014.

[272] K. Ziółkowska, A. Stelmachowska, R. Kwapiszewski, M. Chudy, A. Dybko, and Z. Brzózka, "Long-term three-dimensional cell culture and anticancer drug activity evaluation in a microfluidic chip," *Biosensors and Bioelectronics,* vol. 40, pp. 68-74, 2013.
[273] M. J. Mitchell and M. R. King, "Fluid shear stress sensitizes cancer cells to receptor-mediated apoptosis via trimeric death receptors," *New journal of physics,* vol. 15, p. 015008, 2013.
[274] S. Jadhav, B. S. Bochner, and K. Konstantopoulos, "Hydrodynamic shear regulates the kinetics and receptor specificity of polymorphonuclear leukocyte-colon carcinoma cell adhesive interactions," *The Journal of Immunology,* vol. 167, pp. 5986-5993, 2001.
[275] S. Nagrath, L. V. Sequist, S. Maheswaran, D. W. Bell, D. Irimia, L. Ulkus, M. R. Smith, E. L. Kwak, S. Digumarthy, and A. Muzikansky, "Isolation of rare circulating tumour cells in cancer patients by microchip technology," *Nature,* vol. 450, pp. 1235-1239, 2007.
[276] E. Bouskela, F. Z. Cyrino, and G. Marcelon, "Effects of Ruscus extract on the internal diameter of arterioles and venules of the hamster cheek pouch microcirculation," *Journal of cardiovascular pharmacology,* vol. 22, pp. 221-224, 1993.
[277] V. Turitto, "Blood viscosity, mass transport, and thrombogenesis," *Progress in hemostasis and thrombosis,* vol. 6, pp. 139-177, 1981.
[278] R. W. Lyczkowski, B. R. Alevriadou, M. Horner, C. B. Panchal, and S. G. Shroff, "Application of multiphase computational fluid dynamics to analyze monocyte adhesion," *Annals of biomedical engineering,* vol. 37, pp. 1516-1533, 2009.
[279] J. Tramper, J. Williams, D. Joustra, and J. Vlak, "Shear sensitivity of insect cells in suspension," *Enzyme and microbial technology,* vol. 8, pp. 33-36, 1986.
[280] R. Lu, S. Wu, Y. Zhang, Y. Xia, X. Liu, Y. Zheng, H. Chen, K. Schaefer, Z. Zhou, and M. Bissonnette, "Enteric bacterial protein AvrA promotes colonic tumorigenesis and activates colonic beta-catenin signaling pathway," *Oncogenesis,* vol. 3, p. e105, 2014.
[281] Y. Duan, A. P. Liao, S. Kuppireddi, Z. Ye, M. J. Ciancio, and J. Sun, "β-Catenin activity negatively regulates bacteria-induced inflammation," *Laboratory investigation,* vol. 87, pp. 613-624, 2007.
[282] S. Hashimoto, T. Nishiyama, S. Hayashi, T. Fujishiro, K. Takebe, N. Kanzaki, R. Kuroda, and M. Kurosaka, "Role of p53 in human chondrocyte apoptosis in response to shear strain," *Arthritis & Rheumatism,* vol. 60, pp. 2340-2349, 2009.
[283] J. J. Zhong, K. Fujiyama, T. Seki, and T. Yoshida, "A quantitative analysis of shear effects on cell suspension and cell culture of Perilla frutescens in bioreactors," *Biotechnology and bioengineering,* vol. 44, pp. 649-654, 1994.
[284] I. Abu-Reesh and F. Kargi, "Biological responses of hybridoma cells to defined hydrodynamic shear stress," *Journal of biotechnology,* vol. 9, pp. 167-178, 1989.
[285] R. E. Bachelder, A. Marchetti, R. Falcioni, S. Soddu, and A. M. Mercurio, "Activation of p53 function in carcinoma cells by the α6β4 integrin," *Journal of Biological Chemistry,* vol. 274, pp. 20733-20737, 1999.
[286] N. Resnick, H. Yahav, A. Shay-Salit, M. Shushy, S. Schubert, L. C. M. Zilberman, and E. Wofovitz, "Fluid shear stress and the vascular endothelium: for better and

for worse," *Progress in biophysics and molecular biology,* vol. 81, pp. 177-199, 2003.
[287] H. Yoshisue, K. Suzuki, A. Kawabata, T. Ohya, H. Zhao, K. Sakurada, Y. Taba, T. Sasaguri, N. Sakai, and S. Yamashita, "Large scale isolation of non-uniform shear stress-responsive genes from cultured human endothelial cells through the preparation of a subtracted cDNA library," *Atherosclerosis,* vol. 162, pp. 323-334, 2002.
[288] Y.-S. J. Li, J. H. Haga, and S. Chien, "Molecular basis of the effects of shear stress on vascular endothelial cells," *Journal of biomechanics,* vol. 38, pp. 1949-1971, 2005.
[289] M. A. Kamel, J. L. Picconi, N. Lara-Castillo, and M. L. Johnson, "Activation of β-catenin signaling in MLO-Y4 osteocytic cells versus 2t3 osteoblastic cells by fluid flow shear stress and PGE 2: Implications for the study of mechanosensation in bone," *Bone,* vol. 47, pp. 872-881, 2010.
[290] M. Noris, M. Morigi, R. Donadelli, S. Aiello, M. Foppolo, M. Todeschini, S. Orisio, G. Remuzzi, and A. Remuzzi, "Nitric oxide synthesis by cultured endothelial cells is modulated by flow conditions," *Circulation research,* vol. 76, pp. 536-543, 1995.
[291] L. G. van der Flier and H. Clevers, "Stem cells, self-renewal, and differentiation in the intestinal epithelium," *Annual review of physiology,* vol. 71, pp. 241-260, 2009.

Chapter 8. Publications

1. **Fan R**, Chen X, Wang Z, Custer D, Wan J. Flow-regulated growth of titanium dioxide (TiO_2) nanotubes in microfluidics. ***Small***, 2017. (DOI: 10.1002/smll.201701154)
2. **Fan R**, Wan J. Electrode distance regulates the growth of TiO_2 nanotubes during electrochemical anodization. ***Nanotechnology***, 2017; 28: 25LT01.
3. **Fan R**, Emery T, Zhang Y, Xia Y, Sun J, Wan J. Circulatory shear flow alters the viability and proliferation of circulating colon cancer cells. ***Sci Rep.***, 2016; 6: 27073.
4. **Fan R**, Emery T, Zhang Y, Xia Y, Sun J, Wan J. In vitro microfluidic circulatory system for testing circulating cancer cells. ***Nat. Protoc.*** 2016. [doi:10.1038/protex.2016.037]
5. **Fan R**, Piou M, Darling E, Cormier D, Sun J, Wan J. Bio-printing cell-laden Matrigel/agarose constructs. ***J. Biomater Appl.***, 2016, 0885328216669238.
6. **Fan R**, Naqvi K, Patel K, Sun J, Wan J. Evaporation-based microfluidic production of oil-free cell-containing hydrogel particles. ***Biomicrofluidics***, 2015; 9(5): 052602.
7. **Fan R**, Sun Y, Wan J. Leaf-inspired artificial microvascular networks (LIAMN) for three-dimensional cell culture. ***RSC Adv.***, 2015; 5(110): 90596-601.
8. Koppula KS, **Fan R**, Veerapalli KR, Wan J. Integrated microfluidic system with simultaneous emulsion generation and concentration. ***J. Colloid Interface Sci.***, 2016; 466: 162-7. **[Co-First Author]**
9. Lu T, **Fan R**, Delgadillo LF, Wan J. Stabilization of carbon dioxide (CO_2) bubbles in

micrometer-diameter aqueous droplets and the formation of hollow microparticles. ***Lab Chip.*** 2016; 16(9): 1587-92.